INSIGHTS INTO THE MICROBIAL DEGRADATION OF BONES FROM THE MARINE VERTEBRATE FOSSIL RECORD: AN EXPERIMENTAL APPROACH USING INTERDICIPLINARY ANALYSES

A DISSERTATION
SUBMITTED TO THE FACULTY OF
UNIVERSITY OF MINNESOTA
BY

LAURA ANN VIETTI

IN PARTIAL FULFILLMENT OF THE REQUIREMENTS
FOR THE DEGREE OF
DOCTOR OF PHILOSOPHY

DAVID L. FOX
JAKE V. BAILEY
RAYMOND R. ROGERS

AUGUST, 2014

Acknowledgements

First and foremost I would like to thank my advisers Jake Bailey, David Fox, and Raymond Rogers, for taking a chance on a lady with a dream of watching whales bloat and float, and giving me both space and guidance to pursue my research ideas. I'm especially grateful to Jake for opening his lab doors and making me feel so welcome and included in the Bailey lab group. I'm extremely thankful for all David's help with writing and statistics, and for keeping me grounded to paleontology and being excited about my research when I needed encouragement. Ray kept my passion and excitement alive throughout my dissertation research and I'm extremely appreciative of his guidance concerning future research directions and career advice.

I also give my thanks to Martha Tappen for her time and consideration as my dissertation committee chair, and for all of our great conversations about taphonomy. As one of the only other taphonomists on campus, she and her research group were my academic kin.

I'm also extremely appreciative of the Bailey lab members. Beverly Flood was integral in developing my experiment design, mentoring me in microbial techniques, and helping me interpret the results. Daniel Jones was also extremely helpful in my research methods and analyses, particularly with the entire process of next-generation sequencing and sequence processing. I'm also extremely appreciative of my other great lab-mates (Chris Crosby, Eric Stevens, Palmer Fliss, and Cindy Frickle) who sat through my talks, laughed with me, and shared the steep learning curve of learning microbiology techniques. I also thank the undergraduate interns in the lab, especially a big thanks to Elizabeth Ricci, and all the others!

I'd also like to acknowledge my fellow Fox lab-mate, Andrew Haveless for being such a good friend, sounding-board, and support system through my Ph.D. He was a great academic and QP (quaternary paleoecology) brother and I couldn't imagine my PhD without him in the picture, down the hall.

The anthropology department has also been a great help in my PhD. First I'd like to acknowledge John Soderburg, for without his support and encouragement, I would never have learned about surface texture analyses, nor had the opportunity to use their great scanning instruments. The anthropology grad students, especially Martha Tappen's students and Kieran McNulty's students, have been great friends and made me feel very welcome in the department; especially Kirsten Holt, Niki Garrett, Rebecca Slepkov, and Katrina Yezzi-Woodley. Lastly, I'd like to thank the anthropology department for providing me with a small army of interns over the past few years. Without their help, I would have never have been able to pursue to the surface texture characterization study. Thank you to Sean Carlson-Greer, Alison Rockman, Laura Koski, Dalton Tonga, and Hope Nylander. You all rock!

I also thank Amy Myrbo and other staff members of the Limnology Research Center for the training, use, and support of the SEM. I always enjoyed my time down in the basement with them.

I also would like to thank Colleen Forster of the Bionet histology lab (Minnesota) for her help with the histological sections, Michael Moore at Woods Hole for providing the natural marine mud and seawater, and Rorri Peterson for defleshing the experiment bones and not blaming me for killing off his beetle population when we put in the marine mammals.

I'm also grateful for the Earth Sciences office staff. Sharon Kressler has been such a great friend and support system throughout the whole PhD process. Doug Johnson and Greg Gambowski have been there to answer every money question I ever had, and made it fun! And I thank Kathy Ohler for all her help over the years.

I also have so much appreciation for the good friends I've developed, with a special shout-out to Erkan Toraman, Ben and Val Stanley, Roxanne Renedo, Sara Moron, Anna and Joe Myre, Ben and Julia Tutolo, Ryan Littlewood, Miki Rough, and all the other great friends I didn't mention.

Last but not least, I'd like to thank my family members, especially my Mom (Barbara Vietti) for the years of listening to me and always giving me moral support to

complete the dissertation. My Dad (John Vietti), has also been helpful throughout the process and tried to keep me on track with little hints here and there to keep writing. I've taken advantage of my brother's (Will Vietti) awesome editorial skills and he has looked over many of my documents; below are some suggestions he thought I should title my dissertation when I was tossing ideas around:

> "~~Putting microbes to work: an experimental approach to investigating the effect of microbial activity on the vertebrate fossil record~~ Making microbes your bitch: I watched them eat dead things to figure out stuff about other dead things"
>
> or
>
> "~~Advances in understanding and characterizing pre-burial bone modifications and their applications to the vertebrate fossil record~~ I know more about wet roadkill than you do, but I'm willing to share"

Dedication

I dedicate this dissertation to the generations of strong rock and fossil loving women in my family; in particular my Mom: Barbara Vietti, my Aunt: Janet Chimenti, my Grandma: Ema Jane Tomes, my Grand-Aunt: Ruth Clare Johnson, and my Great-Aunt: Clare Axtell. For without their fascination with rocks and fossils being passed down through the generations, or their role in promoting women's place in earth sciences, I would never have been fortunate enough to have spent the past six years imagining the life of a proto-fossil getting chewed on and tossed around on the paleo-ocean floor, and ultimately discovering a small, yet novel, piece of information about the early fossilization of bone. I look forward to passing on the rock and fossil passion to the next generation of the H1a1 maternal haplogroup when the time comes.

Top Left:
Barbara Vietti with Laura Vietti (1 year old).

Top Right (left to right):
Ruth Clare Johnson, Clare Axtell, Ema Jane Tomes.

Bottom Left:
Janet Chimenti

Bottom Right:
Laura Vietti (5 yrs old)

Abstract

Researchers rely on the fossil record to understand and predict changes in faunal composition and evolutionary trends associated with climatic change. However, taphonomic processes such as scavenging, transport, and weathering, significantly influence the type and quality of information preserved in the fossil record by filtering and diminishing the fidelity of ecological data. To help account for taphonomic biasing, I developed a series of interdisciplinary approaches to better understand the role and characterization of microbes during the fossilization of vertebrate remains, and an additional study that improves a well-established method for estimating time averaging of fossil bone accumulations.

To better understand which bacteria are responsible for bone decay, I simulated aspects of natural whale-falls by adding defleshed bones to mesocosms made of natural marine mud and water. Sequencing the V3 region of the 16S rRNA taxonomic identifier gene of bone-associated microbial communities indicated that the dominant bacterial groups exploiting bone nutrients were taxa within the *Alphaproteobacteria*, *Deltaproteobacteria*, *Gammaproteobacteria*, and *Epsilonproteobacteria*, as well as *Bacteroidetes* and *Firmicutes*. Relative abundances of these bacterial groups changed throughout the experiment, reflecting four community successions.

Sulfidic framboids were observed on the experiment bone surfaces within one week and were interpreted to form as the result of reducing conditions within a dark-colored microbial mat overlain by oxic waters. When compared with published sedimentary framboid populations, the bone-hosted framboids were most similar to framboids formed in anoxic water-columns, even though the bone was overlain by oxygenated conditions, suggesting that the growing periods for framboids are shorter on bone surfaces than those in sediments and do not reflect geochemical conditions.

Bone surface texture is known to degrade in a predictable fashion due to subaerial exposure, and can thus act as a proxy for estimating post-death/ pre-burial time since death which is relevant for assessing time averaging. In the final dissertation chapter I show that traditional weathering analyses can be characterized using quantitative textural

analyses from 3D scans of bone surfaces. Quantifying bone weathering analyses may enable more reliable comparative taphonomic analyses by reducing inter-observer variations and by providing numerical data compatible for use in multivariate statistics.

Table of Contents

List of Tables

List of Figures

Introduction

Microbial activity is recognized as a major constituent of the decay process of modern animal remains (Araujo, 2010; Benninger et al., 2008; Boumba et al., 2008; Carter et al., 2007) and a wide body of evidence also indicates that microbes played a role in the decay of fossil remains (Allison, 1988a; Darroch et al., 2012; Hollund et al., 2012; Jans et al., 2004; Trueman and Martill, 2002; Turner-Walker and Jans, 2008). Bones are a rich source of nutrients, but the organic fraction, primarily collagen, is not easily accessible for microbial degradation. Bones are composed of carbonated hydroxyl-apatite crystallites ($Ca_5(PO_4)_3(OH)$) that gives bone its structural strength, but the mineral also hinders the consumption of bone by other organisms. Bone collagen, the primary organic constituent of bone is also resistant to microbial degradation due to its complex molecular structure. For these reason, bone decays over longer time scales compared to soft tissue and has higher survival rates in the fossil record (Child, 1995b).

Despite bone's resistance to degradation, actualistic studies have shown that bone is not immune to microbial degradation (Ascenzi and Silvestrini, 1984; Balzer et al., 1997; Child, 1995a, b) and several types of biosignatures indicating the presence of microbes during the decay process have been established (Jans et al., 2004; Turner-Walker and Jans, 2008). Microbial biosignatures can generally fall into two categories: features produced by bioerosion or features produced by mineral precipitation. Bioerosion is perhaps the most obvious of the microbial biosignatures in bone due to the easily identifiable tunneling structures such as those described by Jans et al. (2004). The precipitation of authigenic minerals can form indirectly due to microbial activity on decaying material (Allison, 1988a; Brett and Baird, 1986; Daniel and Chin, 2010).

Although microbes play a role in the decay of bones from a variety of environments (Davis, 1997; Reeb et al., 2011), they are especially prevalent on the surfaces of decaying bone on the ocean floor. Marine vertebrates that die in water depths deep enough to prevent post-mortem floating sink to the ocean floor and undergo decomposition, a process termed carcass-fall, or in the case of whales, a whale-fall (Allison et al., 1991; Kemp et al., 2006; Smith and Baco, 2003). Carcass-falls deliver an

organic load several orders of magnitude greater than background organic particulate fluxes and this localized enrichment can stimulate a dynamic and unique food-fall scavenging community, some of which are supported for decades by microbes exploiting bone nutrients (Allison et al., 1991; Goffredi and Orphan, 2010; Smith and Baco, 2003). Bacteria are observed on nearly all types of carcass-fall on the ocean floor including large cetaceans, small cetaceans, and even on terrestrial mammals that float into the ocean and are deposited on the seafloor (Giancamillo et al., 2010). The bacteria occur as a microbial mat covering bone surfaces, and the bacteria in these mats are interpreted to utilize bone organics. However, for the reasons mentioned above, it's not clear if the microbes in the bone surface mats are capable of degrading bone. Some lines of evidence suggest that microbes help in degrading skeletons over time scales as short as 10 years (Lundsten et al., 2010), whereas other studies suggest bacteria degrade bone over much longer time scales (50 to 100s of years) (Bell and Elkerton, 2008; Schuller et al., 2004). Indeed, the role of bacteria in the preservation potential of bone, remains somewhat controversial because bacteria can both promote fossilization by mediating authigenic mineral precipitation (Daniel and Chin, 2010), but microbial processes are also recognized to destroy bone (Trueman and Martill, 2002).

Here, as a first step in understanding the role microbes have on bone survival, I replicated aspects of natural carcass-falls and studied the biofilms and minerals growing the bone surfaces. I identified the bacterial community composition of environmental biofilm growing on bone surfaces at several time points during a year and present my results in **chapter one** of this dissertation. I also discuss the primarily metabolisms likely being expressed over the course of the experiment and how they relate to bone degradation. In **chapter two** I describe and discuss the precipitation of sulfidic framboids that likely formed on bones surfaces as the result of microbial activity. Although not directly tied to the microbial degradation of bone, in **chapter three**, I present a new method for characterizing bone surface textures and discuss how the method could be used to quantify bone surface weathering.

Chapter 1:

INSIGHTS INTO THE MICROBIOME ASSOCIATED WITH EARLY BONE DIAGENESIS FROM rRNA GENE SEQUENCING OF BIOFILMS FROM ACTUALISTIC EXPERIMENTS

INTRODUCTION

Microbes are thought to play a role in the early diagenesis of vertebrate remains deposited in marine environments and evidence of microbial activity is prevalent from fossils recovered from marine strata. Evidence of microbial activity found on fossil bones, illustrated in Figure 1, occurs primarily as two types of features: 1) authigenic mineral precipitates such as calcite and iron sulfides (Brett and Baird, 1986; Clarke, 2004; Pfretzschner, 2004; Vietti et al., (submitted)); and 2) microbial bioerosion features like microborings, corrosion textures, and bone-brecciation (Hollund et al., 2012; Jans, 2008; Turner-Walker and Jans, 2008). These types of putative biosignatures are well documented on marine vertebrate remains from a variety of settings including those interpreted to have been deposited in shallow marine environments (Astibia et al., 2005; Danise et al., 2012) as well as deeper waters (Kaim et al., 2008; Kiel, 2008; Shapiro and Spangler, 2009) suggesting that microbial processes on bone are widespread. Despite the ample evidence of microbial activity on fossilized bone, little is known about the microbial communities involved in the decay process and which microbes may be involved in the mediation of various bone alteration features.

Bone is observed to stimulate microbial growth in modern environments. Most, if not all, large vertebrate skeletons discovered on the ocean floor are found covered by microbial mats (Allison et al., 1991; Amon et al., 2013; Dahlgren et al., 2006; Smith and Baco, 2003) . These microbial mats develop in response to an influx of organics provided by the bone, which can enrich the concentration of labile organic matter by a factor of one hundred over that of the surrounding environment (Goffredi and Orphan, 2010; Smith and Baco, 2003). Microbes are the primary degraders of bone because most other

scavengers are incapable of accessing the bone organics due to the mineral component of the bone. Bone's hardness comes from hydroxyapatite mineral crystallites that are tightly interwoven into the bone molecular structure. Few scavengers are capable of physically or chemically degrading bone; some polychaete worms, echinoids, gastropods, and bivalves are exceptions (Belaústegui et al., 2012; Bromley, 1975; Higgs et al., 2011; Kiel et al., 2010).

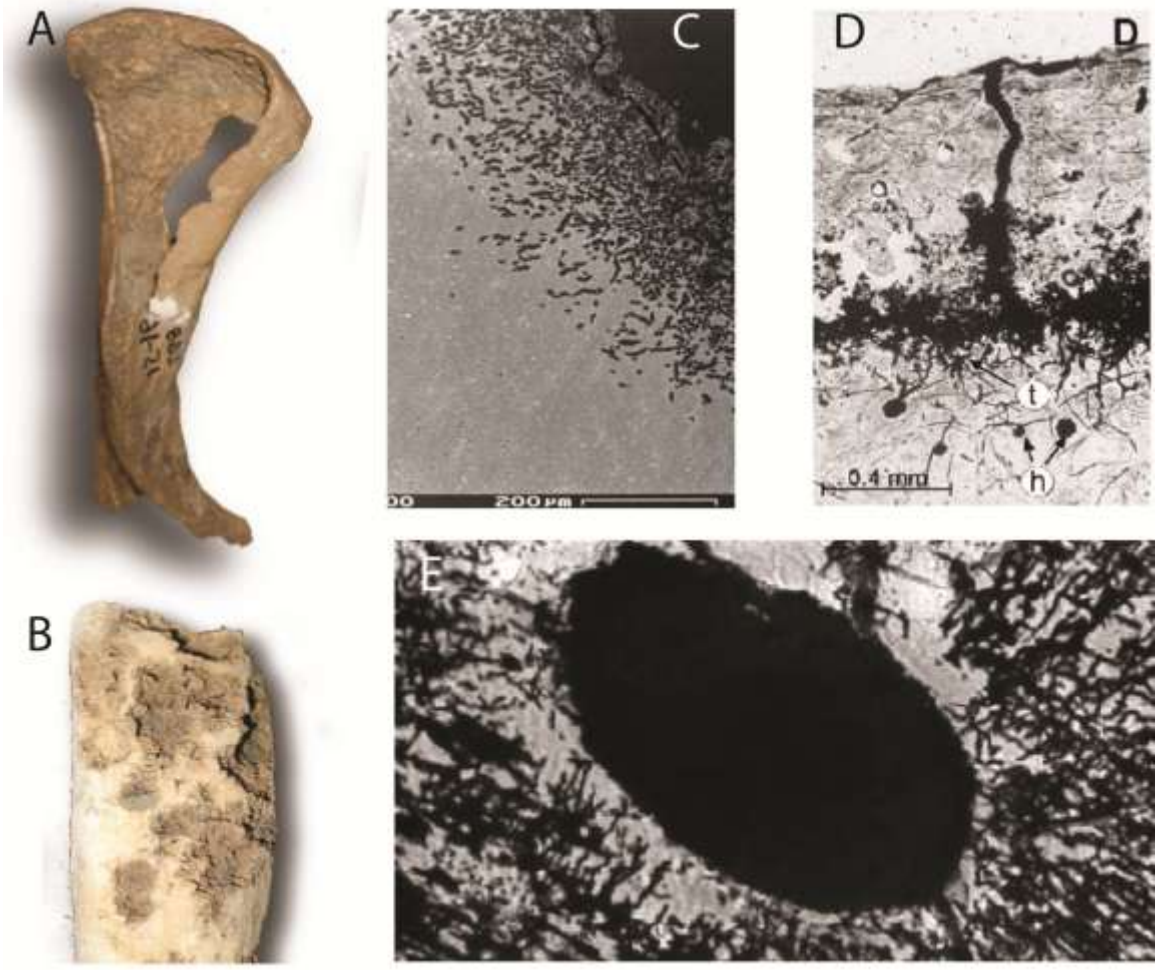

Figure 1. Examples of macro- and micro-bioerosion of bone. A: Macro bone corrosion on a pinniped humerus AMNH, B:Different corrosion texture potentially due to microbial processes, marine mammal rib, AMNH C: Micro-tunneling from Eocene sirenian remains(Astibia et al., 2005), D:microbial micro-tunneling on human recovered from a 15th century shipwreck (Bell and Elkerton, 2008), E: Different morphology of microbial micro-tunneling on Cretaceous marine reptile remains(R. Rogers collection)

Bone is also resistant to microbial degradation due to the complex molecular structure of bone collagen (Child, 1995a, b; Trueman and Martill, 2002). It is hypothesized that for the microbial utilization of bone collagen, the microbial community must be capable of first dissociating the bone collagen from the bone mineral. Once available, bone collagen is still resistant to microbial degradation due to its complex triple-helical structure at the molecular level. In order to lyse collagen molecules and utilize the collagen proteins, a microbe would need to synthesize enzymes like collagenase that are capable of extracellular collagen breakdown (Child, 1995a, b).

Previous studies have explored the microbial communities colonizing archaeological and modern bone in sub-aerial environments (Child, 1995a, b; Marchiafava et al., 1974; Reeb et al., 2011), as well as bacterial and archaea microbiomes from decaying mammals on the ocean floor (Goffredi and Orphan, 2010; Grünke et al., 2010; Tringe et al., 2005). Medical studies have also examined which microbes are capable of infecting and degrading bone (Brook, 2008; Machado de Oliveira et al., 2007). However few, if any, have reported on the community diversity of bone-associated bacteria in marine environments through time using environmental sequencing techniques (Ascenzi and Silvestrini, 1984). A more thorough understanding of community composition of the bone decay microbiome may provide the foundation for better understanding the process of bone degradation and identifying candidate microbial groups responsible for biosignatures found in the fossil bone recovered from marine strata.

In this study, I present a community level analysis of the diversity and taxonomic composition of microbial communities colonizing surfaces of bone decaying in simulated marine environments through time and address the following questions:

1) What is the community composition of bacterial mats colonizing bone surfaces?
2) Does the community change throughout the decay process?
3) Is the bacterial community capable of accessing and degrading bone collagen?

METHODS

Experiment Design

Lab-based mesocosms were used to study the composition of bacterial communities colonizing decaying bone surfaces in marine environments. Mesocosms were created by adding ~1000cm^3 of naturally inoculated marine mud and ~3 L of natural seawater to a 5 L lidded plastic container. Sediments and seawater were collected from the coast of Massachusetts (N 41^0 42'0", W 70^0 45'0", 0.5 m water depth) in early December. The mesocosms were then incubated in near dark conditions at 10^o C for 4 weeks to re-establish stable conditions for sediment-hosted microbial communities. After 4 weeks, 6 defleshed goat rib sections (*Capra aegagrus hircus*) (~2cm x ~1cm x ~1cm), were emplaced on the sediment/water interface of two replicate mesocosms. Rib sections were defleshed using dermestid beetle colonies, a process that has been observed to cause little impact on bone surfaces and bone composition when sufficient soft tissue is available (Hefti et al., 1980). Six holes (3mm diameter) were drilled into the plastic container just above the water/air interface to enable gas exchange and prevent closed-environment conditions. The decay experiment ran for 12 months and each mesocosm replicate was sampled at Months 2, 4, 6, 8 and 12 for a total of 5 sampling points. At each sampling period, oxygen profiles were measured, bones and associated biofilm samples were collected and preserved, and photographs were taken. For comparison, we included a control mesocosm created with sterilized natural seawater and sediment in the experiment design.

Oxygen Concentrations

Dissolved oxygen concentrations were measured as each sampling interval using Clark-type amperometric oxygen censors (Revsbech, 1989; Revsbech and Jørgensen, 1986)(Unisense, Aarhus, Science Park Aarhus, Denmark). Prior to measuring, the microsensor was depolarized and calibrated. Profiles started at ~1.5 cm above the sediment/water interface, extended through the biofilm directly adjacent to the bone, and

extended ~ 1cm into the sediment. Measurements were taken at 0.05 cm intervals and were reported as oxygen micromolar concentrations (μM).

Illumina Amplicon Sequencing of the16S rRNA Gene

DNA was extracted and the hypervariable region V3 of the taxonomic identifier gene 16S rRNA (Figure 2) was sequenced to construct environmental libraries of the biofilm collected from bone surfaces over the course of 12 months. The hypervariable regions of the 16S rRNA gene mutate at slightly faster rates compared to the whole gene, and as such, can provide taxonomic identification of the returned sequences using 150 base pairs as opposed to sequencing the entire gene (~1600 base pairs). Sequencing only the hypervariable region V3 using next-generation sequencing instead of the entire 16S rRNA gene enabled more bacterial phylotypes to be sequenced per sample than with clone libraries.

DNA extraction was done using the MoBio Powersoil DNA Isolated Kit (MoBio Laboratories, Carlsbad, CA). The kit specifies using 0.25 g of sediment to achieve optimal DNA output; however, we used ~ 0.1 g of biofilm sample due to limited biofilm availability. The extraction procedure adhered to the procedures in the MoBio Protocol 12888 (http://www.mobio.com/) with two slight deviations. First, in order to achieve maximal release of DNA, the bead beating was performed in a series of three 5 minute agitations with one third of the supernatant removed between each step. The second deviation occurred during the final elution step where the product was returned to the spin filter and centrifuged an additional time. DNA concentration and purity was evaluated using a Thermo Scientific Nanodrop 2000C Spectrophotometer.

Following the DNA extraction process, each sample was subjected to an initial polymerase chain reaction (PCR). Standard universal bacterial forward and reverse primers (27F: 5’AGAGTTTGATCMTGGCTC3’, 1992R: 5’CGGTTACCTTGTTACGACTT3’) were used to isolate and amplify the 16S rRNA gene in order to confirm the success of the extraction and determined the optimal amount of DNA to be used for each sample in subsequent PCRs. A 25 μl reaction was prepared

using GoTaq Green Master Mix 2X (Promega, Madison, WI) and 0.5 µl of each primer at a 10 µM concentration. The PCR protocol included an initial denaturation step at 95°C for 3 minutes followed by 25 cycles of 95°C for 1 min, 48°C for 90 sec, and 72°C for 2 min with a final extension step at 72°C for 10 min in a Bio Rad C1000 Thermal Cycler. The PCR products were then run through gel electrophoresis on a 1% agarose gel and visualized to confirm amplification. Once each sample had produced a satisfactory band upon visualization, another PCR was prepared using V3 primers with a protocol modeled after Bartram et al. (2011). For this 50 µl reaction, the taq polymerase, 10x loading buffer, and dNTP's were obtained from Qiagen's HotStar Taq plus DNA Polymerase Kit (Valencia, CA). Each reaction mixture included 1 µl of V3 specific primers.

The protocol for the PCR consisted of an initial activation of the taq at 95°C for 5 min, and 25 cycles of 95°C for 1 min, 50°C for 1 min, and 72°C for 1 min with a final extension step at 72°C for 7 min. PCR product for sequencing was collected using a gel-extraction protocol. Gel electrophoresis was prepared using a 2% agarose gel and the appropriate band of target DNA was excised and processed using the Zymoclean Gel DNA Recovery Kit (Zymo Research, Orange, CA). The samples were prepared for sequence analysis and sent to the University of Minnesota Biomedical Genomics Center (Minneapolis, MN) for library processing. Each V3 specific primer assigned to a sample was tagged with a unique barcode, which allowed for multiplexing and pooling of samples on a single lane for paired end Illumina MiSeq analysis. Results from sequencing include ~ 100,000 to 300,000 sequences per sample time period.

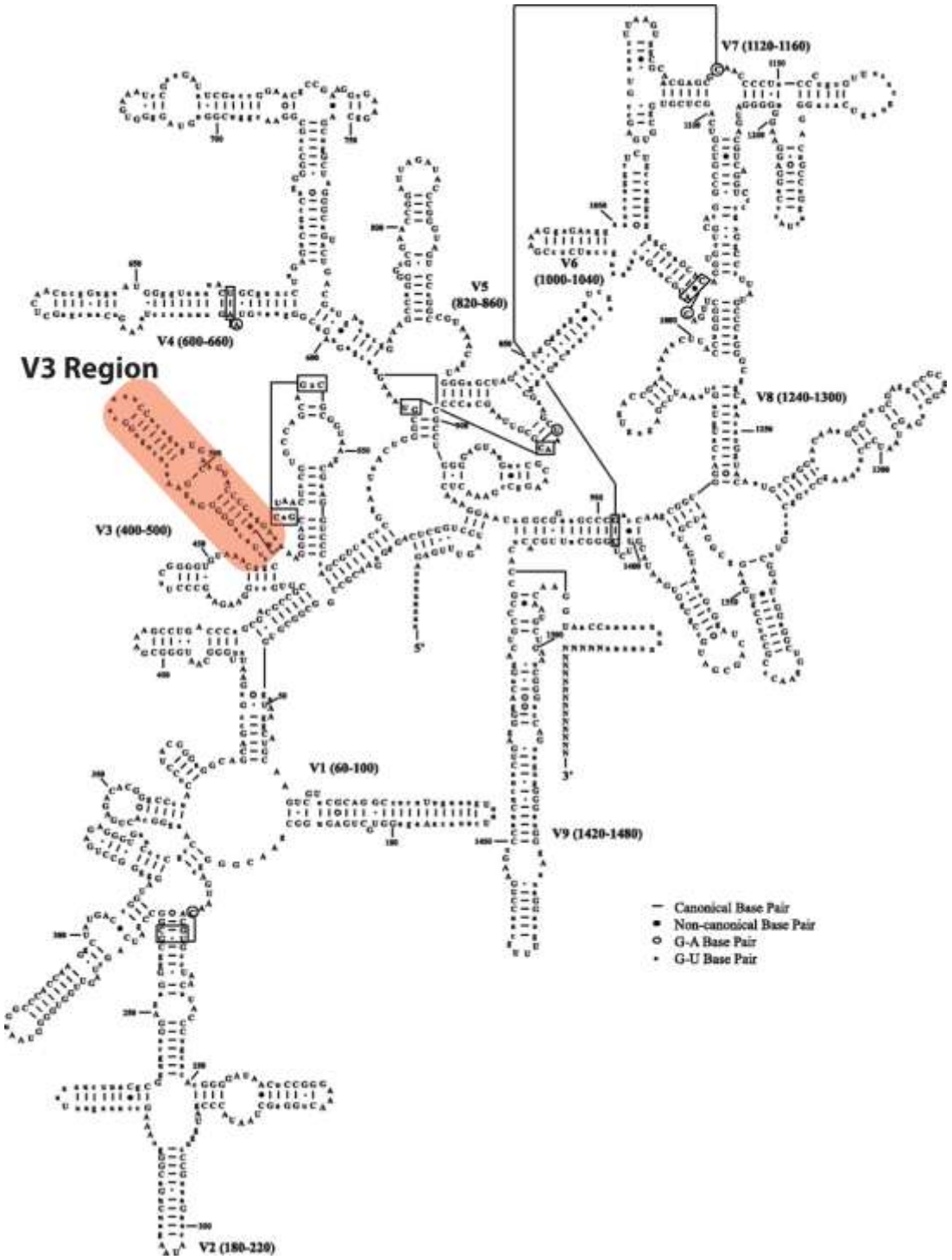

Figure 2: Example of the 16s rRNA gene of A. pyrophilus (Hall et al., 2007) the Hypervariable V3 region is shaded. The Hypervariable V3 region mutates at faster rates compared to the 16S rRNA gene but still provides taxonomic affinity, thus because the V3 region is smaller, more samples can be sequenced.

Sequence Processing and Analyses

Prior to processing, sequences were trimmed to remove the inserted "N" degenerate bases from each primer, and sequences composed of primer-dimers, an unwanted by-product of PCR, were removed from the library (Brownie et al., 1997). Sequences were appraised for quality control using the program SICKLE (https://github.com/najoshi/sickle) and those with Phred quality scores lower than 30 were excluded from further analysis (Del Fabbro et al., 2013). The published workflow developed by Kozich et al., (2013) using the mothur software package (v.1.30) was used for sequence assembly, trimming, filtering, chimera removal, OTU picking (97% similarity), OTU classification, and distance calculations. A version of this published workflow is available and illustrated on the mothur website (http://www.mothur.ork/wiki/MiSeq_SOP (accessed January 2nd, 2014).

Biofilms were sequenced from all sampling intervals of Replicate 1 (Months 2, 4, 6, 8, and 12), but we only sequenced biofilm from three sampling intervals from the second replicate (Months 2, 4, and 12). DNA extracts from Month 4 of the first mesocosm replicate required two extra PCR annealing phases, which generated PCR biases and we believe resulted in a misrepresentation of the microbial consort and was confirmed by inconsistent sequencing results. To account for this error, the second replicate of Month 4 was used in the place of the first replicate for microbial ecology analyses. Although these data came from a different mesocosm, we believe the sequencing results for this replicate are representative because the community composition was not monospecific and the community diversity was consistent with overall trends in diversity throughout the experiment, unlike the first Month 4 replicate. Also, because only two additional sampling points were sequenced for the second replicate (Months 4 &12), I chose to focus my analyses on the first replicate with a complete sequence time series.

Rarefaction analyses and principal coordinate analyses were performed using the mothur software package (www.mother.org(Schloss et al., 2009)). Rarefaction at the 97% similarity level was executed using the rarefaction.seqs command with default

parameters. Principal coordinate analyses, a method for illustrating Beta diversity, were done using the command: pcoa on a phylip-formatted distance matrix, also generated in mothur (command: dist.seqs). In addition to the principal coordinate analyses, hierarchical clustering of OTUs that had similar occurrence patterns over the experiment was performed using JMP Pro 9.0.2 (SAS institute Inc.). The hierarchal cluster function was based on a ward-distance matrix of standardized occurrences of OTUs per sampling point; with singletons OTUs removed to reduce noise in patterns of beta-diversity (Shade et al., 2013). Each OTU was given a cluster number (total of 4 clusters) based on clustering results.

All OTUs determined using the mothur software package were also classified to the phylum, family, order, genus, and species when possible using sequences incorporated in the Silva database (http://www.arb-silva.de)(Pruesse et al., 2007; Quast et al., 2012). Sequences of the most abundant OTUs were also taxonomically assigned using the Basic Local Alignment Tool (BLAST) (Altschul et al., 1990) to compare the experiment sequences to environmental and isolate sequences from hundreds of thousands of organisms curated in the National Center for Biotechnology Information (NCBI) database. Genetic potential of these OTUs was investigated by searching the genomes of related bacteria at the genus, order or family level using the Integrated Microbial Genome database (http://img.jgi.doe.gov/)(Markowitz et al., 2012; Markowitz et al., 2006).

Measures of Temporal Patterns

Temporal patterns of the bacterial community growing on the experiment bone were measured in a variety of ways including comparisons of alpha diversity, beta diversity, and a hierarchical cluster analysis at each sampling interval. Changes in alpha diversity was measured using rarefaction analyses performed using the Mothur software package (Kozich et al., 2013; Schloss et al., 2009; Wang et al., 2012). Rarefaction was calculated at the 97% sequence similarity level and was executed in Mothur using the ‘rarefaction.seqs’ command with default parameters. For illustrating changes in beta diversity across the experiment, a principle coordinates analyses was done using the

command: pcoa on a phylip-formatted distance matrix, also performed in the mothur software package (Kozich et al., 2013). In addition to the rarefaction and principal coordinate analyses, hierarchical clustering of the operational taxonomic units (OTUs) at the 97% similarity level was done using the statistics software JMP Pro 9.0.2 (SAS Institute Inc.). The hierarchal cluster function was performed using methods outlined in Shade et al., (2013) and was based on a ward-distance matrix of standardized occurrences of OTUs per sampling point. As per Shade et al., singleton OTUs were removed to reduce noise in the cluster analysis. A total of four clusters were identified and each OTU was given a cluster number based on clustering results.

RESULTS AND DISCUSSION

Mesocosm Observations

At the time of bone placement in the mesocosms, no distinctive biofilms were observed on the sediment surfaces or bones surfaces; but, within days of introducing the bone, a biofilm developed on the bone and sediment surfaces. Over the 12 month experiment, the bone and sediment biofilm waxed and waned in lateral extent, changed color, as well as changed in morphology throughout the experiment (Figure 3). Days after bone emplacement and lasting through Month 2, the mesocosm was dominated by a dark gray biofilm that covered all bone and sediment surfaces, making it difficult to distinguish individual bones. Starting at Month 2, a buoyant layer of residue and biofilm (~1mm thick) was observed floating on the surface of the tank, but this layer disappeared by Month 4. At Month 4, the dark gray biofilm covering bone and sediment surfaces was reduced in size and only covered the outer edges of bone and extended out to cover the sediment surfaces only between bones. Also, by Month 4, a white colored biofilm had developed on the distal edges of the darker biofilm near bone edges. This white-colored biofilm was always observed in association with the near-dark microbial mat suggesting it may be co-dependent on the dark gray biofilm (Figure 3E).

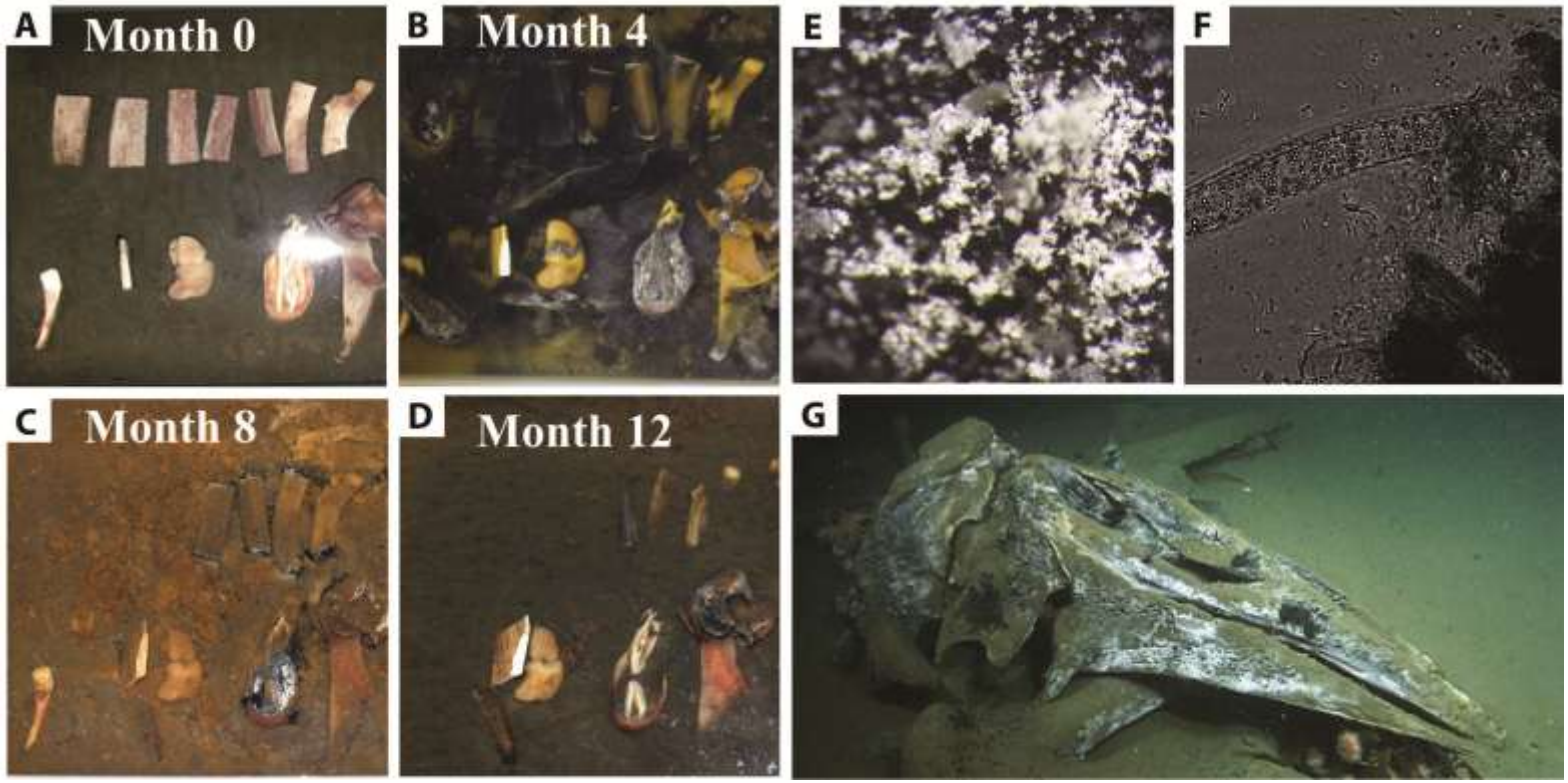

Figure 3: Examples of microbial mats on natural and simulated carcass-falls. A-D are images of the simulated carcass-fall mesocosm through the experiment A: time of emplacement, B:Month 4, C: Month 8, D: Month12. E: enlarged image of biofilm on bone surfaces from Month 4. F: micrograph of the bone-associated microbial mat, the same mat shown in B and E. Beggiatoa, a sulfide-oxidizing filamentous bacterium is prominent in association with smaller bacteria containing elemental sulfur (white specks). G: image taken by remote operation vehicle (ROV) of an experimentally implanted whale-fall observed at Like the mats grown in the carcass-fall simulations, bones from the natural whale-fall are covered in a black and white bacterial mat likely rich in sulfate-reducing bacteria and sulfide-oxidizing bacteria.

In addition to the white-biofilm growing on the distal dark gray biofilm, the central surfaces of bone were first seen to be covered by a brown, texturally ‘fluffy’ microbial mat at Month 4.

By Month 6, the dark gray biofilm was only seen near bone edges, the white-colored mat did not change in lateral coverage, and the brown mat covered nearly all the bone surfaces except for the edges. The bone biofilms at Month 8 were very similar to Month 6 except the white/dark microbial mats covered even less of the bone surface and the brown microbial mat was laterally more extensive. When the experiment ended at Month 12, very little of the white or dark gray mat remained, and the bones were primarily covered by the brown mat. In the sterile control mesocosms, no biofilms were observed on bone or sediment surfaces throughout the experiment.

Dissolved oxygen concentrations were found to change over the 12 month experiment (Figure 4). Before bones were introduced to the mesocosms, the water column was aerobic near the sediment/water air interface (~220 µM dissolved oxygen) and oxygen concentrations decreased along a shallow gradient reaching anoxic conditions near 0.5 cm into the sediment. After bone introduction, the oxygen concentrations remained aerobic, but were lower than the initial concentration in the water column, particularly at Month 4 (~75 µM dissolved oxygen). After Month 4, oxygen concentrations in the water column rose steadily (~95 µM dissolved oxygen at Month 8 and ~140 µM dissolved oxygen at Month 12). The changing oxygen concentrations indicate that the microbial communities were consuming more oxygen than could diffuse through the water columns suggesting the presence of aerobic metabolisms.

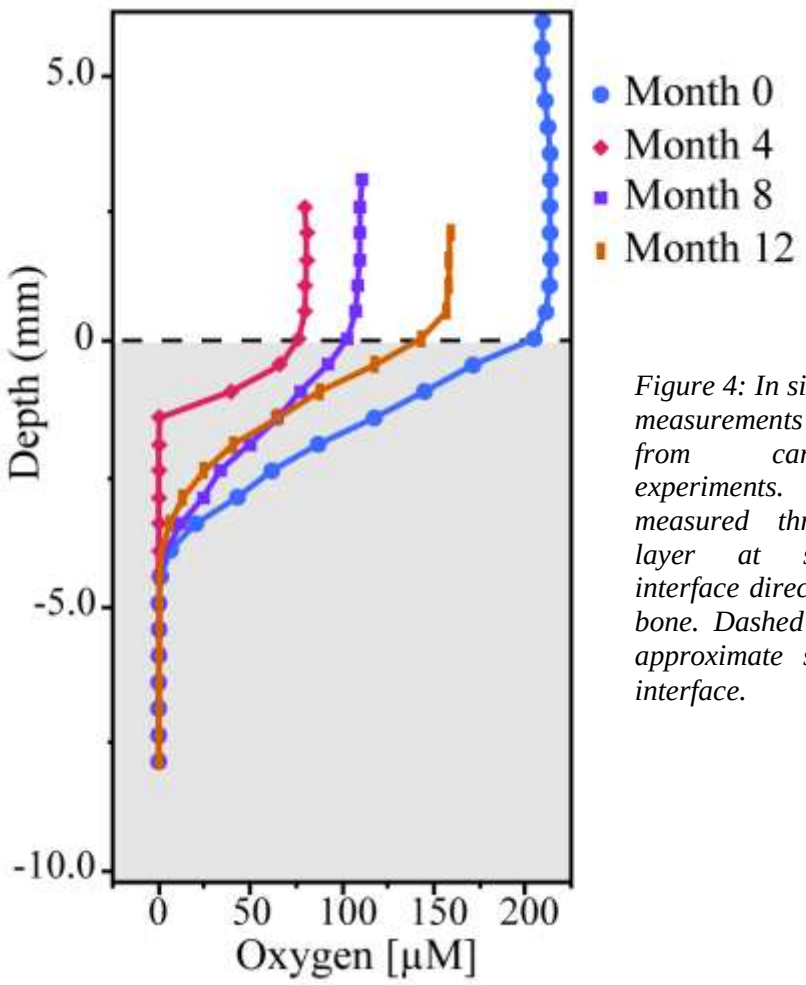

Figure 4: In situ microsensor measurements of oxygen from carcass fall experiments. Profiles were measured through biofilm layer at sediment/water interface directly adjacent to bone. Dashed line indicates approximate sediment/water interface.

Community Composition

The taxonomic affinity of bacteria sampled from the bone surfaces were identified using next-generation, high throughput sequencing of the V3 region of the 16S rRNA gene. Sequencing of surface biofilms across all five sampling intervals (Months 2, 4, 6, 8, and 12) resulted in 1,003,114 quality sequences with the average length of 182±7 base pairs. These sequences were found to represent fifteen phyla that were assigned to 10,381 operational taxonomic units (OTUs). Returned sequences that were at least 97% similar (sequence had ≤5 base pair mismatch) were considered the same OTU. OTUs at the 97% similarity level can generally be interpreted as bacterial species (Stackebrandt and Goebel, 1994), but this is not always the case.

The predominant phyla represented in the bone decay biofilms were the *Proteobacteria* (58% of the community) followed by the *Bacteroidetes* (22% of the community). Of the proteobacteria from the pooled libraries, the *Deltaproteobacteria* were most abundant (19% of total community) followed by the *Gammaproteobacteria* (17% of total community), *Alphaproteobacteria* (16%), and *Epsilonproteobacteria* (7%). Representatives belonging to *Spirochaete, Firmicutes*, *Caldithrix*, *Acidobacteria*, and *Actinobacteria* each represented 1-5% of the sequence library and the combined total of phyla that did not individually represent more than 1% of the community was 7% of the total library.

The bone decay community was not evenly distributed among the identified OTUs. Only 1% of all OTUs from the pooled time intervals had more than 1000 representatives (1000 reps = 0.1% of pooled library) indicating that 99% of the identified OTUs were not well-represented in the experiment. Furthermore, of the OTUs that had more than 1000 representatives in the pooled library, 22% of them could be assigned to six OTUs as illustrated in Figure 5. Even fewer of the common OTUs were found in high numbers throughout the experiment as most were only common at one or two sampling points. Of the OTUs that were common throughout the experiment, they most closely resembled *Phaeobacter* (97% sequence similarity) of the *Alphaproteobacteria*, *Desulfuromusa succinoxidans* (98% sequence similarity), *Desulfofrigus sp.* (100% sequence similarity) of the *Deltaproteobacteria*, and an uncultured *Sulfurimonas sp.* clone (100% sequence similarity) of the *Gammaproteobacteria*.

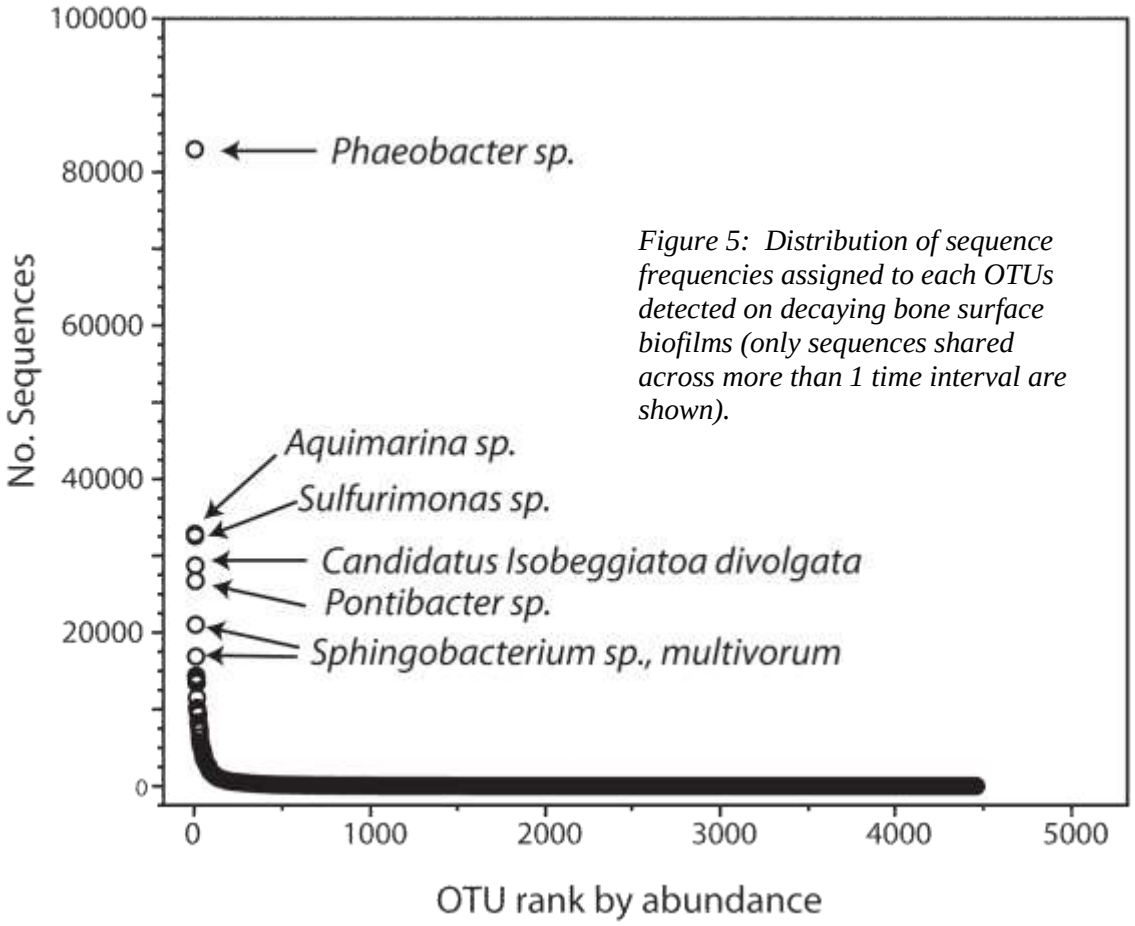

Figure 5: Distribution of sequence frequencies assigned to each OTUs detected on decaying bone surface biofilms (only sequences shared across more than 1 time interval are shown).

Proteobacteria

The *Proteobacteria* were the most dominant phylum identified from the sequence library, totaling more than 60% of the bone degrading community (n=593,045 sequences), which were classified into 4,028 OTUs (37% of community OTUs). The *Proteobacteria* are a very diverse clade and when broken down into the major subphyla, the *Alphaproteobacteria*, *Epsilonproteobacteria*, *Deltaproteobacteria*, and *Gammaproteobacteria* were identified as the most abundant groups in the bone surface community.

Deltaproteobacteria

The *Deltaproteobacteria* subphylum was the most dominant group of the *Proteobacteria* representing 32% of the *Proteobacteria* sequences and nearly 19% of the total community. Of the *Deltaproteobacteria*, nearly 93% of sequences belonged to two dominant clades including the *Desulfobacterales* (80%, n=141,475 sequences) and the *Desulfuromonales* (12%, n=23,172 sequences). Nearly 88% of the *Desulfobacterales* were assignable to phylotypes that most closely resembling the genus *Desulfobacter* (57%, n= 80,306), the genus *Desulfobulbus* (17%, n=24,926 sequences), and the candidate genus *Magnetoglobus* (13%, n= 18,797 sequences). Of the *Desulfuromonales*, 77% of the sequences were assigned to the genus *Pelobacter* (n=17,807 sequences).

Members of both the *Desulfobacterales* and *Desulfuromonales* order are strictly anaerobic sulfur reducing chemolithoheterotrophs or chemoorganotrophs. Both groups are capable of metabolizing H_2, organic acids, ethanol, as well as small molecular weight hydrocarbons (Kuever et al., 2005a; Kuever et al., 2005b; Youssef et al., 2009). Members of the *Pelobacteracea* family are exclusively fermenters, producing acetate (Kuever et al., 2005b). The primary difference between the *Desulfobacterales* and *Desulfuromonales* groups is that members of the *Desulfobacterales* commonly use sulfate (in addition to sulfite, thiosulfate, and possibly even elemental sulfur) as electron acceptors, whereas *Desulfuromonales* members use only ferric iron and elemental sulfur as electron acceptors and they are incapable of reducing sulfate, thiosulfate, and sulfite (Kuever et al., 2005a; Kuever et al., 2005b). In both sulfur reduction pathways, sulfide is the metabolic end-product.

The *Deltaproteobacteria* represented at least 10% of the bone surface community throughout the experiment, with an average representation of 18%, and a peak population at Month 8 where they comprised a maximum of 25% of the community. The abundance of *Deltaproteobacteria* in the bone surface biofilm indicates that sulfur-reduction may have played a large role in the bone degradation process because sulfur-reduction can enable the degradation of bone organics under anoxic conditions. Since the *Desulfuromonales* and *Desulfobacterales* clades can produce H_2S, which reacts to

produce metastable sulfide minerals that are black in color, they likely formed the dark gray microbial mat observed throughout most of the experiment (Figure 2) and indicate that anaerobic conditions existed at the decaying bone surface. The anoxic conditions, however, were either localized or occurred over small gradients (< 500 uM) because microsensor measurements through the biofilm at the sediment/water interface were aerobic as illustrated in Figure 4. Sulfate was the primary electron acceptor for the deltaproteobacteria community based on the predominance of the *Desulfobacterales* order (75% of *Deltaproteobacteria* sequences); however, elemental sulfur and/or ferric iron were presumably available at all time intervals to sustain the *Desulfuromonales* group.

The *Desulfuromonales* and *Desulfobacterales* were likely responsible for the terminal oxidation of bone organics. These *Deltaproteobacteria* groups are capable of degrading a variety of simple organic compounds including long-chain fatty acids, alcohols, pyruvate, polar aromatic compounds, and some hydrocarbons for a source of electrons and carbon (Kuever et al., 2005a; Kuever et al., 2005b). However, their inability to degrade more complex molecules such as lipids, carbohydrates, or collagen suggest these bacteria were dependent on the generation of simple organic compounds produced as metabolites of other bacteria, especially fermenters (Knoblauch et al., 1999; Kraft et al., 2013). The genomes of *Desulfobacter* and *Desulfobacterium* include gene sequences related to the production of collagenase (Gene ID: 638463369 from Desulfuromonas acetoxidans DSM 684 NCBI TAXON ID: 281689; Gene ID:2508601142 from Desulfobacter postgatei 2ac9 NCBI TAXON ID: 879212) suggesting it may be capable of degrading collagen, but has yet to be shown to do so.

Gammaproteobacteria

The *Gammaproteobacteria* was the second-most abundant subphylum representing 28% of the *Proteobacteria* and nearly 17% of the total community (n=166,827 sequences). The orders *Thiotrichales* (28%, n=47,364 sequences), *Vibrionales* (7.5%, n= 12,558 sequences), *Oceanospirillales* (3.4%, n= 5,592 sequences), and *Alteromonadales* (3.2%, n= 5,419) were the most predominant of the

gammaproteobacteria sequences; however, these only represent half of the gammaproteobacteria since half of the gammaproteobacteria sequences could not be assigned to a taxonomic order. From the gammaproteobacteria sequences that could be assigned, 17% of the sequences were assigned to a single OTU most closely resembling a candidate strain of *Isobeggiatoa* (100% sequence similarity n=28,753 sequences), making it the most abundant gammaproteobacteria community member, and the 4th most abundant OTU of all bacteria groups in the community. Of the unidentified gammaproteobacteria, thousands of sequences representing 14% (n=24,066) of the gammaproteobacteria were classified as two OTUs most similar (100% sequence similarity) to a thiotrophic bacterium sampled from the gill of a cold-seep thyasirid clam, *Marithyas hadalis* (Fujiwara et al., 2001).

Although members of the *Gammaproteobacteria* are morphologically, metabolically, and ecologically diverse, at least 50% of the phylotypes sequenced from the bone surface biofilms had potential to oxidize sulfur/sulfide. Studies show that candidate *Isobeggiatoa* was capable of utilizing two sulfur-oxidizing pathways: (1) the reverse sulfate reduction pathway in which sulfide is oxidized to sulfate via sulfite; and (2) the Sox multienzyme system which catalyzes the oxidization of inorganic sulfur compounds (Yamamoto and Takai, 2011). Both pathways require a set of specific enzymes and require 0_2 or NO_3^- as the terminal electron acceptor (Mußmann et al., 2007; Yamamoto and Takai, 2011). The *sox* multienzyme system for *Beggiatoacaea*, the most abundant gammaproteobacteria group in the experiment, lacks the *SoxCD* enzyme subunits and is unable to complete the full oxidation of sulfide and thiosulfate to sulfate in one metabolic pathway. As a consequence, elemental sulfur is produced and stored intracellular for energy acquisition in adverse geochemical conditions. The elemental sulfur likely contributed to the light coloration of the distal white-colored bacterial mat observed bone surfaces from Months 4-12. Under the microscope, these mats were in part composed of large vacuolated filaments that resembled members of the *Beggiatoacaea* clade (Figure 2).

In addition to members of the *Beggiatoaceae* clade, other well represented groups included the *Alteromondaceae* family (8% of gammaproteobacteria, n= 13,279 sequences) and the *Vibrionaceae* family (7.5% of gammaproteobacteria, n= 12,557 sequences). The most common OTU from the *Alteromonadaceae* family (5% of gammaproteobacteria, n=7776 sequences) had 100% sequence similarity to members of the genus *Oceanisphaera*, a heterotroph capable of utilizing organic compounds (Choi et al., 2011). Of the *Vibrionaceae*, many sequences were classified to an OTU with 99% sequence similarity to *Photobacterium*. *Photobacterium* is considered a facultive aerobe and has been shown to degrade a variety of simple and complex organics, undergo fermentation, and is able to utilize nitrate and thiosulfate as an electron acceptor (Freese et al., 2009).

The large numbers of sulfide-oxidizing gammaproteobacteria in the bone degradation experiment indicate that thiotrophy is also a major constituent of the bone degrading microbial mat, and their presence implies favorable oxygen and sulfide gradients in the experiment mesocosms. Direct degradation of bone by the thiotrophic gammaproteobacteria may be minimal since at least 30% of the gammaproteobacteria were lithotrophic; the enrichment in these gammaproteobacteria may simply be the result of favorable conditions afforded by the sulfide generated by the anaerobic sulfate-reducing bacteria utilizing bone organics. Furthermore, sulfide-oxidizers in the white-colored microbial mat would have had very little interaction with the bone surface since the white-mat was not directly adjacent to bone (Figure 2) but was instead located on distal ends of the dark gray biofilm. Some gammaproteobacteria may have interacted with bone however; because nearly 21% of the experiment gammaproteobacteria, including the *Thiotrichales*, had genetic potential for collagenase production that may allow for bone degradation.

Members of the *Vibrionaceae* and *Alteromonaceae* clades represented over 25% of the gammaproteobacteria sequences. Since these groups are heterotrophic they may have played a role in the initial degrading bone organics in the biofilm community, including collagen.

Alphaproteobacteria

The *Alphaproteobacteria* was the third most abundant subphylum comprising 27% of the *Proteobacteria* community (n=158,081 sequences), representing 16% of the entire experiment bacterial community. The *Alphaproteobacteria* includes the most abundant of marine cellular organisms and harbor a wide variety of metabolic strategies, environmental niches, and physiologies including a high capacity for protease activity that allows for the degradation of diverse proteins (Bong et al., 2013; Giovannoni et al., 2005; Williams et al., 2007). The majority of *Alphaproteobacteria* sequences from the experiment were classified to the *Rhodobocterales* order (63%, n= 99,558 sequences) of which most belonged to the *Roseobacter* clade (92%). Members of the *Sneathiellales* order were also well represented in the *Alphaproteobacteria* community (14%, n=21,584).

Members of the *Roseobacter* clade are capable of lithotrophic transformation of organic sulfur compounds (dimethyl sulfide, methanethiol, menthanesulfonate, dimethyl sulfoxide) and/ or inorganic sulfur compounds (elemental sulfur, sulfide, sulfite, thiosulfate) to an oxidized or intermediate form that contribute to sulfur cycling (Buchan et al., 2005; González et al., 1999; Moran et al., 2003). Of the *Roseobacter* sequences, 83% (63% of all *Alphaproteobacteria*) were assigned to a single OTU most closely resembling members of the *Phaeobacter* genus, making it the most well-represented OTU in the entire bone surface community (n=82,965)(Figure 5). Genomic analyses on *Phaeobacter inhibins* reveals the presence of genes for the sulfur-oxidizing enzyme subunits *SoxCD* suggesting that Phaeobacter-related OTUs in this dataset have the potential to oxidize reduced sulfur compounds for chemolithotrophic growth. Members of the *Phaeobacter* genus are also recognized as effective colonizers of both biotic and abiotic surfaces in marine settings and are capable of suppressing other bacterial growth by the production of the antagonistic antibiotic, tropodithietic acid (Thole et al., 2012).

The *Alphaproteobacteria* have the metabolic potential to play many roles in the bone surface community including those of surface colonizers, degraders of complex organic molecules (including collagen), and oxidation of reduced sulfur compounds.

Oxidation of hydrogen sulfide produces sulfuric acid (Yamamoto and Takai, 2011), and acid production at the bone surface has the potential to cause etching or bone dissolution. It has been suggested that collagen, the primary bone organic constituent, must first be released from its bond with bone mineral hydroxyapatite in order to be biodegradable; and, bone demineralization is thought to primarily occur by localized drops in pH through the production of acidic microbial end-products (Child, 1995a, b). Within the experimental tanks, it is possible that sulfide-oxidizing alphaproteobacteria may have generated acid that could have dissolved the apatite mineral component of the bone, making collagen molecules more accessible to enzymatic degradation.

The early timing of the prevalence of *Alphaproteobacteria* within the biofilm (35% of biofilm community in Month 2 that decreased to 5% in Month 12) suggests that their influence was most substantial during the early stages of bone degradation. The potential antagonistic relationship of the *Roseobacter* clade may also explain the high numbers of *Phaeobacter*-related OTUs in the biofilm early in the experiment. Due to their high capacity for protease production, members of the *Roseobacter* clade may also have acted as primary degraders of bone organics. Genes encoding for collagenase were also found in the genomes of *Phaeobacter* representatives indicating that *Phaeobacter* bacteria in the experiment may have been capable of degrading bone collagen. In addition to the ability to degrade complex organics, certain member of the *Roseobacter clade* may have had a competitive edge in the early community due to their ability to oxidize sulfide as an electron source.

Epsilonproteobacteria

The subphylum *Epsilonproteobacteria* was also well represented in the bone degradation community composing 6.85% of the entire bacterial community and 12% of the *Proteobacteria sequences* (n= 68,757 sequences). Over 98% of the *Epsilonproteobacteria* in the bone degradation community were classified as either a member of the *Sulfuricurvales* order (58%) or a member of the *Campylobacterales* order (40%). Like the *Gammaproteobacteria*, the *Epsilonproteobacteria* are metabolically and

ecologically diverse including members capable of heterotrophy and chemolithotrophy, including sulfur-oxidization (Inagaki et al., 2003; Kodama and Watanabe, 2004). The most predominant epsilonproteobacteria metabolism in the experiment was likely chemolithotrophy, which is common in members of both the *Sulfuricurvales* and *Campylobacterales* order.

Almost 50% of the *Epsilonproteobacteria* community sampled from the bone biofilm (n=32,581 sequences) were classified as a single OTU most closely resembling bacteria from the *Sulfurimonas* genus, particularly *Sulfurimonas gotlandica* (100% sequence similarity). Genome analysis of *Sulfurimonas gotlandica*, a sulfide oxidizing chemolithoautotroph, indicates that this particular species exceeds other *Epsilonproteobacteria* in metabolic versatility, which enables it to thrive successfully in oxygen depleted environments (Grote et al., 2012). Since bone surfaces were likely anoxic sulfur-rich environments based on the abundance of *Deltaproteobacteria* in the bone biofilm, the ability of the *Sulfurimonas* group to oxidize sulfide and to cope with anoxia may explain its proliferation in the bone decay community. Sequencing analyses also indicate that members from the *Sulfuricurvum* genus of the *Campylobacterterales* order were also abundant in the bone biofilm (18% of *Epsilonproteobacteria* community). Like *Sulfurimonas*, the *Sulfuricurvum* group is chemolithotrophic and capable of oxidizing sulfide, elemental sulfur, thiosulfate, and H_2. Both members of the *Sulfurimonas* and *Sulfuricurvum* generea are documented from environments like hydrothermal vent fields, crude-oil spills, and as endosymbionts suggesting members of these groups are selected for in environments with steep redox gradients such as those found in carcass-falls (Inagaki et al., 2003; Kodama and Watanabe, 2004). 51% of the *Campylobacterales* (23% of the *Epsilonproteobacteria*) were not classifiable to the genus level.

Like the *Gammaproteobacteria*, the primary metabolism of *Epsilonproteobacteria* in the bone biofilm community was likely sulfide oxidation under anoxic conditions. If the *Sulfurimonas*- and *Sulfuricurvum*-like OTUs were strict autotrophs, as some representatives of this clade are known to be, they would likely have

had very little interaction with the bone organics. However, genes potentially encoding for collagenase (gene ID: 2531204094 from genome of Sulfurimonas sp. GD1 NCBI taxon ID: 929558; gene ID: 648192621, from genome of Sulfurimonas autotrophica OK10, DSM 16294 NCBI ID:563040; term object ID: 4008 from genome of Sulfurovum sp. NBC37-1 NCBI ID: 387093) were also identified from members of both the *Sulfurimonas* and *Sulfuricurvum* clades, suggesting that the sulfur-oxidizing *Epsilonproteobacteria* from the experiment may have extracted some necessary nutrients directly or indirectly from the bones.

Bacteroidetes

The *Bacteroidetes* was the second-most abundant phylum composing 22% (n= 224,624 sequences) of the bone surface bacterial community. The *Bacteroidetes* phylum is recognized as being abundant in marine habitats, including natural whale-falls (Goffredi and Orphan, 2010; Tringe et al., 2005), and are involved in the extracellular degradation of macromolecular organic matter into smaller subunits which can then be taken up intracellularly (Bauer et al., 2006). The majority of the bacteroidetes community members were distributed among the *Flavobacterales* (43% of bacteroidetes), the *Sphingobacteriales* (17% of bacteroidetes), and the *Cytophagales* (12% of bacteroidetes). Members of the *Flavobacterales*, *Sphingobacteriales*, and *Cytophagales* are typically found in nutrient rich environments including activated sludge of waste-water treatment plants, human abscesses, and even as endosymbionts of biota endemic to natural whale-falls (Haiyan et al., 2007; Marinellama, 1995; Ranieri and Boor, 2009; Verna et al., 2010). These bacterial clades are commonly associated with the aerobic degradation of high molecular weight compounds including biopolymers such as proteins and polysaccharide chitins (Bauer et al., 2006; Kirchman, 2002). Few of the *Bacteroidetes* sequences generated in this experiment could be classified at the family or genus level, suggesting that the bacteroidetes bone-associated bioflm community is novel and yet to be characterized.

The bacteroidetes in the bone surface biofilm may have been involved in the degradation of bone-derived organics since the dominant *Bacteroidetes* clades from the

experiment were most likely capable of degrading complex proteins. Little genetic potential for the production of collagenase was found in the genome of *Sphingobacterium and Cytophaga* (86% sequence similarity to experiment OTUs), which suggests the *Bacteroidetes* may not have degraded the collagen fraction of bone; although, without knowing the physiology of more closely related phylotypes, we cannot rule out the ability of *Bacteroidetes* members in the degradation of collagen. Further interpretations of the bacteroidetes role in the bone surface biofilm would be purely speculative because at least half (≥ 48%) of the *Bacteroidetes* sequences from the experiment were not classified past the order level, including the most abundant OTUs.

Other Phyla

Although less abundant, representatives belonging to the *Spirochaete* phylum were also constituents of the bone biofilm community (5% of community, n=51,847 sequences). Members of the *Spirochaete* phylum, predominantly from the *Leptospirales* order, are free-living and inhabit soil, freshwater, saltwater, as well as being symbionts for a variety of hosts (Ananyina, 2010). The *Leptospira* genus in particular is recognized as an extremely pathogenic group to animals and humans, capable of virulence, cell surface adhesion, as well as synthesizing numerous enzymes capable of destroying cell wall components and degrading long-chain fatty acids (Evangelista and Coburn, 2010; Ko et al., 2009). The *Spirochaete* community was likely capable of collagen degradation since the genomes of the most similar spirochaete isolate to those in the experiment, belonging to *Leptospira borgpetersenii* (86% sequence similarity), encoded for genes related to the synthesis of microbial collagenase.

The *Firmicutes* phylum represented nearly 3% of the bone biofilm community (n= 29,707 sequences) of which 80% of the sequences were classified to the *Clostridia* order. The *Clostridia* are generally considered to be chemoorganotrophs, but some *Clostridia* species are chemolithotrophic as well. Members of the *Clostridia* may metabolize, often through fermentation, a variety of organic compounds including carbohydrates, alcohols, amino acids, purines, and steroids (Ludwig et al., 2009). Most species of the *Clostridia* are obligate anaerobes, although some species are

microaerophillic. Members of the *Clostridia* are not known to carry out dissimilatory sulfate reduction (Ludwig et al., 2009). Like the *Bacteroidetes*, the *Clostridia* members of the bone biofilm community were likely capable of the degradation of complex bone organics, and since the *Clostridia* are commonly capable of fermentation, they may have produced secondary organic metabolites like acetate and pyruvate as end-products that other community members such as the *Deltaproteobacteria* would have been dependent upon.

Temporal Changes

Community Composition

Several temporal trends that were not previously known to be associated with bone-associated biofilms were observed throughout the experiment. Sequencing results indicated that the biofilms covering bones surfaces were not static and that the bacterial community varied in composition and diversity over the course of the 12-month experiment. Figure 6 illustrates the changes in the bone surface biofilm community at the phylum level throughout the experiment. Large scale trends in composition include the steady decline of alphaproteobacteria throughout the experiment from 35% of the community sequences in Month 2 to 5% of the community sequences by Month 12. Representatives of the deltaproteobacteria display an inverse relationship to the alphaproteobacteria and generally increase over the experiment with their peak abundance in Month 8. The gammaproteobacteria and epsilonproteobacteria were most abundant mid-experiment during Month 6.

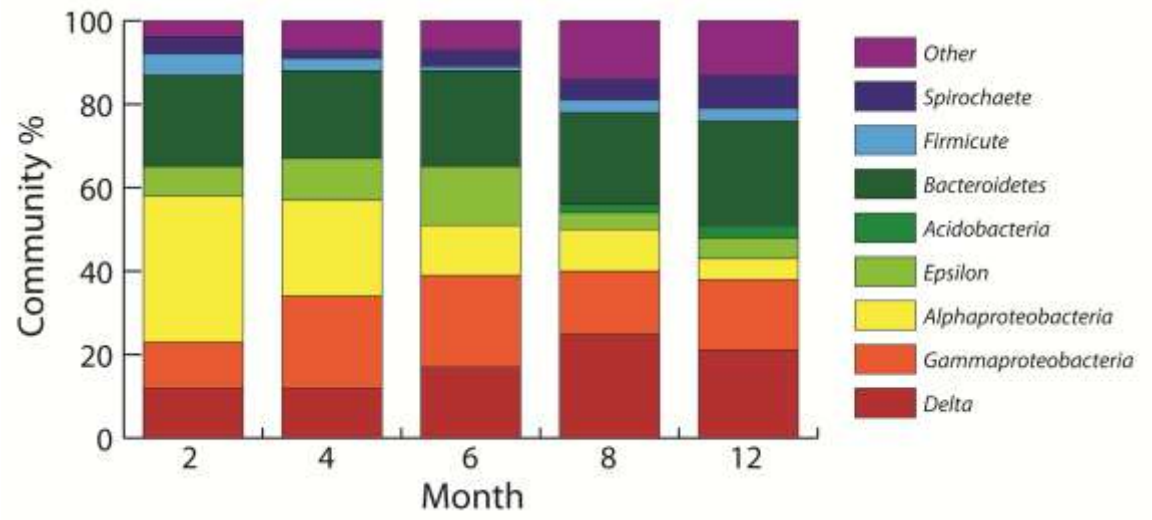

Figure 6: Sequence representation of bone-associated biofilm microbial community changed throughout the experiment. Shown here are the stacked percentages of the major phylums and sub-phylums at each sampling interval in the experiment. Major trends include decrease in Alphaproteobacteria over time, peak in members of the Gammaproteobacteria and Epsilonproteobacteria mid-experiment, and a steady increase in Bacteroidetes, Deltaproteobacteria, and other less abundant groups over time.

Alpha and Beta Diversity

Alpha diversity, calculated as the number of observed species level OTUs (defined at the 97% similarity level) per time interval, also changed throughout the experiment. Initially, species richness ranged from 2,000 OTUs early in the experiment to over 6,000 OTUs by the end of the experiment (out of 10,831 total OTUs). Rarefaction analyses, a different metric of alpha diversity that is based on species richness for a given number of samples, indicated that Months 2, 4, and 6 had relatively low species richness and the community was well represented due to the near plateau of the curve after 100,000 sequences were sampled (Figure 7). But after Month 6, the biofilms on decaying bone surfaces were found to have much higher species richness for the same number of sequences sampled. The later communities are also not fully resolved after sampling 100,000 sequences as indicated by the still-sloped curve for Months 8 &12.

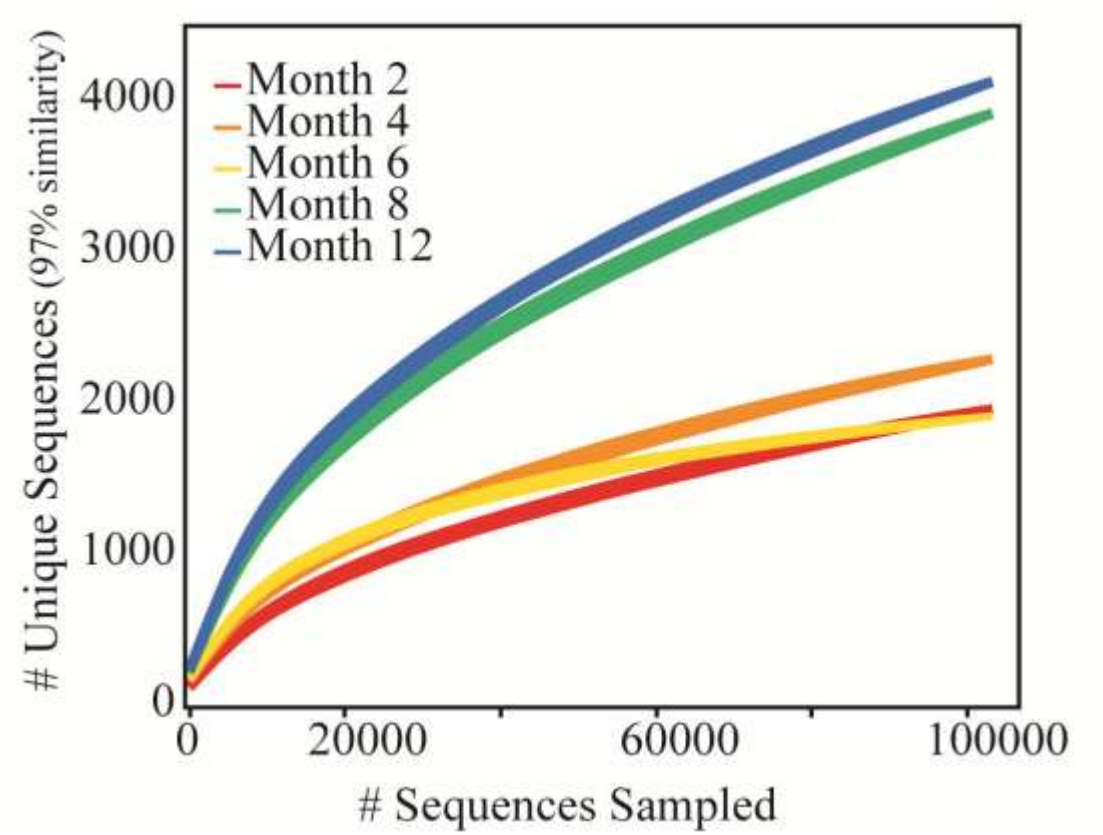

Figure 7: Rarefaction curves from the V3 region of the 16S rRNA libraries constructed at each time point and sampling up to 100,000 sequences per sample. Samples from Months 2, 4, and 6 show less diversity (fewer unique sequences) compared with Months 8 and 12.

Beta diversity, which measures differences in community composition between samples, was visualized using principal coordinate analysis based on a distance matrix generated from all samples in the mothur software package (Schloss et al., 2009). The resulting principal coordinate plot is shown in Figure 8, and illustrates that like the rarefaction analyses, Months 2 & 4 plot closer together suggesting similar community composition and species richness; whereas Month 6 plots closer to Months 8 & 12 suggesting Month 6 had lower species richness (Figure 7) but is compositionally more similar to bacterial communities from Month 8 &12. Months 8 & 12 have relatively similar species richness and composition compared to the other time intervals.

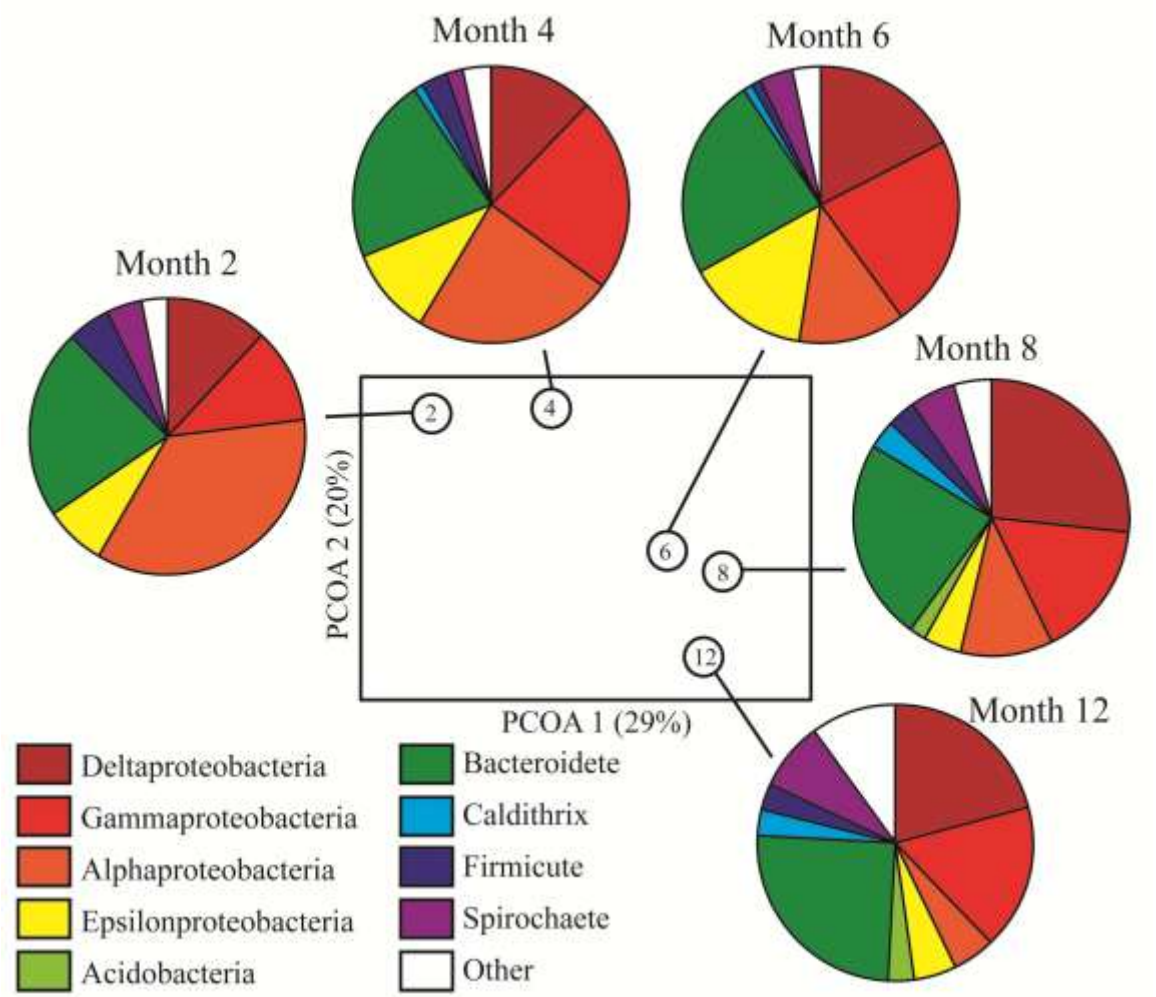

Figure 8: Principal coordinate plot of distances between samples. The results presented here illustrate the phylogenetic clustering of the bacterial communities by sampling time. Numbers in plot indicate month biofilm was sampled. Pie charts show the relative abundance of the dominant bacterial phyla at each sampling time.

Succession of Bone Degradation Biofilm

Observed temporal patterns in the relative abundance of various bacterial phyla, OTUs, and diversity over the course of the experiment were indicative of a bacterial successional series associated with the progressive decay of bone in marine environments. To test for a successional time series, a hierarchical cluster analysis was performed on the occurrence patterns of OTUs throughout the experiment following an analysis described by Shade et al (2013). The hierarchal cluster analysis was based on a distance matrix of standardized occurrences of OTUs per sampling point; with singleton

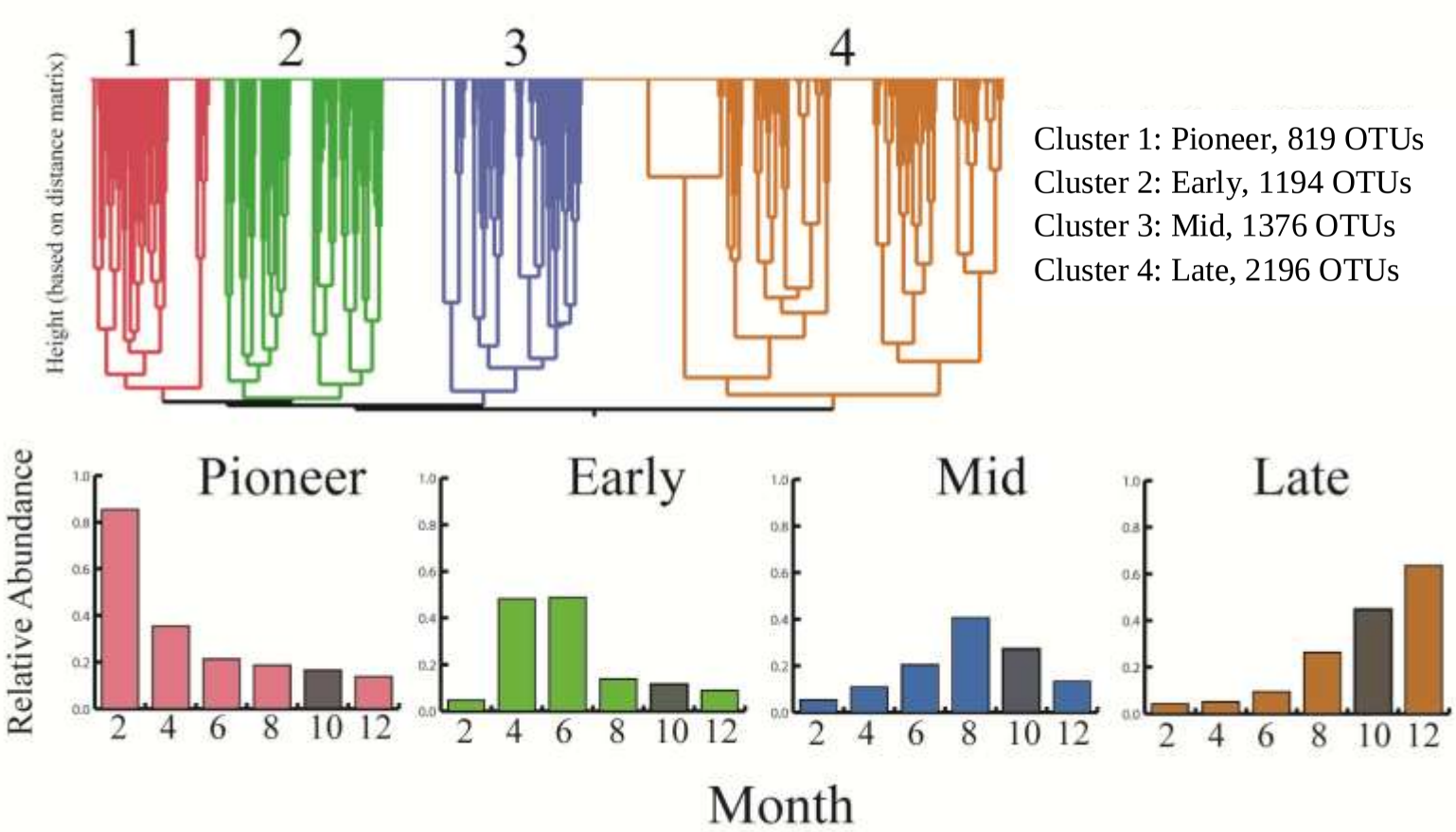

Figure 9: Bacterial Succession groups of biofilm growing on bone in lab-simulated marine environments. (a) Hierarchical clustering (Ward linkage-based distance matrix among OUT's defined at 97% sequence identity) to determine OUT's having coherent dynamics. The analysis was conducted on 6,306 OTUs (singletons removed) each represented by a branch tip of the dendrogram. The y axis represents within-cluster distances. (b) Successional group dynamics indicating the relative abundance of members belonging to each group over the course of the simulated carcass-fall experiment. Shaded bars are interpolated values because biofilms were not sampled at the Month 10 interval. Interpolations calculated by simple average of before and after time points.

OTUs removed to reduce noise in patterns of beta-diversity (Shade et al., 2013). Results

of the hierarchical cluster analysis distinguished four aggregated clusters, each composed of OTUs that have similar temporal patterns throughout the experiment (Figure 9A). Each cluster of OTUs is interpreted as a distinct microbial successions associated with the progressive decay of bone surfaces in response to changes in environmental gradients and nutrient supply. These clusters are thus interpreted to represent a (i) Pioneer Succession, (ii) an Early Succession, (iii) a Mid Succession, (iv) and a Late Succession (Figure 9B). The environmental conditions, taxonomic composition, and role in the bone decay process are discussed for each microbial succession.

Pioneer Succession

The pioneer succession stage was composed of OTUs (n=819) that were most abundant during the first sampling interval at Month 2 and are thought to represent the initial microbial consortia associated with bone decay in marine environments. The initial placement of the bone within the mesocosms stimulated a laterally extensive dark gray-colored biofilm that covered all bone and sediments surfaces in the mesocosm observed at Month 2. Although no oxygen concentrations were measured at this sampling interval (calibration error), oxygen profiles from a similar experiment and time frame by Vietti et al., ((submitted)) suggests that oxygen concentrations at the sediment water interface during Month 2 were likely dysoxic to anoxic (0_2 - 30 µM) as a result of the extensive microbial activity. The pioneer successional community was composed primarily of *Alphaproteobacteria* (27%), *Bacteroidetes* (20%), and *Deltaproteobacteria* (18%) and manifested macroscopically as a near-dark biofilm on the bone surfaces

The phylogenetic composition of the pioneer succession suggests a syntrophic bacterial community formed on the bone surfaces within two months. A schematic of hypothesized trophic interactions is presented in Figure 10. At the base of the nutrient web were aerobic and anaerobic heterotrophic bacteria most closely resembling *Sphingobacteriales* and *Flavobacterales* orders from the *Bacteroidetes*, as well as *Vibrionales* and *Arlteromondales* of the *Gammaproteobacteria*. Since members of these heterotrophic groups are commonly capable of degrading complex organic molecules and

closely related taxa possess putative collagenase genes, representatives of these may have been involved in the initial degradation of complex bone organics including collagen.

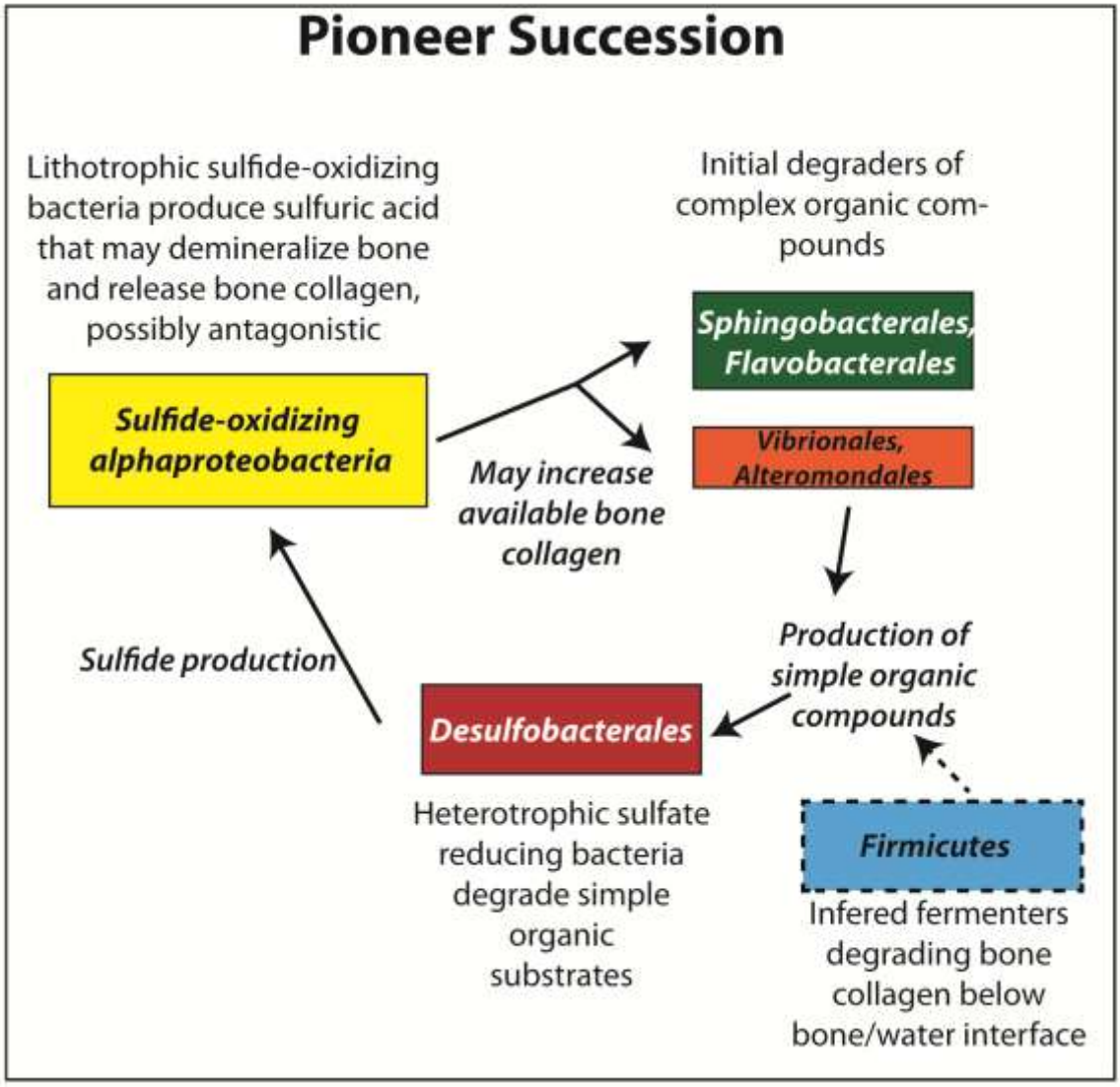

Figure 10: Hypothetical flow chart of dependency on end-products and metabolites of the Pioneer Succession. The height of each box is relative to the group's abundance in the community.

The *Flavobacterales*, *Sphingobacteriales*, *Vibrionales*, and *Alteromondales* most likely degraded macromolecular organic matter into smaller, less complex subunits of organic compounds which could then be used as growth substrates by sulfate-reducing *deltaproteobacteria* (Bauer et al., 2006; Knoblauch et al., 1999; Kraft et al.,

2013)(Knoblauch et al., 1999; Kraft et al., 2013). The sulfide generated by the sulfate-reducing deltaproteobacteria was then utilized as an electron donor for the chemolithotrophic *Phaeobacter*-like bacteria that may have produced bone demineralizing acid via sulfide oxidation.

Early Succession

The Early Succession is characterized by the group of OTUs (n=1194) with peak abundances during Months 4 & 6 (Figure 9). At this time interval, oxygen concentrations in the bone-associated biofilm returned to oxic conditions (Figure 4), but were lower compared to initial oxygen concentrations. At Month 4, a white–colored biofilm developed in association with the dark gray colored biofilm adjacent to the edges of bone surfaces (Figure 3 E) and the brown-colored biofilm replaced the dark grey biofilm in the central portion of bone surfaces.

Sequencing results of the Early Succession microbial community show a marked taxonomic turnover. Although lithotrophic sulfide-oxidizing bacteria were still the most abundant type of bacteria in the Early Succession, the taxonomic affinity changed from *Phaeobacter*-like representatives of the *Alphaproteobacteria* subphylum to predominantly members of the *Sulfurimonas* genus within the *Epsilonproteobacteria* (17% of succession, n= 32,824 sequences), as well as thiotrophic members of the *Gammaproteobacteria* (20% of succession= 37,167 sequences). The percentage of the *Bacteroidetes* and *Deltaproteobacteria* community representatives dropped from 47% in the Pioneer Succession to 27% in the Early Succession community indicating a marked decrease in primarily heterotrophic bacteria in the Early Succession.

The predominance of lithotrophic sulfide oxidizing bacteria and the decrease in heterotrophic bacteria in the Early Succession suggests that the nutrient and energy cycling community was unbalanced and/or not constrained to the bone surface in the Early Succession community, likely due to changes in oxygen concentrations. Oxygen concentrations in the bone biofilm must have been low because the sulfide-oxidizers identified in the biofilm during Months 4 and 6 most closely resembled *Sulfurimonas*

gotlandica (17% of the Succession community) , and relatives of thiotrophic endosymbionts which are recognized to specialize in sulfide-oxidation under anaerobic conditions.

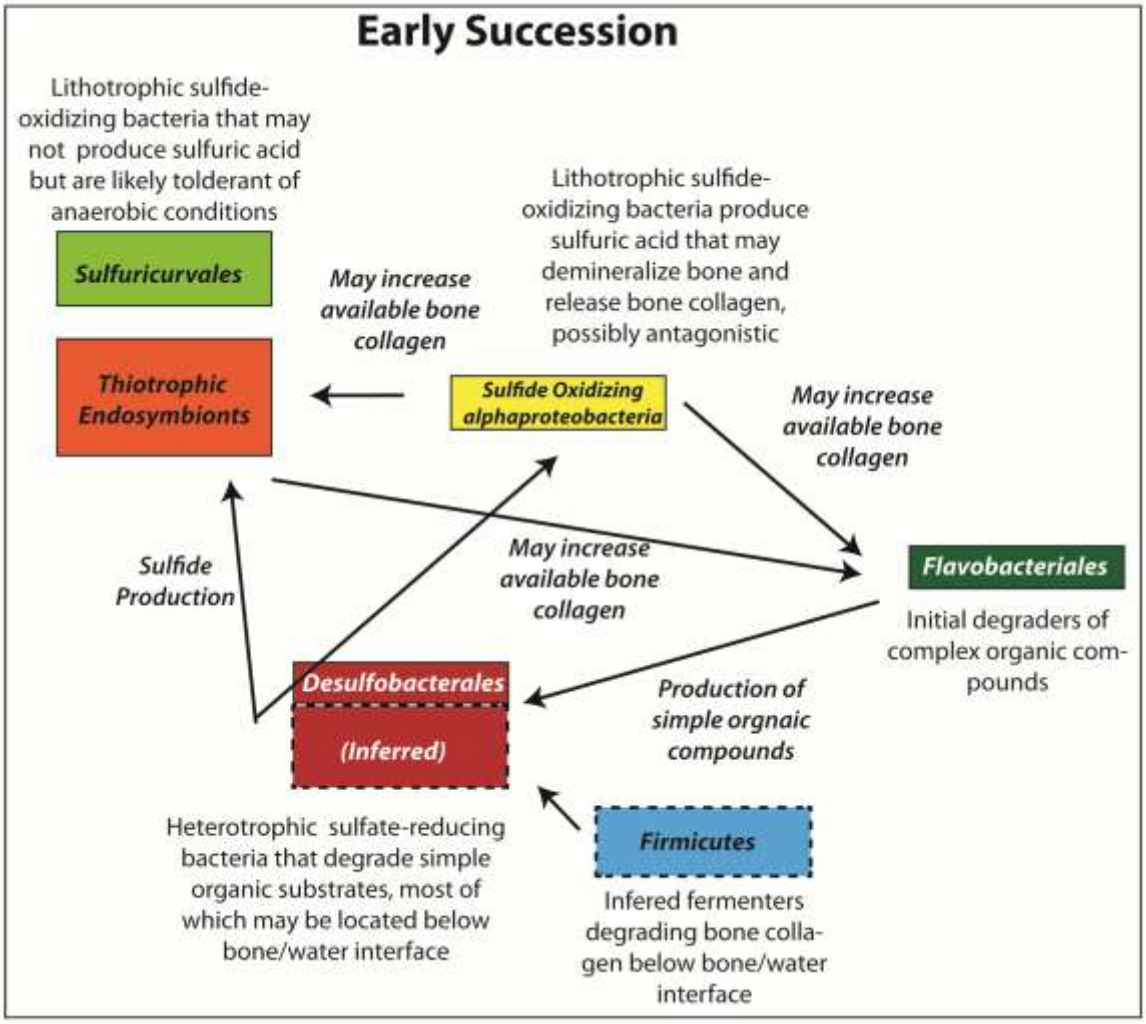

Figure 11: Hypothetical flow chart of dependency on end-products and metabolites of the Early Succession. The height of each box is relative to the group's abundance in the community. Dashed box boundaries indicate inferred bacterial groups that may have been located adjacent to the bone surface.

However, depending on the oxygen conditions, these sulfide-oxidizers may have produced sulfuric acid in aerobic environment, but where not likely capable of producing sulfuric acid in anaerobic conditions. Potentially less labile organic matter resulted in fewer *heterotrophs* to degrade the complex organics which and consequently resulted in

fewer sulfate-reducing bacteria that are dependent on metabolites of the complex degraders. Since *Deltaproteobacteria* were not well represented during this interval, the source of the sulfide may not have been localized within the biofilm. Sulfate-reducing deltaproteobacteria may have been more abundant in the bone interior biofilm or in the surrounding sediment during this interval and sulfide would diffuse out of the bone or sediments to fuel sulfide-oxidation in the biofilm. Sequencing the bacteria from the bone interior would be needed to support this hypothesis.

Mid Succession

The mid succession bacterial community is assigned to the group of OTUs (n=1376) that were most abundant on bone surfaces at Month 8 of the decay experiment (Figure 9). At this time, the dark-colored biofilm and associated white biofilm was reduced to only the edges of bone, and the majority of bone surfaces were covered by the brown colored biofilm (Figure 3). Also at this time, oxygen concentrations had risen to ~ 100 µM in the water column and at the sediment/water interface, an increase of nearly 50 µM from four months prior (Figure 4).

The bacterial community of the Mid Successional Stage changed drastically from a lithotrophic sulfide-oxidizing community in the previous succession, to primarily a heterotrophic community. Sequencing results show that over 75% of the succession was composed of heterotrophs from the *Bacteroidetes* (33%), and *Deltaproteobacteria* (30%), *Alphaproteobacteria* (13%), and *Caldithrix* (6%) groups. Of the sequences classified as bacteroidetes, 51% were assigned to an unidentified *Cytophaga* OTU related to *Krokinobacter sp*. and *Dokdonia sp*. (89%) from the *Flavobacterales.* Of the sequences classified as deltaprotoebacteria, 54% were assignable to three OTUs most closely related to the genus *Desulfobacter* (98% sequence similarity), the genus *Desulfobacula* (95% sequence similarity), and the genus *Desulfobacterium* (96% sequence similarity). The *Alphaproteobacteria* community at the Mid Succession was composed primarily of an OTU (57%) most closely resembling *Sneathiella* genus (100% similarity).

The Mid Successional community appears to be composed primarily of heterotrophic bacteria. A schematic showing hypothetical trophic relationships associated with this succession is provided in Figure 11. Members like the *Flavobacterales* and *Snethiella* capable of degrading high weight molecular compounds (Bauer et al., 2006; Jordan et al., 2007; Kirchman, 2002) were present, as were heterotrophs, such as certain d*eltaproteobacteria*, that were only capable of degrading simple organic compounds (Youssef et al., 2009).

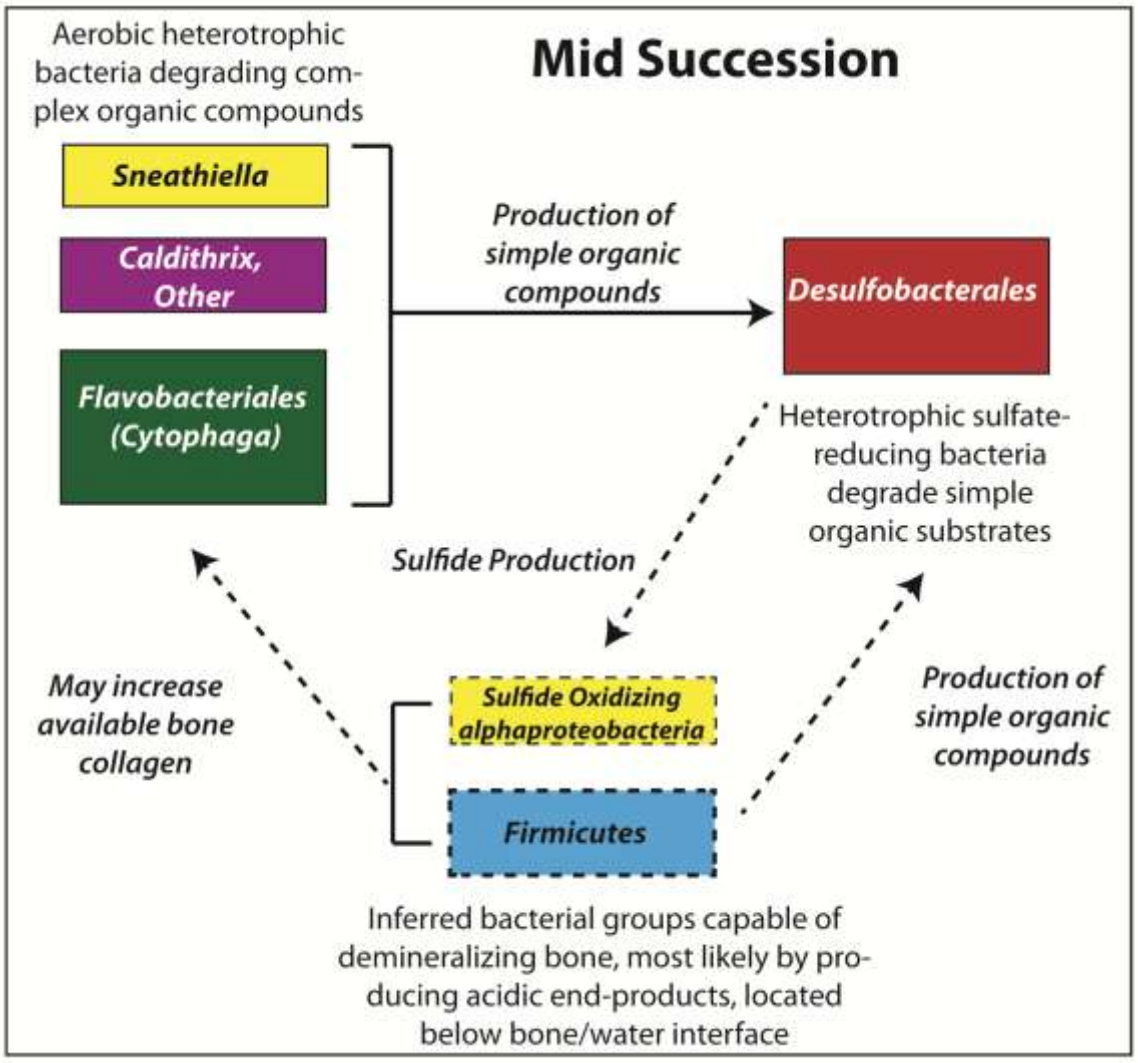

Figure 12: Hypothetical flow chart of dependency on end-products and metabolites of the Mid Succession. The height of each box is relative to the group's abundance in the community. Dashed box boundaries indicate inferred bacterial groups that were likely located adjacent to bone surface.

Heterotrophy in the Mid- Succession community was also likely carried out by aerobes such as the *Flavobacterales* as well as anaerobes such as members of the *Deltaproteobacteria* and *Sneathiella* genus (Jordan et al., 2007). It is reasonable to hypothesize that representatives of the *Bacteroidetes* and *Sneithiella* genus provided simple organics molecules as waste metabolites to the *Deltaproteobacteria*. However, of the cytophaga isolate genomes queried, only a few have genetic potential for collagenase production (n= 7 out of 56 queried genomes), suggesting that the *Bacteroidetes* group was likely not directly involved in the degradation of collagen during the Mid Succession. Certain members of the *Deltaproteobacteria* do have genetic potential for collagen degradation.

Although there was an abundance of heterotrophs in the Mid Succession, there were few bacteria types that could have produced acid end-products to demineralize the bone and make the bone collagen accessible. The lack in acid-producers suggests a number of possibilities: (1) the collagen degrading bacteria were able to access the collagen without additional demineralization, (2) there was a surplus in available collagen from previous succession, (3) bone collagen was abiotically being dissociated from the bone mineral by hydrolysis, and/or (4) the heterotrophic bacteria were not utilizing bone collagen.

.

Late Succession

The Late Successional stage is characterized by a group of OTUs (n=2196) that was most abundant during Month 12, the last sampling interval of the experiment (Figure 9). At this time, the experiment bone was almost completely buried in the sediment due to sediment and water agitation during repeated sampling over the course of the 12 month experiment, but a small sliver of dark gray biofilm could still be seen on the cut edges of bone samples (Figure 3). All other unburied bone surfaces were covered by a brown-colored biofilm. At Month 12, oxygen concentrations had risen again by 50 µM over the course of 4 months and reached concentrations around ~ 150 µM in the water column and

at the sediment/water interface when sampled marking it as the highest recorded oxygen concentration since bones were added, but not quite as high as the initial oxygen concentrations at ~200 µM (Figure 4). Sequencing results suggest that the microbial mat on the edge of bone surfaces at Month 12 was composed primarily of *Bacteroidetes* (25%), *Gammaproteobacteria* (20%), *Deltaproteobacteria* (17%), as well as members of the *Spirochaete* phylum (10%).

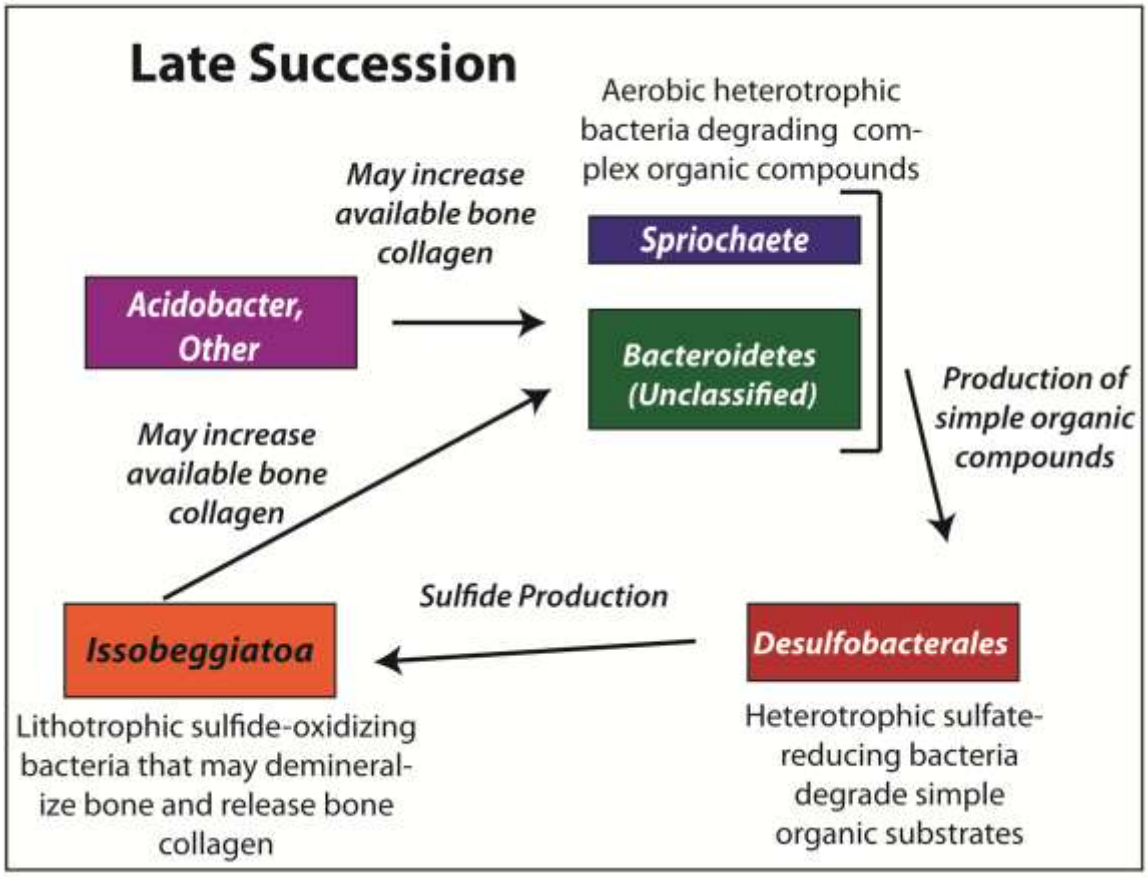

Figure 13: Hypothetical flow chart of dependency on end-products and metabolites of the Late Succession. The height of each box is relative to the group's abundance in the community.

The relative proportion of the bacterial clades in the Late Succession indicates that the community was well balanced with nearly equal representation of the major bacteria groups and most metabolic types were expressed (Figure 13). As in the previous succession, representatives of the *Bacteroidetes* phylum, predominantly members of the *Sphingobacteria* class (69% *Bacteroidetes* sequences), likely fueled a diverse web of

nutrient and energy cycling by aerobically degrading complex molecules into simpler organic molecules. However, since members of, the *Sphingobacteria,* the predominant Bacteroidetes group in the Late Succession, have little potential for collagen degradation due to the paucity of genes associated with collagenase in the genomes of sphingobacteria isolates (*Sphingobacterium sp*. 21 NCBI Taxon ID: 743722), the Bacteroidetes may not have been the only heterotrophs capable of degrading complex organ substrates. Alternatively, representatives of the *Leptospirales* family of the *Spirochaetes* are capable of degrading complex organic compounds and are also likely capable of collagen degradation based on genetic potential of published *Leptospirales* genomes (Evangelista and Coburn, 2010; Ko et al., 2009).

The *Deltaproteobacteria* represented 16.5% of the Late Succession stage, and were primarily composed of sequences belonging to the *Desulfobacter* family (73% of *Deltaproteobacteria*). The *Deltaproteobacteria* were likely secondary degraders of bone organics and their presence suggests anaerobic conditions and sulfide production in the Late Succession mat. Sulfide and steep oxygen gradients produced by the *Deltaproteobacteria* would have then selected for the growth of members of the *Beggiatoaceae* family from the *Gammaproteobacteria*. The *Gammaproteobacteria* represented 20% of the Late Succession, and of these sequences, 52% (n=28,753 sequences) were classified to an OTU most closely resembling a candidate strain of *Isobeggiatoa* (100% sequence similarity) from the family Beggiatoaceae (Mußmann et al., 2007). Members of the *Beggiatoaceae* are sulfide-oxidizing bacteria that can be lithotrophic, mixotrophic, or even heterotrophic. Beggiatoa is most often found in filamentous trichomes that can form extensive white mats covering sulfidic sediments (Beutler et al., 2012; Mußmann et al., 2007). Large vacuated filaments with elemental sulfur inclusions were observed in the Month 12 biofilm under the microscope and were interpreted to be the Isobeggiatoa bacteria (Figure 3). Since *Beggiatoaceae* lack the *SoxCD* subunit, this group likely contributed in bone demineralization when localized conditions were aerobic. Copies of genes related to the synthesis of collagenase were identified in the genomes of *Beggiaota alba* and *Beggiatoa sp*., which suggests members

of the *Beggiatoaceae* from the experiment may have utilized collagen and were capable of mixotrophic growth.

Comparisons with Modern Whale Falls

Comparisons of the communities from the bone decay experiments with natural whale-fall microbial communities is difficult because the sequence libraries from natural whale falls do not record the same microenvironments investigated here. For example, some published samples of natural whale-fall community microbiomes are sampled from the sediment near the bones, and do not include bone surface biofilms (Goffredi and Orphan, 2010; Goffredi et al., 2008). Most natural samples are not part of a time series and only represent one point in the decay history of a whale-fall; and often the age of the whale-fall correlating with the biofilm sample was unknown (Tringe et al., 2005). Comparisons of experiment samples with natural biofilm are also questionable because the sequencing technology used in this study were different from the published natural whale-fall microbial community analyses; differences in sequencing technology will result in drastically different sequence yields (~100 vs. >100,000 sequences), different taxonomic resolution (V3 vs. complete 16S rRNA gene), and different biases inherent in the sequencing technology and sample prep. Despite these differences, comparisons made between the experiment communities and natural whale-falls still provides valuable insights into the reliability of the experiment results and interpretations of them. Furthermore, comparisons with natural whales may also highlight areas of the experiment that may not represent natural bone decay.

Comparisons of the relative abundance of six major bacterial groups indicated that the community composition of the experiment biofilms were overall similar to biofilms from natural whale fall environments, with some marked differences. Figure 14 illustrates the relative abundance of these six bacterial groups compared to biofilms from bone surfaces published in Tringe et al., (2005)(called Whale Fall 1,2,3), microbial communities sampled from sediment near a whale-fall over the course of 6 years from the Goffredi et al. (2010) study (called Whale-Sediment 1,2,3), and the bacterial

endosymbiont community sampled from a bone eating worm (*Osedax mucofloris*) on a whale-fall published by Goffredi et al., (2007)(callede: osedax). ANOVA results of the data plotted in Figure 14 indicate that the experiment communities are statistically similar to whale-fall populations based on relative abundances of *Bacteroidetes*, *Epsilonproteobacteria*, and *Firmicutes* (α=.05). For the other bacterial groups, the *Deltaproteobacteria* abundance of the experiment community was not similar to any whale-fall community, and for the *Alphaproteobacteria* and *Gammaproteobacteria*, the experiment composition was statistically similar to the abundances sampled from sediment near a whale-fall (Goffredi and Orphan, 2010), but not the whale fall bone surface biofilms or *Osedax* endosymbionts.

When considering the entire microbial community using multivariate statistical analysis of the major phylum abundances, the experiment microbial communities were also very similar to natural bone decay communities. Ordination of the data using a principal component analysis (Figure 15) indicated that 75% of the data could be accounted for on two eigenvectors that were most heavily weighted by *Firmicutes* abundances (eigenvector 1), and *Gammaproteobacteria* abundances (eigenvector 2); see vector plot in Figure 15. Experiment communities did not overlap with microbial communities from natural whale-falls on the PCA plot, but they did plot adjacent and between the bone biofilm and sediment natural samples.

The comparisons at the bacterial group level and multivariate level indicate that the experiment results are mostly consistent with the community composition of bacteria associated with bone decay in natural environments. As such, many bacteria involved in the early decay of fossil bone from the fossil record are also likely to have been similar to those sequenced identified in this study.

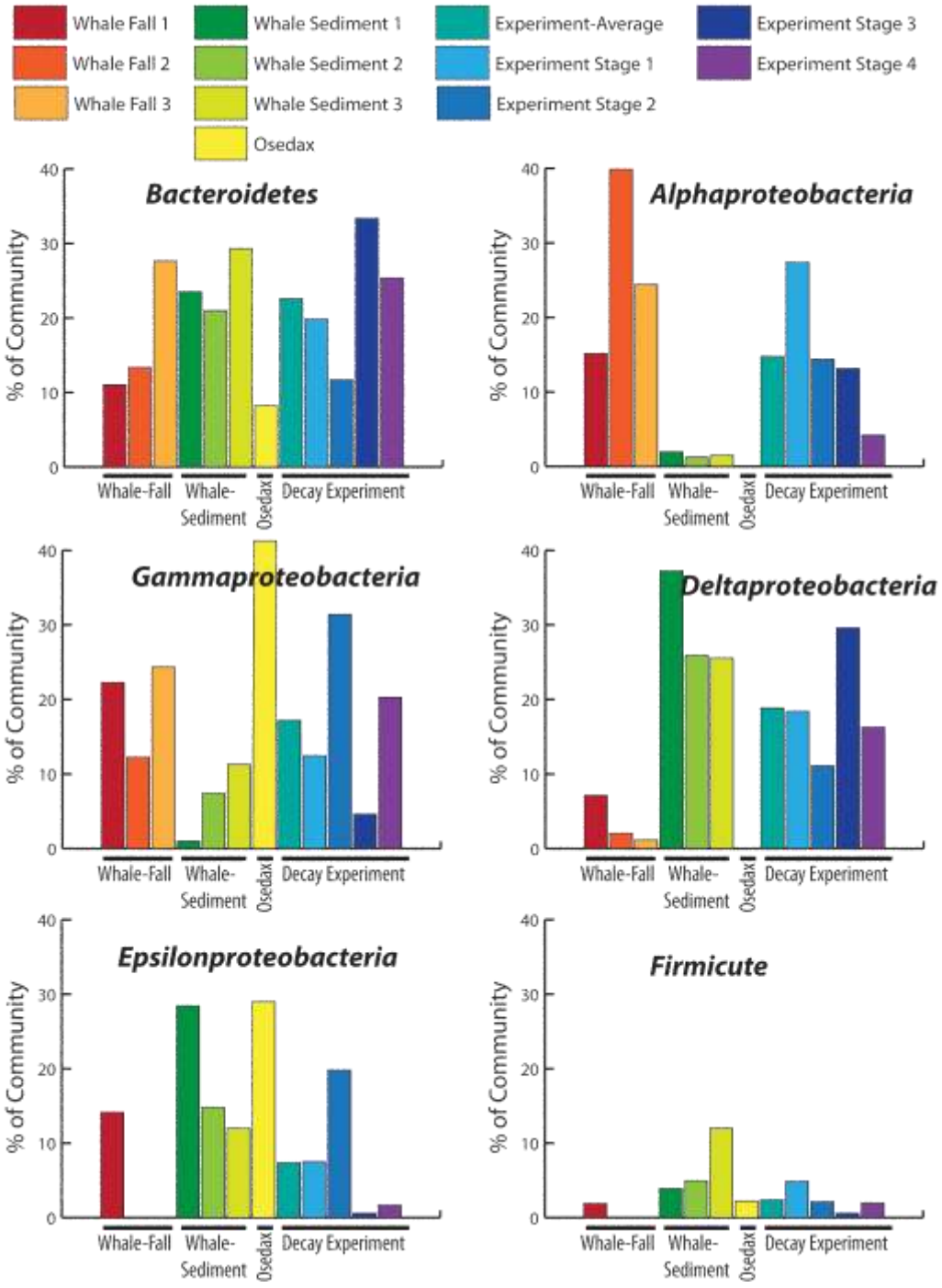

Figure 14: Comparisons of experiment bacteria with natural whale falls from bone surfaces published in Tringe et al., (2005)(Whale Fall 1,2,3), microbial communities sampled from sediment near a whale-fall over the course of 6 years from the Goffredi et al. (2010) study (sample name: Whale-Sediment 1,2,3), and the bacterial endosymbiont community sampled from a bone eating worm (Osedax mucofloris) on a whale-fall published by Goffredi et al., (2007)

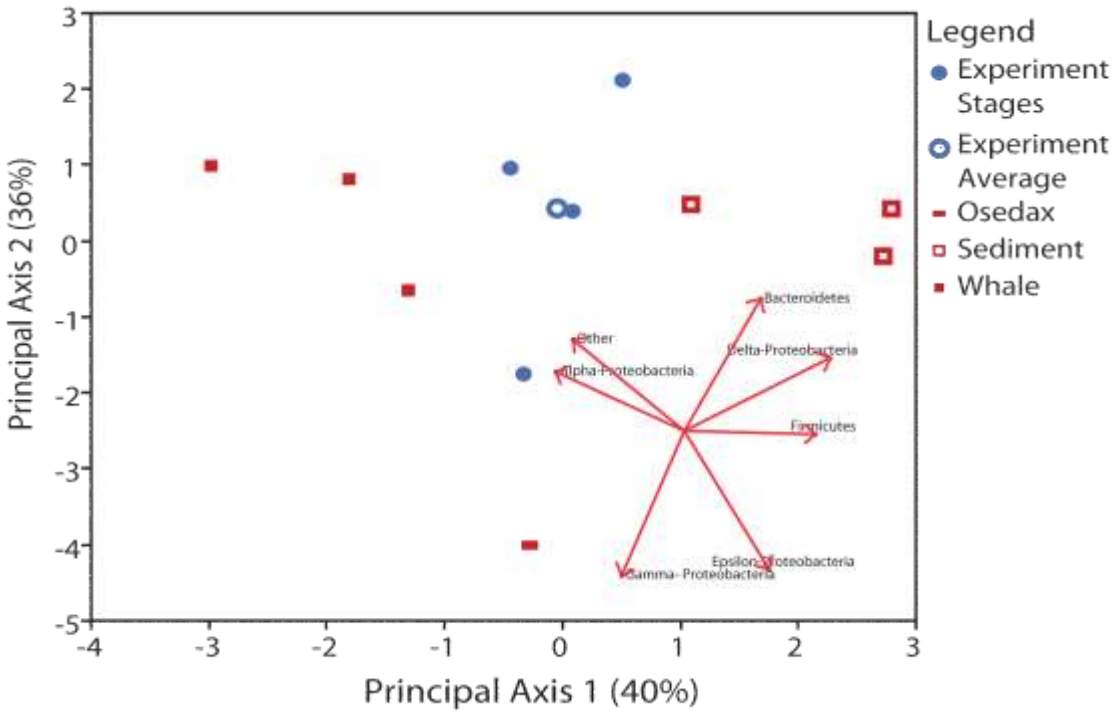

Figure 15: Principal Component plot of experiment communities compared to natural communities. Closed Squares are natural whale falls from Tringe et al., (2005), open squares are from sediment near natural whale fall from Goffredi et al., (2010), and the blue dots represent communities from the mesocosm experiment (open circle is experiment average).

CONCLUSIONS

The marine vertebrate fossil record is rich in putative microbial biosignatures suggesting that microbes were involved in the decay of the remains prior to fossilization. However, little is known about the microbes associated with the microbial degradation of bone in marine environments. In an effort to better understand the bone decay microbial consortia, we conducted lab-based experiments simulating aspects of natural bone decay and sequenced the biofilms covering bone surfaces five times throughout the 12 month experiment. From the returned sequences, we performed a community level analysis of the diversity and taxonomic composition of the microbial communities colonizing bone surfaces and specifically sought out to answer the following two questions: (i) what is the community composition of bacterial mats colonizing bone surfaces? And (ii) how does the bacterial community change during the bone decay process?

Results from the experiment suggest that the primary groups associated with decaying bone surfaces are the *Proteobacteria* (58% pooled time intervals, primarily members of the *Deltaproteobacteria*, *Gammaproteobacteria*, *Alphaproteobacteria*, *Epsilonproteobacteria*) followed by the *Bacteroidetes* (22%). From these groups over 10,000 operational taxonomic units (OTUs) were identified, but the community members were not equally distributed among them and the majority of the sequences were classified to < 100 OTUs.

Throughout the experiment, we observed several temporal trends that were not previously known to be associated with bone decay biofilms including changes in biofilm morphology and local oxygen concentrations. The relative abundance of bacterial phylum, OTUs, and diversity over the course of the experiment also changed over the course of the 12-month experiment, which was indicative of a bacterial successional series associated with the progressive decay of bone in marine environments. A hierarchical cluster analysis was used on the occurrence patterns of OTUs throughout the experiment to test if trends in bacterial composition had similar occurrence patterns. Results of the hierarchal cluster analysis confirmed that the bacteria composing biofilms on bone surfaces occurred at specific times throughout the experiment and likely represent four temporal successional stages that we interpreted as a (i) Pioneer Succession, (ii) an Early Succession, (iii) a Mid Succession, (iv) and a Late Succession.

There were significant environmental differences in the lab-based mesocosm experiment compared to natural bone decay on the ocean floor. However, comparisons of sequences from the experiment with those from several natural whale falls indicate that the experiment mesocosms do indeed capture realistic aspects of natural bone degradation and their associated microbial communities. When considering multivariate statistics at the phylum level, the experiment microbial communities were also very similar to natural bone decay communities, including samples from a variety of whale-fall types, depths, and decay stage. Geochemical gradients may have also been similar in the mesocosm to natural environments based on the presence of sulfide and oxygen sensitive species.

My results provide the first community level analysis of bacteria which colonize decaying bone surfaces in marine environments. Similar bacterial communities were likely involved in the decay of fossil bone. With additional investigations, more detailed information about the microbe-bone interaction, as well as the use of microbes for paleo-environmental and taphonomic analyses may be possible.

Chapter 2:

EARLY FRAMBOIDAL SULFIDES FROM A SIMULATED CARCASS-FALL: INDICATORS OF THE ROLE OF MICROBES IN MARINE VERTEBRATE TAPHONOMY

INTRODUCTION

Taphonomic processes that act on organic materials prior to deep burial reflect conditions in the local depositional setting (Behrensmeyer and Kidwell, 1985; Best and Kidwell, 2009; Brett and Baird, 1986; Fürsich and Oschmann, 1993; Hogler, 1994; Meldahl and Flessa, 1990; Norris, 1986). In marine settings, physical properties such as wave action, geochemical properties such as oxygenation, and biological factors such as the composition and activity of the local scavenging community can all influence the taphonomic history of skeletal material(Brett and Baird, 1986). Since taphonomic modification of vertebrate remains can be reflective of the depositional environment, reconstructing taphonomic histories may provide important paleoenvironmental information that can both constrain and inform paleobiological, paleoecological, and paleogeographic reconstructions.

A variety of indicators are used to interpret taphonomic histories, including the presence of authigenic minerals, such as calcite or pyrite, which serve as indicators of depositional conditions (Brett and Baird, 1986). Authigenic minerals may be used to draw inferences about various environments because certain minerals precipitate only under specific geochemical conditions. A great number of theoretical models and empirical results from experiments provide further constraints on the chemical concentrations, as well as the Eh, and pH conditions necessary for the precipitation of specific authigenic minerals (Butler and Rickard, 2000; Farrand, 1970; Krumbein and Garrels, 1952; Skei, 1988; Sweeney and Kaplan, 1973; Wilkin and Barnes, 1996, 1997). Consequently, authigenic minerals found in association with fossil material can act as paleoenvironmental proxies and aid in the reconstruction of taphonomic histories and depositional environments (Koenig et al., 2009; Sagemann et al., 1999; Wings, 2004).

Authigenic pyrite framboids, which are spherical aggregates composed of densely packed microcrystals, are common in marine sediments. Pyrite framboids are well studied and have been used as indicators of local and regional geochemical conditions (Bond et al., 2004; Wignall and Newton, 1998; Wignall et al., 2005; Wilkin et al., 1996). They have also been employed to infer diagenetic histories, including the presence of bacterial sulfate reduction during early diagenesis (Brett and Baird, 1986; Canfield and Raiswell, 1991). Since pyrite framboids are commonly found on vertebrate fossils recovered from marine sedimentary rocks (Grimes et al., 2002; Jensen and Thomsen, 1987; Kenrick and Edwards, 1988; Martill and Unwin, 1997; Raiswell et al., 1993; Zhou and Jiang, 2009), the potential exists for them to inform taphonomic reconstructions (Brett and Baird, 1986; Canfield and Raiswell, 1991; Pfretzschner, 2004). However, because most actualistic framboid studies to date have occurred in environments where bacterial mediated sulfide was fueled by finely-disseminated organic matter or plant remains, it remains unclear whether or not framboids formed in settings of decaying bone can be used as indicators of the conditions of decomposition and/or the prevailing geochemical conditions in the depositional setting. Indeed, there are few reported examples of pyrite framboid formation on modern vertebrate remains. Consequently, a better understanding of how framboids develop on bones in marine settings has the potential to improve our understanding of bone-associated framboids. In order to explore the formation of framboids associated with vertebrate fossils from marine strata, we documented the growth of framboids from lab-simulated carcass-falls. This work provides new insights and constraints on the formation of framboids in marine vertebrate decay scenarios.

METHODS

Experiment Design

Lab simulated carcass-falls were used to study various aspects of organic loading associated with natural carcass-falls (sunken vertebrate remains on the ocean floor). Simulated carcass-falls were created by adding 50 ml of naturally-inoculated marine mud

and 200 ml of natural seawater to a 300 ml lidded plastic container (Figure 16). Sediment and seawater were collected from the coast of Massachusetts (N 41° 42’0”, W 70° 45’0”, 1 m water depth). Mesocosms were then incubated in near-dark conditions at 10° C for two weeks to re-establish stable conditions for sediment-hosted microbial communities. After two weeks, two defleshed domestic pig rib sections (~ $1cm^3$) were emplaced on the sediment/water interface of each mesocosm. Syringe tips connected to an aquarium air pump were extended approximately 1cm into the water column to better simulate open ocean circulation.

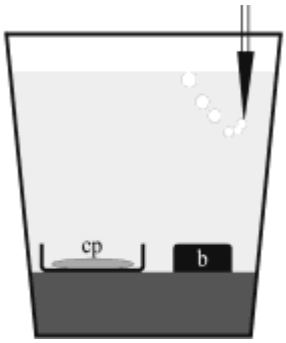

Figure 16: Diagram of carcass-fall mesocosm.

The experiment utilized three separate carcass-fall simulations. Framboid populations were sampled from the sediment of each carcass-fall simulation prior to bone emplacement to control for preexisting framboid populations. After bone emplacement, one mesocosm was sampled each week over the course of the three week experiment. A different carcass-fall mesocosm was sampled at each interval to avoid disturbing any biofilms and the sediment during sampling. At each sampling period, oxygen profiles were measured, biofilm and sediment samples were collected and preserved, and photographs were taken of the sampled carcass-fall mesocosm.

Analytical Methods

To measure microbial oxygen consumption, oxygen profiles were measured in the carcass-fall mesocosm at each sampling interval using Clark- type amperometric oxygen sensors (Revsbech, 1989; Revsbech and Jørgensen, 1986)(Aarhus, Science Park Aarhus, Denmark). Prior to measuring, the microsensor was depolarized and calibrated. Profiles

started ~1.5cm above the sediment/water interface, extended through the biofilm directly adjacent to bone, and extended ~1cm into the sediment. Measurements were taken at 0.05 cm intervals and were reported as oxygen micromolar concentration (μM).

Framboids found on bone surfaces and in sediment were examined during each sampling period using a low vacuum Hitachi TM-1000 E-SEM housed at LacCore (National Lacustrine Core Facility, University of Minnesota – Twin Cities). Framboids were initially identified by their shape and high contrast compared to surrounding bone, biofilm and sediment. Elemental abundances were then measured using the EDAX energy dispersive X-ray spectrometer (EDS) running Quantax 50 software (www.bruker-axs.com). Observations were made at an accelerating voltage of 15kV, with acquisition times of 90 seconds for framboid EDS spectra. Relative, corrected, and atomic counts of main elements were reported. Framboid diameters were measured directly on the SEM image capture.

Framboid populations from the sediment and bone surfaces were characterized using a variety of qualitative and quantitative observations. Information about framboid microcrystal shape, packing, and biofilm association was collected in a qualitative manner. SEM and EDS analyses provided information about framboid diameter, microcrystal diameter, atomic %Fe , S, C, and Fe: S. Since observations about framboid diameter and microcrystal diameter were parametric, these observations were compared using ANOVA with a post-hoc all pairs comparison Tukey-Kramer test ($\alpha = 0.05$) for multiple group comparisons, and a Student's T-test for pair-wise comparisons. Since the majority of elemental data was skewed, we used non-parametric tests for elemental statistical analyses. Multiple group comparisons of elemental data were performed using Kruskal-Wallis Tests, and post-hoc pairwise comparisons were done using Wilcoxon tests; p-values are based on the χ-square test statistic. Because multiple variables were reported per observation, discriminant analyses were performed to test group membership based on a multivariate approach. Groups were cross-validated to assess if the discriminant function has any predictive ability on data that was not used to build the function.

Framboids from this study were compared with framboid populations reported in the literature. Information about the mean diameter, standard deviation, and environments of formation were recorded. In instances when framboid populations were not summarized in the literature, framboid size distributions were measured from published images of a given population. This method is recognized to underestimate the true diameter of framboids because not all framboids are cut directly through the center (Wignall and Newton, 1998). However, calculations by Wilkin et al. (1996) suggest that distributions measured from polished thin section differ from the true mean diameter by less than 10%.

RESULTS

Bone-hosted framboids were observed to form in association with microbial biofilms at the macroscopic and microscopic level. Within the first week after bone deployment, dark microbial mats developed on bone surfaces where framboids were also observed. By the third week of the experiment, white-colored mats developed at the peripheries of the dark mats (Figure 17B). Under the microscope, the white mats contained filaments, likely *Beggiatoa*, recognized by their distinctive morphology (Larkin and Strohl, 1983; Nelson et al., 1989; Sassen et al., 2004) as well as other non-filamentous bacteria housing intra-cellular elemental sulfur (Figure 17C). At the microscopic level, framboids were often found adjacent to or encapsulated in biofilm; biofilm-associated organic matter was identified on SEM images as a feature with amorphous and homogenous texture that was distinct from bone surface texture (Figure 19). This material likely represents a mixture of microbial cell material and extracellular polymeric substances.

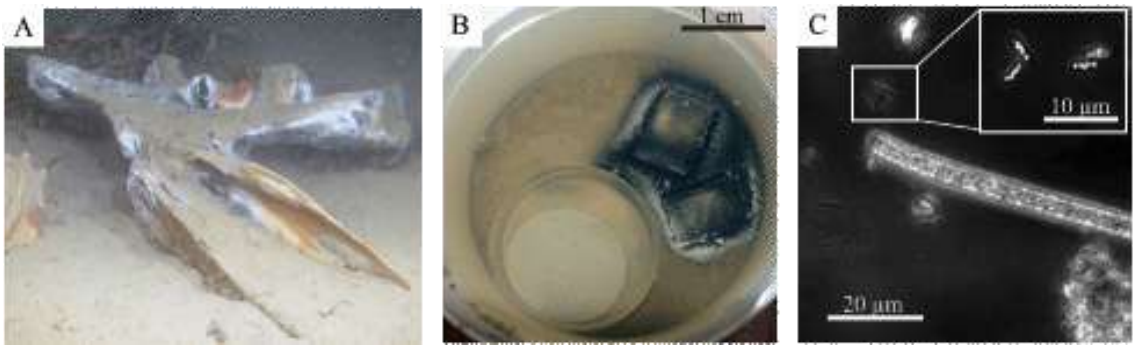

Figure 17: Examples of microbial mats on natural and simulated carcass-falls. A) Image of an experimentally implanted whale-fall observed at 125 m off the coast of Sweden (Dahlgren et al., 2006). Like the mats grown in the carcass-fall simulation, bones from the natural whale-fall are covered in a black bacterial mat likely rich in sulfate-reducing bacteria, which in places is overlain by a white bacterial mat containing sulfide-oxidizing bacteria. Photo courtesy of Thomas Dahlgren, Adrian Glover, and Thomas Lundalv (remotely operated vehicle (ROV) pilot). B) Bones covered with black (sulfate-reducing) and white (sulfide-oxidizing) microbial mat after three week of experimentation. C) Photomicrograph of a bone-associated microbial mat similar to those seen in carcass-fall simulations at Week 3. Beggiatoa, a sulfide-oxidizing filamentous bacterium is prominent and the inset shows smaller bacteria containing elemental sulfur (white circles).

Oxygen profiles measured through the microbial mats adjacent to the bones indicate that dissolved oxygen concentrations were affected by the microbial communities in the mesocosm (Figure 18). Before bones were introduced to the mesocosms, the water column was aerobic near the water/air interface (0_2>30µM) and oxygen concentrations decreased along a gradient typical of abiotic diffusion with depth (Jorgensen and Revsbech, 1985). One week after bone placement the water column remained oxygenated, but the oxygen concentrations dropped steeply at the water/microbial mat interface near the bone. Two weeks into the experiment, the water column above the bone became dysoxic (0_2< 30µM) and anoxic (no measureable 0_2) at the sediment/water/biofilm, interface (Wilkin and Barnes, 1996) (Figure 3). By the third week of the simulation, conditions became more aerobic with the water-column becoming oxic (0_2>30µM), and the pore-waters moving from anoxic to dysoxic conditions. The sterilized control mesocosms showed little change in oxygen concentration throughout the experiment.

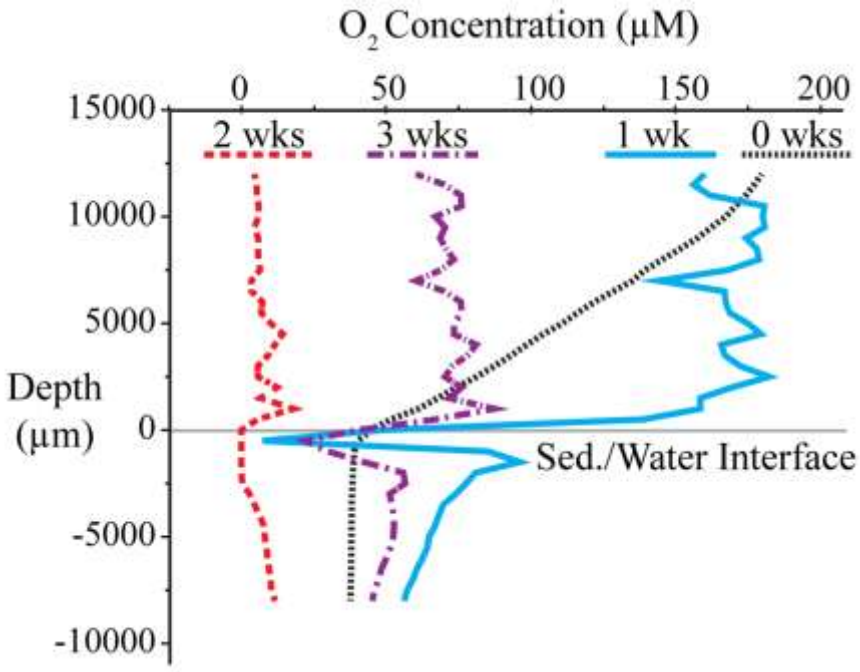

Figure 18: Oxygen microsensor profiles of carcass-fall mesocosms during the experiment. Profiles show the progression from a typical oxygen diffusion (Week 0) to a near anoxic water column in Week 2, and the return of dissolved oxygen in Week 3.

Framboids were observed on bone surfaces from the carcass-fall simulations as early as the first week of experimentation and were observed through the third week when the experiment ended. See Table 1 for summary statistics for the framboid populations, and Figure 17 for images of representative images of framboids on bone surfaces. Mean framboid diameter for all framboids observed on bones surfaces throughout the three week experiment was 3.9 µm ± 1.1µm (SD) (n=59), and the mean microcrystal size was 0.7 µm ± 0.3 µm (SD) (n=57). The medians and standard deviations of elemental data for the bone-associated framboids were: atomic %Fe=7.9 µm ± 3.0 µm, atomic %S= 10.6 µm ± 5.8 µm, and atomic %C= 47.0 µm ± 16.6 µm. The median Fe:S ratio for the bone-hosted framboid population was 1.3 µm ± 1.7 µm. In addition to the framboids, sulfide clusters, which are framboid-like but do not have consistently shaped, sized, or ordered microcrystals(Canfield and Raiswell, 1991; Ohfuji and Rickard, 2005), were also observed on bone surfaces (n=4). These sulfide clusters were found to be statistically similar in size and elemental composition to the bone hosted

framboid populations (P-values > 0.3); although the sample size is likely too low to detect differences between framboids and clusters. Raw data for bone-derived framboids and clusters is shown in Table 2. No framboids were observed on bone surfaces from the sterilized control at any point during the experiment.

Population Type	Week Sampled	n	Framboid Diameter (µm)	Microcrystal Diameter (µm)	Atom % Fe	Atom % S	Atom % C	Fe: S
Bone Total	1-3	59	3.9 ± 1.1	0.7 ± 0.3	7.9 ± 3.0	10.6 ± 5.8	47.0 ± 16.6	1.3 ± 1.7
Sed. Total	0-3	36	4.3 ± 1.7	0.8 ± 0.4	3.3 ± 1.2	5.5 ± 1.8	34.2 ± 11.2	0.6, 0.3

Table 1: Shown here are the statistics calculated for characteristics measured from framboid populations from framboids associated with bone and from framboids associated with sediment; mean and standard deviation are reported. Grey shadowed boxes indicate statistical differences (p<.05) between the bone-hosted and sediment- hosted framboid populations. See text for description of tests used.

As framboids were found in the sediment prior to bone placement, framboids were also characterized from the sediment before and after bone deployment to distinguish pre-existing framboids from newly formed framboids. To do this, we tested if the sediment and bone framboid populations were statistically similar (null hypothesis) using Student's T-test, α=0.05; results are summarized in Table 1 and raw data is included in Table 2. Our results indicate that the sediment-associated framboid diameters were not statistically different from the bone-hosted framboid populations (sediment framboids: 4.3 µm ± 1.7µm , SD, n=36, p-value=0.1313). Framboid microcrystal diameters were also found to be similar in size to bone-associated framboids (sediment microcrystal diameter: 0.8 µm ± 0.4µm, SD, n=36, p-value=0.1405). Conversely, statistical results on elemental data do distinguish sediment-hosted framboid populations from bone-hosted populations ($p < 0.05$ for all comparisons). The mean values of bone-associated framboids had over double the At.% Fe compared to sediment framboids (7.9% vs. 3.3%), nearly double the At. %S compared to the sediment framboids (10.6% vs. 5.8%), and also had elevated median At. %C (47.0% vs. 34.2) In addition to elemental percentages, the Fe:S ratio of the bone-hosted framboid population was statistically higher compared to sediment framboid population (1.3 vs. 0.6). Sulfidic clusters were

also observed in the sediment samples and were found to be statistically similar in diameter and atom %Fe, %S, %C, and Fe:S to the sediment hosted framboid populations (n=3). Like the bone vs. sediment framboid comparisons, results from comparing the sulfidic clusters indicate that bone-hosted sulfide clusters have similar sizes as the sediment-hosted clusters, but are different in elemental makeup compared to the sediment hosted clusters.

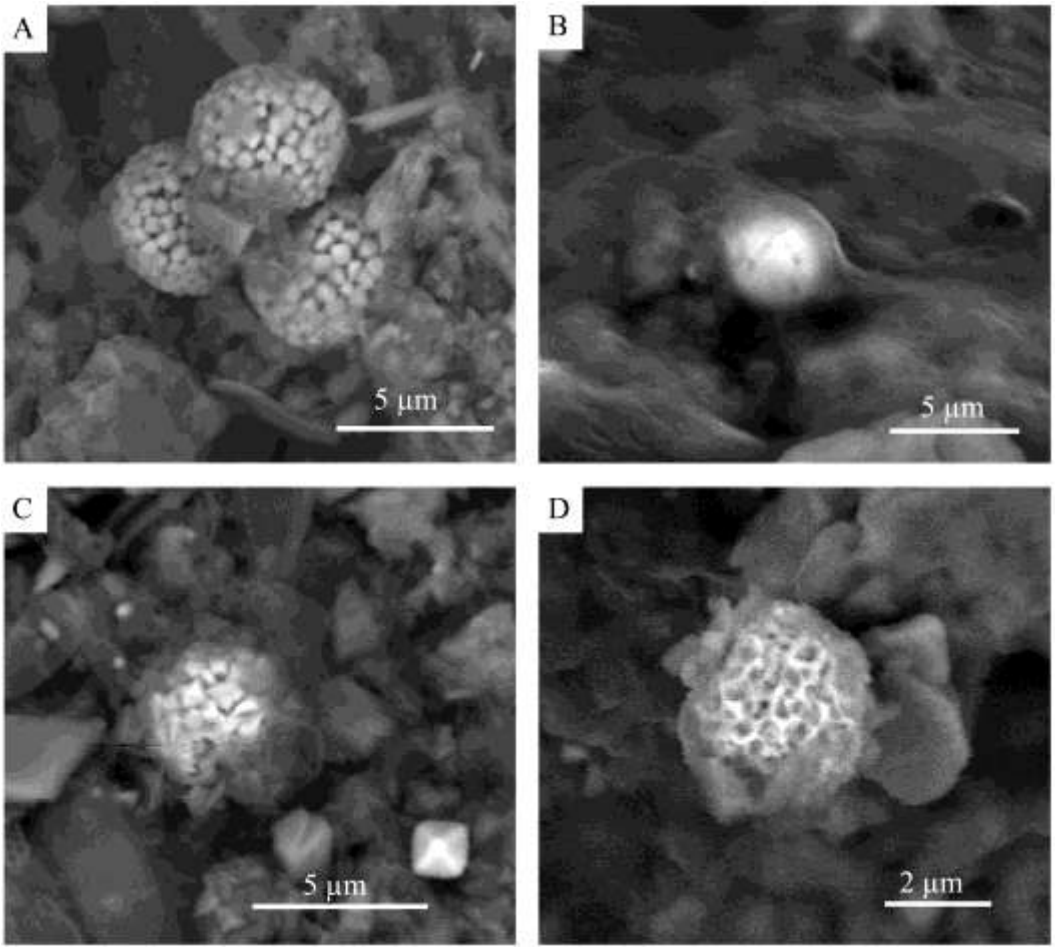

Figure 19: Images of framboids found on bone surfaces from carcass-fall simulation. A) Typical framboid morphology observed on bones. B) Framboid from the microbial mat surface encapsulated in probable extracellular polymeric substances. C) Framboid with octahedral crystallites, also associated with putative biofilm. D) Example of framboid with anhedral crystallites, thought to be a proto-framboid, also associated with putative biofilm.

Because framboid populations differed across many variables, we also used a multivariate approach to characterize the different framboid populations. A discriminant analysis was performed on *a priori* groups (bone and sediment) to determine the probability of framboid group relationships based on framboid diameter; microcrystal diameters; At. % Fe, At.%S, At.%C; and Fe:S ratios. Discriminant analyses generate independent linear axes that maximize separation among *a priori* groups. Group membership is then tested by cross-validation (removing a sample and re-preforming discriminant groups). Figure 18 illustrates the discriminant analysis in a canonical plot. Results of this analysis confirm that framboids from bone are distinct from sediment-associated framboids with only a 2% cross-validation mismatch rate and significant test statistics for both the Wilks'-Lambda and Pillai's Trace tests ($p<0.001$, DF=6). Loading scores on each axis indicate that the elemental composition of framboids, primarily At. %Fe and At. %C, distinguish bone framboids from sediment framboids Figure 18.

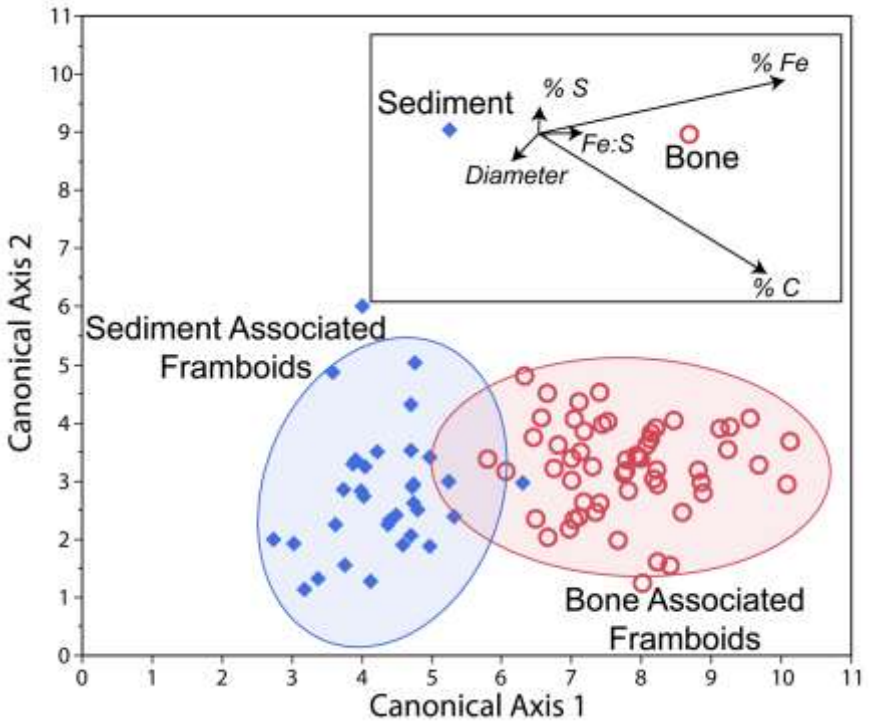

Figure 20: Discriminant analyses of framboids associated with bone (open red circle) and framboids associated with sediment (closed blue diamond). 95% Confidence ellipses are drawn around groups. Axis loading plot in top right corner indicates that loading vectors of each variable (italicized), and the sediment and bone, and framboid means.

DISCUSSION

Pyrite framboids found in association with vertebrate material deposited in marine environments can yield diagenetic, taphonomic, and environmental information. However, to date, most experimental studies of framboidal pyrite formation on organic material have focused on the decay of plant matter (Grimes et al., 2002) or were performed in synthetic environments (Sweeney and Kaplan, 1973; Wilkin et al., 1996). While these efforts are informative, they are not particularly useful with respect to the conditions promoting framboid development on decaying bone in marine environments. Indeed, there are no accounts of framboidal pyrite developing on modern bone and little is known about the timing and mechanisms of pyrite framboids formation associated with fossil material. This in turn limits the use of framboidal pyrite in taphonomic reconstructions. Here, we characterize pyrite framboids that form in association with decaying bone in simulated marine environments.

Framboid Development

Results from the carcass-fall experiments show that a distinctive framboid population developed on bone surfaces within one week of experimentation. Elemental analyses indicate that framboid populations found on bone surfaces were chemically distinct from sediment populations (Table 1). Although framboid diameters and microcrystal diameters did not differ between bone and sediment-hosted framboids, bone-associated framboids were found to be enriched in iron and carbon, especially after the first week of experimentation. The division in framboid populations is more evident in multivariate analyses (Figure 18). Although discriminant analyses are designed to ensure maximum group separation, the low misclassification percentage in conjunction with significant results from group comparison tests support the conclusions that bone framboids are different from sediment framboids. We interpret these observations and analyses to indicate that the bone-associated framboids formed on the bone and were not derived from a pre-existing framboid population that was re-suspended and deposited on bone surfaces.

The distinct elemental composition and amorphous microcrystal habit of the bone-associated framboids are consistent with pyrite framboids in the early stages of development. Pyritic framboids are believed to form through successive replacement by progressively more sulfide-rich minerals (Wilkin et al., 1996). As such, the iron to sulfur ratio of early framboids is expected to start around a 1:1 ratio reflective of ordered mackinawite (Fe_8S_9), pass through a 3:4 ratio found in greigite (Fe_3S_4), and approach a 1:2 ratio, typical of pyrite (FeS_2). Our results show that the iron to sulfur ratio of framboids forming on bone lie closer to an Fe: S ratio of mackinawite (1.3 ± 1.7 SD), whereas framboid populations from the sediment before and after bone introduction lie closer to those Fe: S ratios expected for pyrite (0.6 ± 1.7 SD). The formation of greigite framboids has never been documented in a laboratory setting, but they are observed in nature (Bailey et al., 2010; Jiang et al., 2001; Nuhfer and Pavlovic, 1979).

The elemental carbon enrichment and occasional anhedral microcrystalline habit of bone framboids may also be indicative of early framboid development. In a study characterizing framboids forming in a low temperature microbial mat, MacLean et al. (2008) described a proto-framboid composed of amorphous microcrystals that appeared to have formed within an organic matrix composed of bacteria and biopolymers. They concluded that pyrite framboids inherit their shape and microcrystals from this organic matrix (MacLean et al., 2008, fib. 3b) and develop into more euhedral shapes later in the framboid growth history as the organic matrix degrades or becomes engulfed in the mature framboid structure. Like the proto-framboid described by MacLean et al. (2008), we also identified framboids with anhedral microcrystals and one instance of a similar scaffolding surrounding microcrystals (Figure 17D). We also documented that carbon concentrations from the bone derived framboids forming early in the experiment were 22% higher compared to sediment associated framboids. Furthermore, the carbon concentration of the bone-associated framboids in our study decreased each week of experimentation by ~9%,, and this may reflect the loss of the organic matrix as the framboid matures, a phenomenon noted by MacLean et al. (2008). However, unlike the

proto-framboids in the MacLean et al. (2008) study, the framboids observed in our study were closer in composition to mackinawite as discussed above.

Framboid Formation in Bone-Associated Microbial Mats

Observations from the lab-simulated carcass-fall experiments suggest that framboids nucleated as the result of microbial activity. Although not necessary for formation (see Ohfuji and Rickard (2005) and references therein), microbes, specifically sulfate-reducing bacteria (SRBs) are generally thought to play a role in framboid formation (Donald and Southam, 1999; Grimes et al., 2001; MacLean et al., 2008; Popa et al., 2004). SRBs, often members of the Deltaproteobacteria sub-phylum, use sulfate as their terminal electron acceptor and generate sulfide as an end-product, which then can react with iron monosulfide constituents to form framboids. Our observations and measurements suggest that the framboids in the carcass-fall mesocosms also formed due to sulfide produced by the microbial consortia colonizing bone. Although not directly measured in this study, the generation of sulfide due to bone emplacement in the lab simulated carcass-fall mesocosms is indicated by the sharp decrease in oxygen concentrations near the bone biofilm (Figure 16), the blackening of the bone surfaces and surrounding sediments (Figure 15B), and the presence of sulfide-oxidizing bacteria (Figure 15C). The low oxygen concentrations near the biofilms on bone surfaces indicate that the microbial community was likely living in anoxic conditions, which is favorable for the production of sulfide by sulfate-reducing bacteria. Additionally, the dark staining on bone and sediment also suggests that sulfide was generated in the mesocosm; sulfide often reacts with ambient ferrous iron and produces nanocrystallites composed of iron monosulfide, which can stain sediment black (Amon et al., 2013; Canfield and Raiswell, 1991; Darroch et al., 2012; Thamdrup et al., 1994).

Under the microscope, several types of sulfide-oxidizing bacteria were identified from bone surface biofilms including filamentous *Beggiatoa*, which are easily identified (Larkin and Strohl, 1983; Nelson et al., 1989; Sassen et al., 2004) and are known to occur in natural carcass-falls as seen in Figure 15A (Deming et al., 1997; Smith and Baco, 2003). Sulfide-oxidizing bacteria are often found adjacent to sulfate-reducing bacteria

because they depend on the sulfide produced by the sulfate-reducing bacteria as their energy source. Thus, the presence of sulfide-oxidizing bacteria in bone biofilms indirectly supports the presence of sulfide in the mesocosm experiments. Biofilms were not observed on the mesocosm sediment before bone addition suggesting that the microbial communities developed as a direct result of the bone which implies the bone organics and associated secondary metabolites fueled mat formation.

Framboids as Indicators of Taphonomic Condition

Pyrite is commonly found associated with fossil vertebrate material in the form of framboids, euhedral crystals, void fillings, cements, and as surface coverings. In particular, pyrite framboids are generally found on fossil bone surfaces, in sediment adjacent to bone, or in voids such as Haversian canals. Framboids are documented to co-occur with fossil bone from Mesozoic marine reptiles (Martill, 1987; Kaim et al., 2008) and Cenozoic marine mammal specimens (Naganuma et al., 1996; Amano and Little, 2005; Amano et al., 2007; Shapiro and Spangler, 2009). Framboids associated with modern bone have yet to be observed. Here, we discuss how our results, which better constrain the timing and mechanisms of framboid formation on bone in marine environments, can be used to indicate more specific information about the diagenesis, taphonomic history, and depositional environment of vertebrates deposited in marine settings.

In the carcass-fall simulation, bone-hosted framboids developed on bone surfaces within one week of introducing bone to the mesocosm, suggesting that framboid formation can initiate within days of soft-tissue removal in natural carcass-falls - occurring extremely early in the diagenetic history of fossilized remains. The decay process of natural carcass-falls, especially of large marine mammals, is dynamic and long-lived, and prior to our experiment, it was unclear at which point during the decomposition history framboids would form (Kiel, 2008; Shapiro and Spangler, 2009). Smith and Baco (2003) studied the decomposition of whale-falls extensively and established four successional decomposition stages characterized by predominant scavenger types and their targeted whale tissue: (1) a mobile-scavenger stage during

which most soft tissue is removed primarily by mobile scavengers; (2) an opportunist-enrichment phase composed of sessile scavengers that target organics leached into the surrounding sediment and remaining soft tissue on the bone; (3) a sulphophilic stage fueled by sulfate-reducing bacteria exploiting bone lipids, a stage that can support complex trophic assemblages; and (4) a reef stage during which nutrient-depleted bone acts as a substrate for epibionts (Smith and Baco, 2003). Microbes are present and actively degrading tissue in each stage, including the initial scavenger-stage as shown by aqueous decomposition studies (Giancamillo et al., 2010). The duration of each decomposition stage is dependent on environment conditions as well as the size, age, and taxon represented by the vertebrate remains (Smith and Baco, 2003). In general, the consumption of soft-tissue and labile organics is fast and occurs within a few years, but the degradation of bone during the sulphophilic stage is much slower, sometimes occurring over a time scale of many decades (Jones et al., 1998; Smith and Baco, 2003).

We would expect framboids to form during the sulphophilic scavenging stage when sulfide concentrations are thought to be at their highest (Smith and Baco, 2003). Indeed, a previous study used the association of sulfide framboids, in the presence of fossil mollusks and gastropods known to harbor sulfide-utilizing symbiotic bacteria, to identify the sulphophilic scavenging stage of a fossil whale-fall (Amano and Little, 2005). However, since microbes were also present during the other decomposition stages, and based on the rapid formation of framboids in our experiment, it is possible that framboid formation is not limited to just the sulphophilic stage, and may also occur much earlier in the decomposition history. Our experiments indicate that sulfate-reducing bacteria colonizing bone surfaces at the very early stages of microbial decay can provide sufficient sulfide to initiate framboid nucleation. Thus, our findings suggest that framboid formation can occur as early as the opportunistic-enrichment phase when bones are initially exposed. Due to the limited scope of our study, we cannot confirm at which other decomposition stages framboids may form, although it is likely that if sulfide is being produced, even in small amounts, then framboids have the potential to form.

Sulfate-reducing bacteria, a primary source for sulfide in the formation of framboids, naturally exist in shallow sediment, often with their activities concentrated within localized reduction sulfate-reduction zones in the sediments (Allison, 1988b). Kiel et al., (2008) have suggested that framboids forming in association with vertebrate material likely formed when the vertebrate remains are buried at shallow depths. Our experiments also show that bones need not be buried in the sulfate reduction zone to act as substrates for framboid formation, but can also form on the surfaces of bone exposed at the sediment/water interface, even if the overlying water column is well oxygenated as was the case in our experiment mesocosms.

Geochemical Indicators

Much of the framboid literature focuses on their use as an indicator of regional geochemical conditions (Bond et al., 2004; Marynowski et al., 2007; Skei, 1988; Wilkin and Barnes, 1996). Previous experimental and actualistic studies indicate that framboid populations originating in euxinic ocean basins typical of stagnant closed basins or ocean anoxic events tend to be smaller and less variable in size compared to framboid populations that from in oxygenated ocean basins (Bond et al., 2004; Marynowski et al., 2007; Wilkin and Barnes, 1996). Framboids from anoxic settings are thought to be smaller and less variable (5.1 μm ± 1.5 μm SD) because they form in the water column and quickly sink to the seafloor after precipitation, limiting the supply of iron in a sulfide-dominated system and halting framboid growth (Skei, 1988; Wilkin and Barnes, 1996). In comparison, framboids that form in oxygenated water columns tend to be larger and more variable in size (8.0 μm ± 2.2 μm SD) because they likely nucleate near or at the sediment/water interface where both iron and sulfide are available, and the framboids remain in conditions ideal for framboid growth for a longer time (Wilkin and Barnes, 1996). The formation of framboids in euxinic, dysnoxic, and oxic conditions is further illustrated in Figure 20.

To date, few if any studies have compared framboid populations associated with vertebrate material with sedimentary framboid populations. Although the sulfide involved in framboid formation likely originates from the microbial decay of organic matter in

both the sedimentary and carcass-fall scenarios, it is unclear if the disparity in amount of available organics (planktonic in sedimentary systems vs. large vertebrate remains) has any impact on the size distribution of framboid populations on carcass-falls. Our study offers an opportunity to compare the experimental bone-hosted framboid population where the location and some environmental conditions are known, with those from the literature to determine if framboids found in association with vertebrate material can also be used as regional environmental indicators. Additionally, since the mechanisms responsible for governing framboid size in sedimentary environments are relatively well known, comparisons of bone-hosted framboids to published framboid populations may provide additional insights into the formation and time of framboid populations derived from bacterial decay of vertebrate remains.

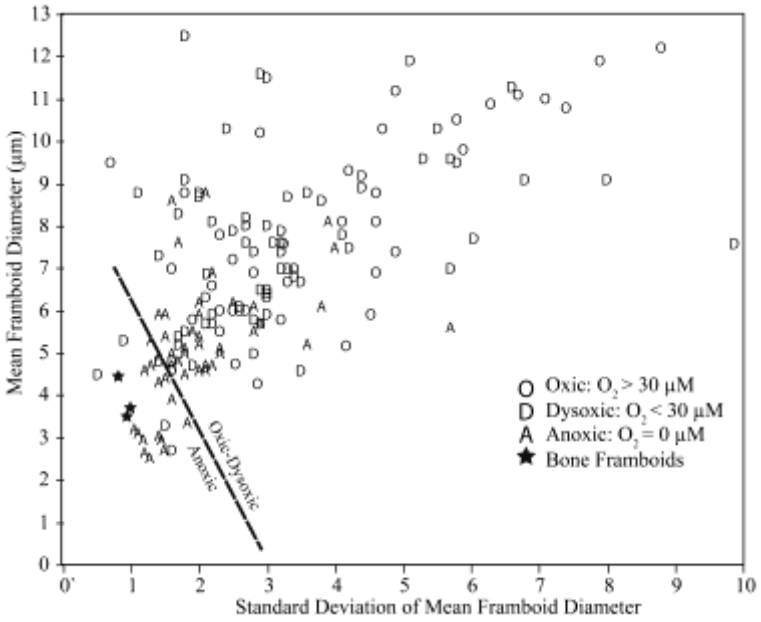

Figure 21: Scatter plot of mean framboid diameters plotted against the standard deviation of sedimentary framboids from known environments and from bone hosted-framboids from this study (stars, one for each week of experimentation). Oxic-Dysoxic: Anoxic line is the same as identified in Wilkins et al (2006). Values and sources for each data point are provided in Table 3.

When the mean framboid diameter and corresponding standard deviation of framboids growing on bone surfaces from this study are plotted against those from published framboid population originating from known environments, bone associated framboids plot closest to framboids forming in anoxic water columns (Figure 21).

However, our microsensor measurements show an oxygenated water column in the mesocosm experiments (Figure 18). If the water column is taken to be representative of regional oxygen concentrations, then we might have expected the bone framboids to plot closer to the dysoxic and oxic framboid populations. On closer inspection, measured oxygen concentrations from the carcass-fall simulations indicate that framboids grew in localized anoxic environments in the biofilm (0_2 concentrations = 0 μM), despite the oxic conditions in the surrounding mesocosm water (0_2 concentrations > 30 μM). We interpret these results to indicate that larger volumes of organic matter can promote steep oxygen gradients and localized anoxic conditions that extend above the sediment water interface to above the bone surface, even though the regional water chemistry is oxic.

Additionally, because the framboids in our mesocosm experiment are small and likely formed in the biofilm covering bone, yet plot closest to sedimentary framboid populations that formed in suspension, we suggest that bacterially-mediated anoxic and sulfidic conditions surrounding the bone were transient, likely due to nutrient availability and changing microbial communities (Figure 22). Subtle Eh or pH changes may abruptly stop framboid formation; and once stopped, framboids typically do not resume formation (Wilkin and Barnes, 1996). Thus, we propose that the smaller framboids that form in the microbial mat result from shorter exposure to conditions that favor framboid growth than those that precipitate in sediment pore waters. Framboid populations originating from the decay of vertebrate material, and possibly other transient conditions such as bacterial biofilms, may be reliable indicators of localized conditions, but not necessarily of regional geochemical conditions.

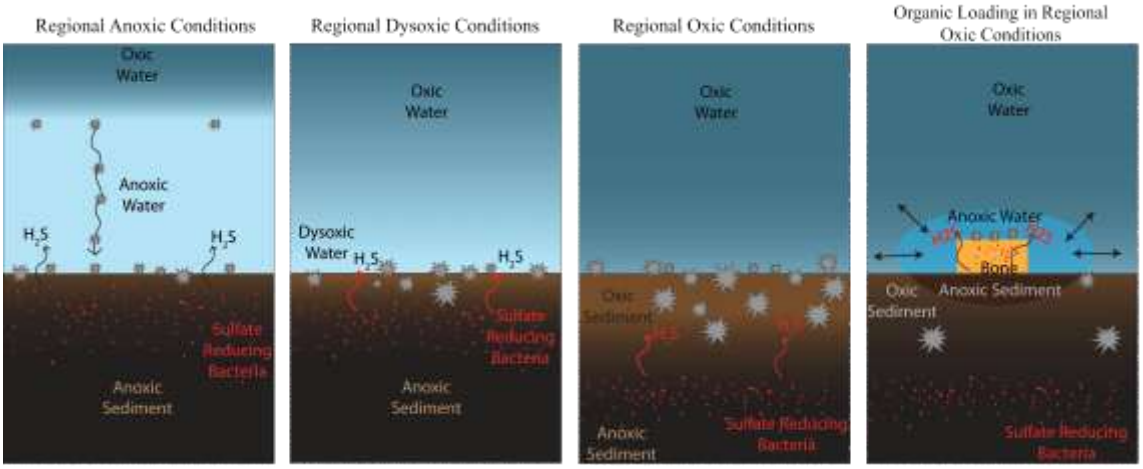

Figure 22: Cartoon depicting the formation of iron sulfide framboids in various environments. In anoxic water columns, framboids tend to form in the water column near the redox boundary, but fall out of suspension resulting in small and less variable framboid sizes. In dysoxic and oxic environments, framboids are interpreted to form at or below the sediment/water interface enabling them to potentially form for longer periods of time which results in larger and more varied framboid sizes. We show that framboids forming in association with bone decomposition are more similar to framboids forming in anoxic water columns likely due to transient geochemical conditions near the bone. As a result, framboids forming in organic loading environments may not be reliable geochemical indicators.

CONCLUSIONS

These are the first lab-based experiments to document the formation of framboidal iron sulfide growth on vertebrate material decaying in a simulated marine setting. Analyses of individual framboid characteristics combined with discriminant analyses support our conclusion that framboids forming on bone are distinct from the pre-existing framboid population in the sediment. Our experiments provide a lower bound on the timing of framboids development associated with vertebrate material. The framboids were first discovered on bone surfaces within a week of starting the experiment, and appeared in conjunction with a dark-colored microbial mat that covered bone surfaces. The black color of this microbial mat, in addition to the presence of sulfide-oxidizing bacteria suggest that sulfide was produced in the mesocosms, likely as the product of heterotrophic sulfate-reducing bacteria degrading bone organics or associated secondary metabolites. Framboids formed as a result of the localized sulfide production. Also in

support of the microbial association, many framboids on bone were found encapsulated in probable biofilm associated with the bone-covering mat. Furthermore, the direct association of framboid appearance with the development of microbial growth on bone surfaces, and not in controlled sterile experiments, attests to the indirect formation of framboids by microbial activity.

We conclude from our experiments that bones, once defleshed from scavenging, can sustain sufficient rates of sulfide production to induce framboid precipitation early, within weeks, of exposure. Our experiments show that framboids may not necessarily indicate the sulphophilic decomposition stage as they may also form at the initial time of bone exposure that develops during the opportunistic-enrichment phase of large vertebrate decay. Furthermore, our experiments also suggest that burial is not required for framboid formation. On comparing bone-hosted framboid populations from the carcass-fall simulation with those from previous studies that looked at framboid size distributions in sediments, we found that framboids formed on vertebrate bones, or possibly other large organic loading scenarios, may not be reliable indicators of regional oxygen, but instead represent highly-localized anoxic and transient microenvironments. We found that the framboids forming on bone surfaces under an oxic water column are close in size distribution to framboid populations originating under regional anoxic conditions. We suggest that geochemical conditions associated with microbial mats developing on bone and other organic loading situations are dynamic, and that framboids developing in microbial mats may have shorter growing periods due to these transient conditions. Because our experiments address only the initial stages of decay more experimentation will be needed to investigate the formation of framboids at later stages of decay.

Table 2: Raw data of experiment framboids

Population Type	Framboid Diameter (µm)	Microcrystal Diameter (µm)	Atom % Fe	Atom % S	Atom % C	Fe: S
Bone	3.4	anhedral	7.6	10.6	65.6	0.7
Bone	5.0	1.1	3.8	5.6	78.3	0.7
Bone	4.7	0.9	0.0	5.5	75.1	0.0
Bone	3.6	0.4	8.1	12.0	63.2	0.7
Bone	2.0	0.3	9.9	12.5	62.2	0.8
Bone	4.2	0.6	9.3	15.2	61.9	0.6
Bone	4.0	0.5	6.5	10.4	65.5	0.6
Bone	2.4	0.3	5.4	7.3	68.6	0.7
Bone	3.9	0.5	7.4	3.8	68.4	2.0
Bone	3.8	1.4	10.5	17.3	38.7	0.6
Bone	4.0	1.6	10.7	10.7	32.5	1.0
Bone	3.1	0.4	6.0	11.4	54.2	0.5
Bone	4.0	0.5	8.7	12.9	47.9	0.7
Bone	3.6	1.3	9.1	14.9	45.3	0.6
Bone	3.5	0.7	7.4	11.8	55.9	0.6
Bone	6.5	1.3	8.8	17.8	36.8	0.5
Bone	3.1	0.4	12.9	20.0	39.7	0.6
Bone	4.0	1.1	16.3	22.8	52.5	0.7
Bone	3.4	anhedral	6.0	11.1	13.9	0.5
Bone	3.5	0.5	11.2	17.3	26.8	0.6
Bone	3.5	anhedral	8.6	9.1	34.7	0.9
Bone	2.9	0.6	6.6	12.9	39.8	0.5
Bone	4.6	0.5	8.9	14.2	38.2	0.6
Bone	3.1	0.4	13.0	21.4	28.0	0.6
Bone	4.0	0.6	12.2	18.9	39.2	0.6
Bone	3.1	0.7	8.1	6.6	39.9	1.2
Bone	2.8	0.5	8.5	1.6	22.6	5.5
Bone	3.0	0.5	7.8	1.4	30.4	5.4
Bone	3.0	0.5	8.0	2.9	49.2	2.8
Bone	5.0	0.9	8.1	12.6	51.8	0.6
Bone	3.9	0.5	7.8	2.4	47.0	3.3

Bone	3.2	0.4	5.1	3.0	66.0	1.7
Bone	3.5	0.7	3.1	0.4	75.9	8.5
Bone	6.2	1.0	4.7	1.1	49.7	4.4
Bone	3.0	0.4	8.0	14.3	46.8	0.6
Bone	4.0	0.7	6.4	11.2	58.0	0.6
Bone	3.7	0.5	3.7	6.4	66.8	0.6
Bone	4.0	1.0	4.8	9.0	68.1	0.5
Bone	1.8	0.1	7.7	10.2	61.2	0.8
Bone	3.4	1.0	7.6	16.2	48.0	0.5
Bone	4.9	0.4	5.7	9.4	49.1	0.6
Bone	6.5	1.3	4.9	8.3	59.7	0.6
Bone	4.6	0.4	6.9	8.3	46.6	0.8
Bone	5.5	1.0	4.9	7.4	52.0	0.7
Bone	4.8	0.8	7.0	10.8	42.5	0.6
Bone	2.9	0.3	7.7	10.7	39.1	0.7
Bone	3.6	0.8	6.4	11.5	50.0	0.6
Bone	5.6	0.8	4.5	7.1	66.3	0.6
Bone	4.0	0.7	4.1	3.7	62.0	1.1
Bone	4.5	0.8	5.1	6.2	44.6	0.8
Bone	2.0	0.3	6.7	11.1	45.0	0.6
Bone	3.1	0.5	15.6	16.8	12.3	0.9
Bone	5.6	0.9	10.0	10.0	32.8	1.0
Bone	4.4	0.5	10.1	16.6	40.1	0.6
Bone	3.7	0.8	10.6	8.2	21.7	1.3
Bone	4.0	0.5	13.9	27.7	12.7	0.5
Bone	6.3	0.7	7.2	12.5	37.0	0.6
Bone	3.6	0.4	8.3	14.0	33.0	0.6
Bone	4.2	0.6	11.3	1.3	9.9	8.5
Sediment	1.9	0.3	2.3	4.7	42.6	0.5
Sediment	6.6	1.4	3.2	6.4	31.8	0.5
Sediment	5.6	1.0	2.3	4.4	41.0	0.5
Sediment	2.8	0.4	2.8	5.8	37.8	0.5
Sediment	4.5	0.5	2.2	5.7	37.0	0.4
Sediment	4.9	1.6	3.7	4.8	17.9	0.8

Sediment	3.0	anhedral	3.6	5.1	33.7	0.7
Sediment	3.2	0.5	3.7	4.8	22.6	0.8
Sediment	5.0	1.0	1.6	2.6	38.9	0.6
Sediment	7.5	1.3	3.9	3.1	37.4	1.2
Sediment	3.3	0.9	3.0	7.2	28.9	0.4
Sediment	4.6	0.6	3.8	5.9	28.6	0.6
Sediment	2.4	0.4	2.8	1.9	40.1	1.5
Sediment	3.0	anhedral	2.5	4.7	27.7	0.5
Sediment	4.0	0.6	3.3	5.9	30.7	0.6
Sediment	3.4	0.6	2.5	3.3	41.0	0.8
Sediment	5.0	1.1	2.1	5.2	47.9	0.4
Sediment	3.0	0.5	2.4	4.3	45.4	0.6
Sediment	7.8	0.5	4.0	2.1	28.2	1.9
Sediment	6.3	0.6	2.6	6.6	46.9	0.4
Sediment	3.4	0.4	2.5	5.7	35.9	0.4
Sediment	2.9	0.9	3.7	6.4	28.9	0.6
Sediment	3.6	1.0	2.1	4.3	50.1	0.5
Sediment	3.4	0.9	4.7	9.3	13.4	0.5
Sediment	10.0	1.9	4.2	8.3	24.3	0.5
Sediment	4.2	0.8	6.4	8.7	39.5	0.7
Sediment	3.3	0.5	2.8	5.4	42.5	0.5
Sediment	4.0	1.0	2.5	5.7	52.0	0.4
Sediment	4.6	0.8	3.4	5.0	39.5	0.7
Sediment	4.1	0.7	2.3	5.7	52.5	0.4
Sediment	2.6	0.3	3.5	6.3	12.7	0.6
Sediment	5.4	anhedral	3.6	5.9	27.3	0.6
Sediment	5.0	1.3	3.6	7.0	17.1	0.5
Sediment	2.9	0.4	6.1	9.2	16.8	0.7
Sediment	5.3	0.8	6.1	8.0	22.6	0.8
Sediment	4.0	0.5	2.1	4.2	50.4	0.5

Table 3: Table of mean and standard deviation of published framboid populations from specified geochemical environments (Wilkin et al., 1996; Suits and Wilkin, 1998; Taylor and Macquaker, 2000; Nielsen and Shen, 2004; Popa et al., 2004; Wignall et al., 2005; Marynowski et al., 2007; Shen et al., 2007; Zhou and Jiang, 2009; Bond and Wignall, 2010).

Environment	Average Framboid Diameter (μm)	Stan. Dev. (μm)	Source
Anoxic	4.8	1.7	Wilkin et al., 1996
Anoxic	4.7	1.6	Wilkin et al., 1996
Anoxic	5.0	1.6	Wilkin et al., 1996
Anoxic	5.1	1.8	Wilkin et al., 1996
Anoxic	6.1	2.0	Wilkin et al., 1996
Anoxic	5.1	1.8	Wilkin et al., 1996
Anoxic	4.8	1.7	Wilkin et al., 1996
Anoxic	5.2	2.0	Wilkin et al., 1996
Anoxic	5.0	1.6	Wilkin et al., 1996
Anoxic	4.4	1.5	Wilkin et al., 1996
Anoxic	5.0	1.8	Wilkin et al., 1996
Anoxic	4.3	1.4	Wilkin et al., 1996
Anoxic	4.9	1.4	Wilkin et al., 1996
Anoxic	5.4	2.0	Wilkin et al., 1996
Anoxic	3.1	1.1	Wignall et al., 2005
Anoxic	3.2	1.05	Wignall et al., 2005
Anoxic	5.2	3.6	Popa et al., 2004
Anoxic	2.95	1.45	Nielsen and Shen, 2004
Anoxic	3.34	1.83	Nielsen and Shen, 2004
Anoxic	3.03	1.4	Nielsen and Shen, 2004
Anoxic	2.7	1.48	Nielsen and Shen, 2004
Anoxic	2.51	1.28	Nielsen and Shen, 2004
Anoxic	2.64	1.19	Nielsen and Shen, 2004
Anoxic	2.94	1.18	Nielsen and Shen, 2004
Anoxic	4.7	2.1	Suits and Wilkin, 1998
Anoxic	6.9	2.2	Bond and Wignall, 2010
Anoxic	6.4	2.1	Bond and Wignall, 2010
Anoxic	6.2	2.5	Bond and Wignall, 2010
Anoxic	8.8	2.1	Bond and Wignall, 2010
Anoxic	8.6	1.6	Bond and Wignall, 2010
Anoxic	4.6	2.1	Bond and Wignall, 2010
Anoxic	6.2	2	Bond and Wignall, 2010
Anoxic	6.1	3.8	Bond and Wignall, 2010

Anoxic	8.1	3.9	Bond and Wignall, 2010
Anoxic	7.5	4	Bond and Wignall, 2010
Anoxic	6.3	2.1	Bond and Wignall, 2010
Anoxic	5.1	2.3	Bond and Wignall, 2010
Anoxic	4.5	1.8	Bond and Wignall, 2010
Anoxic	5	2.3	Bond and Wignall, 2010
Anoxic	5.6	5.7	Bond and Wignall, 2010
Anoxic	5.9	2	Bond and Wignall, 2010
Anoxic	5.5	2.8	Bond and Wignall, 2010
Anoxic	7.6	1.7	Bond and Wignall, 2010
Anoxic	6.1	2.8	Bond and Wignall, 2010
Anoxic	4.7	2.2	Bond and Wignall, 2010
Anoxic	3.9	1.6	Bond and Wignall, 2010
Anoxic	4.7	1.3	Bond and Wignall, 2010
Anoxic	5.7	2.9	Bond and Wignall, 2010
Anoxic	5.9	1.4	Bond and Wignall, 2010
Anoxic	4.7	2.1	Bond and Wignall, 2010
Anoxic	4.6	2	Bond and Wignall, 2010
Anoxic	5.5	1.9	Bond and Wignall, 2010
Anoxic	5.4	1.5	Zhou and Jiang, 2009
Anoxic	5.9	1.5	Zhou and Jiang, 2009
Anoxic	4.6	1.2	Zhou and Jiang, 2009
Anoxic	5.3	1.3	Zhou and Jiang, 2009
Dysoxic	6.5	2.9	Wilkin et al., 1996
Dysoxic	6.1	2.6	Wilkin et al., 1996
Dysoxic	6.4	3.0	Wilkin et al., 1996
Dysoxic	5.7	2.9	Wilkin et al., 1996
Dysoxic	6.7	3.5	Wilkin et al., 1996
Dysoxic	7.0	3.2	Wilkin et al., 1996
Dysoxic	2.7	1.6	Wignall et al., 2005
Dysoxic	3.3	1.5	Wignall et al., 2005
Dysoxic	5.7	2.1	Wignall et al., 2005
Dysoxic	7.5	4.2	Wignall et al., 2005
Dysoxic	6.88	2.12	Wignall et al., 2005
Dysoxic	7.58	3.25	Wignall et al., 2005
Dysoxic	7.59	9.88	Wignall et al., 2005
Dysoxic	7.71	6.05	Wignall et al., 2005
Dysoxic	5	2.8	Shen et al., 2007
Dysoxic	8.7	2	Shen et al., 2007

Dysoxic	4.6	3.5	Shen et al., 2007
Dysoxic	6	2.7	Shen et al., 2007
Dysoxic	5.4	1.7	Shen et al., 2007
Dysoxic	4.5	.5	Shen et al., 2007
Dysoxic	7.4	2.8	Bond and Wignall, 2010
Dysoxic	7.6	3.1	Bond and Wignall, 2010
Dysoxic	8.3	1.7	Bond and Wignall, 2010
Dysoxic	9.2	4.4	Bond and Wignall, 2010
Dysoxic	7.9	2.5	Bond and Wignall, 2010
Dysoxic	8.8	3.6	Bond and Wignall, 2010
Dysoxic	9.1	1.8	Bond and Wignall, 2010
Dysoxic	7.6	3.1	Bond and Wignall, 2010
Dysoxic	8.2	2.7	Bond and Wignall, 2010
Dysoxic	9.1	8	Bond and Wignall, 2010
Dysoxic	9.6	5.3	Bond and Wignall, 2010
Dysoxic	8.7	3.3	Bond and Wignall, 2010
Dysoxic	9.1	6.8	Bond and Wignall, 2010
Dysoxic	22.1	7.4	Bond and Wignall, 2010
Dysoxic	10.3	2.4	Bond and Wignall, 2010
Dysoxic	8.8	2	Bond and Wignall, 2010
Dysoxic	11.3	6.6	Bond and Wignall, 2010
Dysoxic	11.5	3	Bond and Wignall, 2010
Dysoxic	5.2	1.7	Bond and Wignall, 2010
Dysoxic	16	12.2	Bond and Wignall, 2010
Dysoxic	8.8	1.1	Bond and Wignall, 2010
Dysoxic	7.3	1.4	Bond and Wignall, 2010
Dysoxic	5.9	2.2	Bond and Wignall, 2010
Dysoxic	4.7	1.9	Bond and Wignall, 2010
Dysoxic	11.6	2.9	Bond and Wignall, 2010
Dysoxic	7.4	3.2	Bond and Wignall, 2010
Dysoxic	4.8	1.4	Bond and Wignall, 2010
Dysoxic	10.3	5.5	Bond and Wignall, 2010
Dysoxic	7	3.3	Bond and Wignall, 2010
Dysoxic	7	5.7	Bond and Wignall, 2010
Dysoxic	12.5	1.8	Bond and Wignall, 2010
Dysoxic	9.5	5.8	Bond and Wignall, 2010
Dysoxic	5.8	2.8	Bond and Wignall, 2010
Dysoxic	5.7	2.2	Bond and Wignall, 2010
Dysoxic	4.8	1.6	Bond and Wignall, 2010

Dysoxic	5.5	1.8	Bond and Wignall, 2010
Dysoxic	6.1	2	Bond and Wignall, 2010
Dysoxic	6.3	2.1	Bond and Wignall, 2010
Dysoxic	7.9	3.2	Bond and Wignall, 2010
Dysoxic	7.6	2.7	Bond and Wignall, 2010
Dysoxic	8	2.7	Bond and Wignall, 2010
Dysoxic	5.3	.9	Bond and Wignall, 2010
Dysoxic	7.8	4.1	Bond and Wignall, 2010
Dysoxic	8	3	Bond and Wignall, 2010
Dysoxic	6.8	3.4	Bond and Wignall, 2010
Dysoxic	8.1	2.2	Bond and Wignall, 2010
Dysoxic	4.6	1.6	Taylor and Macquaker, 2000
Dysoxic	9.6	5.7	Marynowski et al., 2007
Dysoxic	5.9	3	Marynowski et al., 2007
Dysoxic	11.9	5.1	Marynowski et al., 2007
Dysoxic	8.9	4.4	Marynowski et al., 2007
Dysoxic	8.6	3.8	Marynowski et al., 2007
Oxic	5.16	4.17	Nielsen and Shen, 2004
Oxic	5.92	4.54	Nielsen and Shen, 2004
Oxic	4.28	2.87	Nielsen and Shen, 2004
Oxic	4.73	2.53	Nielsen and Shen, 2004
Oxic	7.4	4.9	Suits and Wilkin, 1998
Oxic	10.3	4.7	Bond and Wignall, 2010
Oxic	9.5	.7	Bond and Wignall, 2010
Oxic	11	7.1	Bond and Wignall, 2010
Oxic	19.5	2.1	Bond and Wignall, 2010
Oxic	18.9	12.5	Bond and Wignall, 2010
Oxic	36	24.3	Bond and Wignall, 2010
Oxic	7	1.6	Bond and Wignall, 2010
Oxic	8.8	1.8	Bond and Wignall, 2010
Oxic	9.3	4.2	Bond and Wignall, 2010
Oxic	10.2	2.9	Bond and Wignall, 2010
Oxic	12.2	8.8	Bond and Wignall, 2010
Oxic	11.2	4.9	Bond and Wignall, 2010
Oxic	6.7	3.3	Bond and Wignall, 2010
Oxic	6	2.3	Bond and Wignall, 2010
Oxic	6.6	2.2	Bond and Wignall, 2010
Oxic	7.2	2.5	Bond and Wignall, 2010
Oxic	7.8	2.3	Bond and Wignall, 2010

Chapter 3:

QUANTIFYING BONE WEATHERING STAGES USING THE SURFACE ROUGHNESS PARAMETER Ra MEASURED FROM 3D DATA

SUMMARY

Bone surface texture is known to degrade in a predictable fashion due to subaerial exposure, and can thus act as a relative proxy for estimating temporal information from modern and ancient bone assemblages. To date, the majority of bone weathering data is collected on a categorical scale based on descriptive terms. While this qualitative classification of weathering data is well established and quite successful, 3D textural analyses of bone surfaces may provide means to quantify weathering stages. Here we test whether different weathering stages are characterized by statistically distinct surface textures. To do so, we first measured the surface roughness parameter Ra, which is the average vertical deviation of surface from the mean line of roughness profiles measured from 3D scans, from four adult ungulate taxa to identify regions with similar initial bone texture. We found that points measured from the lateral and medial sides of the rib-shaft were similar to each other, and that the rib-shaft in general was less rough compared to the rib-ends and rib-heads. Furthermore, rib-shafts are good candidates for high resolution textural analyses because taxa rib-shafts from unweathered ungulate skeletons were similar. After establishing that ribs-shafts would be most suitable candidates for weathering analyses, we measured the average roughness of weathered ungulate rib-shafts and assigned them to a descriptive weathering stage. We found that Ra was a reliable predictor for weathering stages and may provide means for quantifying bone weathering stages. Using Ra, or other textural analyses, may enable more reliable comparative taphonomic analyses by reducing inter-observer variations and by providing numerical data more compatible for multivariate statistics**.**

INTRODUCTION

Bones exposed to subaerial conditions undergo mechanical and chemical degradation at the ground surface, a process recognized as weathering (Shipman, 1981). Bone weathering is attributed primarily to exposure to UV, changes in temperature, changes in humidity, wetting-drying, and freezing-thawing (Behrensmeyer, 1978; Tappen, 1994; Trueman et al., 2004). These factors and processes progressively alter the crystallography of the bone and degrade collagen, which can result in the micro-cracking, macro-cracking, flaking, splintering, exfoliation, and ultimate breakdown of the bone (Behrensmeyer, 1978; Tappen and Peske, 1970; Tuross et al., 1989).

In arid environments, the weathering of bone occurs in a progressive and predictable pattern that often correlates with amount of time bones are exposed to subaerial conditions after death. Behrensmeyer (1978) was the first to document the pattern of bone degradation and use it as an indicator of temporal information in taphonomic investigations. In her original study, Behrensmeyer (1978) revisited natural bone assemblages actively weathering on the ground in Amboseli Park, Kenya and documented patterns of bone surface changes over time. She developed a classification scheme of weathering stages that documented the progressive destruction of bone over time (summarized in Table 4). Subsequent studies have since employed bone weathering stages to assess temporal information about modern and fossil bone assemblages (Cutler et al., 1999; Eberth et al., 2007; Fiorillo et al., 2000; Miller, 2011; Shipman, 1981; Tuross et al., 1989).

In arid environments, bone weathering trends are manifested on the surface of bones as the development and propagation of micro-cracks into large-scale bone splinters that exfoliate off the bone surface (Behrensmeyer, 1978). Because subaerial weathering is shown to progressively modify bone surface texture, likely by becoming rougher, 3D surface analyses may provide means to further constrain and modify previously established weathering stages. 3D surface analyses are commonly used in the fields of mechanical engineering as a means for characterizing turned metal, for standardizing surface production, and as a method for assessing surface quality of manufactured parts.

Cost-efficient instruments capable of measuring surfaces are becoming more available, and the use of industrial surface texture parameters are now being used in archaeologic and paleontologic studies, primarily for studying the micro-wear of stone tools and teeth (Evans and Donahue, 2008; Kaiser and Brinkmann, 2006; Kaiser and Katterwe, 2001; Schulz et al., 2010; Stemp, 2013; Stemp and Stemp, 2003). To date, the use of industrial surface texture analyses have not been applied to characterize bone surfaces.

Weathering Stage	*Description*
Stage 0	Fresh, unaltered bone with no cracking or flaking.
Stage 1	Fine cracks on bone surface, usually parallel to fiber structure. Incipient cracks in flat, short, and irregular bones, initial stages of exfoliation.
Stage 2	Flaking of outer bone layers usually associated with cracks. Crack edges are angular, fissures are longer and wider. Inner bone layers may be exposed.
Stage 3	Rough, cracked surface, with patches of fibrous texture. Crack edges are rounded. Tissue rarely present.
Stage 4	Deep, open cracks penetrate inner portions of bone. Portions of splintered surface may break off when bone is moved.
Stage 5	Bones severely deteriorated and mechanically falling into pieces. Very deep cracks, with many splinters broken away. Bone is extremely fragile and its only shape may be difficult to determine.

Table 4: Descriptive bone weathering stages adapted from Behrensmyer (1978), Lyman and Fox (1989), Tuross et al., (1989), Cutler et al., (1999), and Todisco and Manchot (2008).

Here we investigate if 3D surface characterization methods can be used to study bone surfaces. Our project goals were to:

1) Measure fresh bone texture across a single bone, within a skeleton, and across mammal species to ensure downstream analyses of weathering texture is not due to natural variation of fresh bone.

2) Test if different weathering stages are characterized by statistically distinct surface textures using standardized surface characterization methods.

METHODS

3D textural analyses of bone surfaces were done using the software package StereoExplorer (Leica Microsystems Schweiz AG, CH-9435 Heerbrugg, Switzerland). StereoExplorer uses pixel shifts from digital stereo-image pairs captured from a standard microscope with an integrated stereo camera (here a Leica MZ 16A from Leica Microsystems Schweiz AG, CH-9435 Heerbrugg, Switzerland) to generate surface data models (Schwaller et al., 2009). Bone surfaces were measured at the same magnification (25x) and with the bone fibers oriented in the horizontal direction. Prior to textural analysis, surface models were leveled to remove form and cropped to areas in focus. StereoExplorer was set to measure 100 vertical profiles of the surface and calculated 26 ISO (International Organization for Standardization) parameters for the selected surface.

We chose to focus primarily on the ISO parameter Ra, a metric of surface roughness. Ra is calculated by subtracting the waviness profile from the primarily profile. The cut-off for what is deemed waviness is rough and waviness profiles were generated using a 0.999 mm cutoff-length filter. This cutoff-length filter value subtracts vertical changes in bone surface that occur on frequencies over 1mm (such as natural features like bone shape and/or fibers) from the primary profile. Subtracting vertical changes due to bone fibers will highlight smaller surface textures. Ra is the industrial standard for profile average roughness and it calculated by averaging vertical deviations of measured points from the mean line (Kaiser and Katterwe, 2001). See Figure 23 for illustration on how Ra is measured from bone surface.

Unweathered bone specimens used in this study came from the osteological teaching specimens housed at the University of Minnesota-Twin Cities, Anthropology Department. Two groups of specimens were considered: large mammal (all ungulates > 100kg); and small mammals (mammals < 25kg). See Figure 25 for general species types. Only adult specimens were measured. Bone cleaning and other curation methods varied for each specimen. Most were defleshed and degreased by boiling; however, some specimens were cleaned using dermestid beetles. Since the

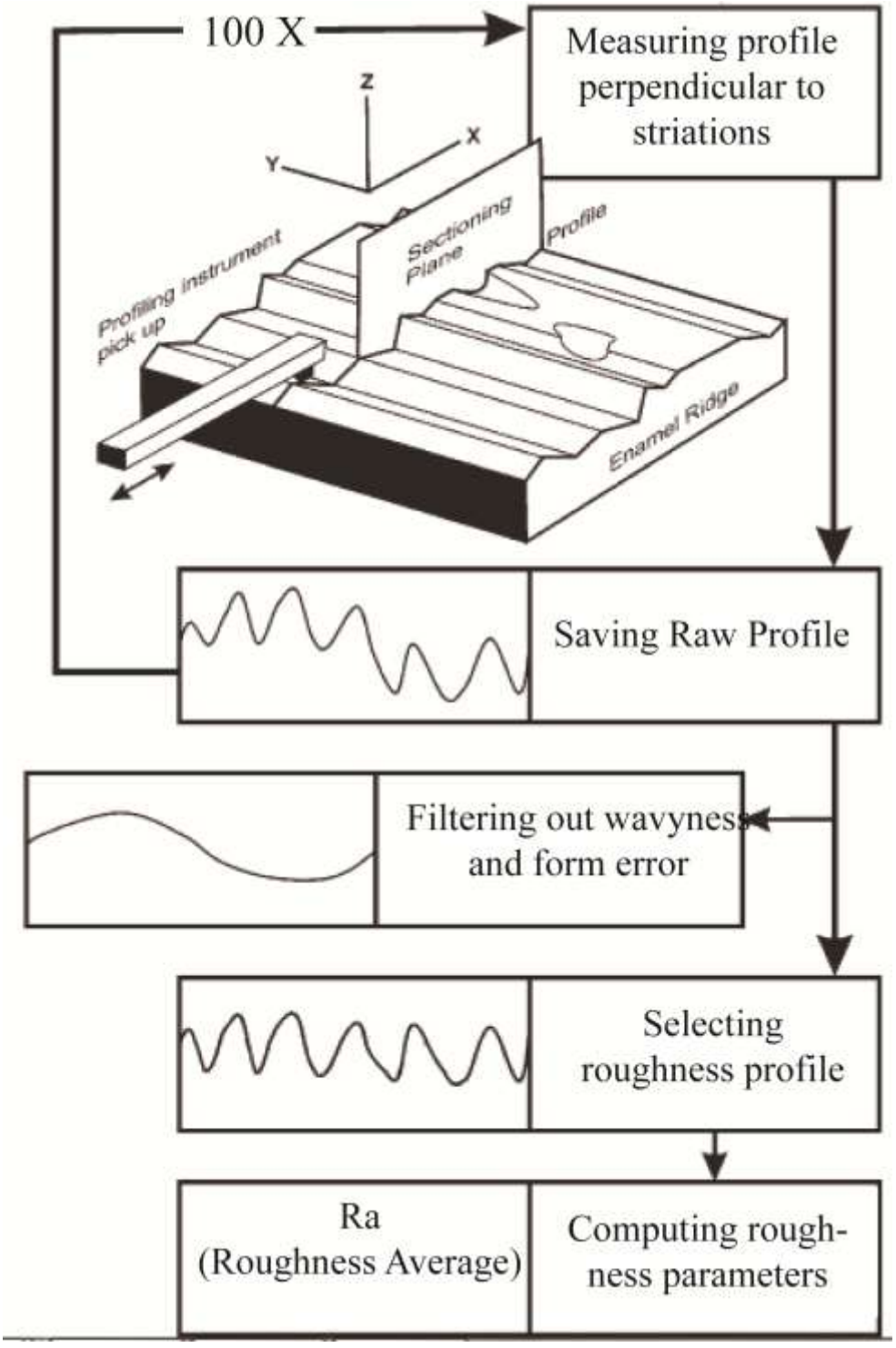

Figure 23: Figure adapted from Kaier and Katterwe (2001), illustrating the process for collecting and analyzing Ra, a surface texture measurments sampled from bone surfaces.

method of bone preparation varies and is unknown, we are considering the collection a random sample of bone preparation techniques. To minimize the effects of natural bone variation on the weathering stage analyses, we limited analyses to rib bones. All rib references here on out refer to dorsal rib bones.

Weathered ribs analyzed in this study come from the Isaac collection also housed at the University of Minnesota-Twin Cities Anthropology department. The Isaac collection is composed of naturally weathered bones collected from the ground surface in Kenya. Since these specimens were weathered in a very similar climate as the Behrensmeyer (1978) study, surface textures and weathering stages should be similar to the original classification scheme. As such, this study only pertains to bone surface textures caused by subaerial weathering in arid (savannah-like) climates. To keep the study consistent, only ribs or rib fragments from ungulate species were measured from the Isaac collection.

The variation in Ra values was compared across individual ribs, within a skeleton, between species, and ultimately between weathering stages. The disparity of Ra across and individual rib was calculated using the mean absolute percentage formula (Grine et al., 2002). Group comparisons were performed first by an analyses of variance (ANOVA), often followed by post-hoc pair-wise mean comparisons using Tukey's Honesty Significant Difference (HSD) with α=0.5).

To test if weathering stages are characterized by distinct surface texture, we measured the surface roughness parameter Ra from ~50 unidentified mammal rib shafts (some fragments) and assigned them a weathering stage. ANOVA and post-hoc pair-wise T-tests were used to investigate statistical differences in surface roughness.

RESULTS/DISCUSSION

Surface Texture Variation of Unweathered Bone

In order to test if weathering stages are characterized by different surface textures and can be quantified, we first had to investigate the natural variation of unweathered bone to ensure differences in surface texture of weathered bone are not due to natural bone variation. Here, we present the results of unweathered bone texture variation using the average roughness parameter Ra. We measured the Ra from five specific regions of

each rib, for six ribs per skeleton, and did this for large (>50 kg) ungulate taxa. We also compared the Ra of rib bones from smaller mammalian taxa (<25kg); however, only two points from the lateral and medial rib-shaft were measured.

Our results indicate that the average roughness (Ra) varied across an individual rib bone. Depending on the species, roughness measurements deviated from the mean by 30-40%. However, when comparing all ribs within in a skeleton, ANOVA results indicated that the Ra of each rib (points pooled) is statistically similar to the other rib bones ($P>0.1$) These results suggest that, although the rib texture varies across an individual rib, this variation is similar across each bone within a skeleton. When comparing the rib textures of different species, ANOVA results showed that the Ra values of the rib regions pooled are statistically similar across taxa ($P = 0.3852$). These results may signify that, even though the roughness varies within an individual rib, these intrinsic variations across the rib are similar across taxa and are not confounding, as long as Ra is measured from multiple points along a whole rib bone.

Although we found the natural variation in surface texture of rib bones to be insignificant if the whole bone is measured, rib bones are often recovered as fragments (Bown and J Kraus, 1981; Fiorillo, 1991; Holz and Barberena, 1994). For this reason, we investigated which regions of the rib bone have similar roughness values and would be suitable for comparative surface analyses. To do so, we compared different points of a rib bone within a skeleton and across taxa. For each rib, five points were measured in homologous locations: 1) lateral rib-head; 2) lateral mid-shaft; 3) medial rib-end; 4) medial ventral rib-shaft; and 5) medial dorsal rib-shaft. Flatter regions of the rib bone were chosen because they generated higher quality 3D surface models (more area in focus).

The average roughness of unweathered bone texture was found to be similar for specific regions of the rib bone across taxa as illustrated by Figure 22. ANOVA results confirmed textural differences among rib regions for all observed species, and post-hoc pair-wise Tukey's HSD tests indicated that the lateral rib-head (Point 1) was texturally different from the medial rib-shaft (Points 4,5) for all species. Textural similarities for the

lateral mid-shaft (Point 2) and medial rib-end (Point 3) were less consistent across taxa. For example, the medial rib-end (Point 3) of llama rib bones was found to be texturally similar to the medial rib shaft (Points 4 and 5), whereas the same region in the horse skeleton grouped more closely with the lateral rib-head and medial rib-end (Points 1 and 3, respectively). However, when analyzing rib regions together (species pooled), we found that the lateral mid-shaft (point 2) is closer in texture to the other rib-shafts (points 4, 5) than the later rib-head and medial rib-end (points 1 and 3) (values given in Table 5). Similarly, a mean comparison of lateral vs. medial Ra measurements of the rib shaft (excluding points 1&3), shows they are statistically similar (2.5 ± 0.2µm vs. 2.2 ± 0.1µm for lateral vs. medial rib shafts, respectively).

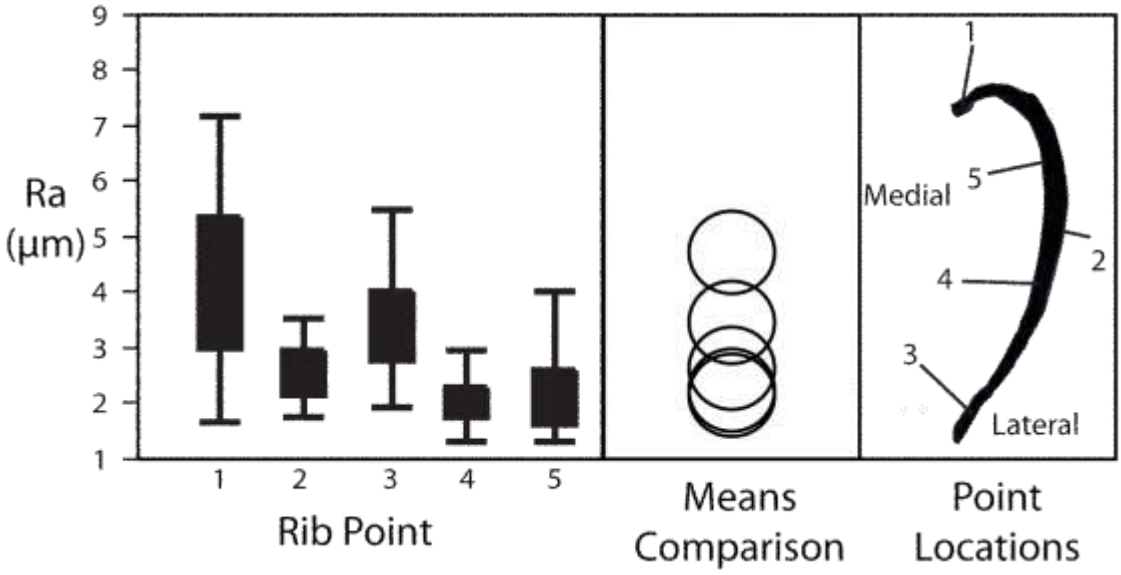

Figure 24: Box plot showing the distribution of roughness measurements (Ra) at specific points across the rib bones (n=6) of 4 large ungulate skeletons

Our results indicate that rib-shafts from large ungulate skeletons are texturally similar to each other, but different from rib-ends and rib-heads. We attribute this pattern of textural differences to bone morphology. Distal portions of ribs are often the loci of muscle attachments, and, as a result, the bone surface at these regions is more rugose. Since rib-head and rib-ends are initially rougher than rib shafts, we suggest that these regions should be compared separately in weathering analyses when using high-resolution scale data at the sub-micron scale. Our results imply that as long as weathering

analyses are restricted to rib-shaft regions, differences in initial bone texture should be negligible. Our results also suggest that locations of tissue connectivity may not be suitable for weathering stage analyses due to differences in initial bone texture.

While rib-shaft fragments may be plentiful in the fossil record (González Riga and Astini, 2007; Moore, 2012); they can be difficult to identify to the genus level. For this reason, we compared rib shaft textures from different types of mammals to determine if unweathered rib-shafts from different species were similar. We analyzed the rib shafts from the four large ungulate skeletons, also used for the single-rib analyses, in addition to four other smaller mammal types (see Table 5 for species). An ANOVA of all species indicated that there were differences among species ($p<0.0001$). Post-hoc comparisons of means distinguished two levels of similarity; the first grouped the non-ungulate smaller mammals, and the second level grouped the larger ungulates, illustrated in Figure 23. An ANOVA comparing the rib shaft roughness values among these animals groups showed that the rib-shaft Ra values are statistically indistinguishable from others classified in the same group (large/ungulate $p= 0.3121$; small/non-ungulate $p=0.4430$). Our results suggest that select smaller mammal groups have more rough ribs than larger mammal groups (4.7± 0.3µm SE vs. 2.3± 0 µm SE, Figure 24). This relationship may also correlate with ungulate group affinity; however, more analyses would be needed to further interpret the cause for rib-texture differences. Our results also suggest that it is not important to assign taxonomy to large ungulate mammalian rib fragments prior to analyses; and we predict the same may be true for smaller mammal taxa.

Group	Animal	Scientific	N	Point 1	Point 2	Point 3	Point 4	Point 5	Rib Mean	Shaft Mean
Large	Deer	*Odocoileus virginianus*	6	5.9 ± 1.4	2.7 ± 0.5	3.7 ± 0.5	2.8 ± 0.8	1.9 ± 0.2	3.4 ± 0.4	2.1 ± 0.1
	Elk	*Cervus canadensis*	6	4.3 ± 0.2	2.6 ± 0.2	3.9 ± 0.5	2.0 ± 0.2	2.0 ± 0.2	3.0 ± 0.2	2.3 ± 0.1
	Horse	*Equus ferus*	6	3.2 ± 0.5	2.7 ± 0.6	3.3 ± 0.4	2.0 ± 0.1	1.9 ± 0.2	2.6 ± 0.2	2.2 ± 0.2
	Llama	*Lama glama*	6	5.9 ± 1.1	2.4 ± 0.2	3.0 ± 0.3	2.2 ± 0.2	2.9 ± 0.3	3.3 ± 0.3	2.5 ± 0.1
	Pooled		24	4.7 ± 0.5	2.6 ± 0.1	3.5 ± 0.2	2.2 ± 0.2	2.2 ± 0.1	3.0 ± 0.2	2.3 ± 0.1
Small	Beaver	*Castor Canadensis*	6		4.1 ± 0.3			4.7 ± 0.3		4.4 ± 0.2
	Hare	*Lepus timidus*	6		3.9 ± 0.7			4.1 ± 0.3		4.0 ± 0.4
	Mongoose	*Atilax paludinosus*	2		4.9			7.9		6.4 ± 1.6
	Opposum	*Didelphis virginiana*	6		4.7 ± 0.6			6.2 ± 0.8		5.5 ± 0.5
	Pooled		18		4.3 ± 0.3			5.2 ± 0.4		4.7 ± 0.3
Non-Mammal	Fish		6		5.3 ± 0.4			5.9 ± 0.4		5.6 ± 0.3
	Ostrich	*Struthio camelus*	6		3.2 ± 0.5			3.4 ± 0.5		3.3 ± 0.3
Weathered	Stage 0	Mixed Ungulate	90							2.4 ± 0.1
	Stage 1		25							3.4 ± 0.3
	Stage 1.5		33							6.7 ± 0.6
	Stage 2		6							14.4 ± 1.2
	Stage 3		4							23.5 ± 1.5

Table 5: Summary Table of the rib roughness average (Ra) measurements across the rib for several types of taxa that are grouped into three classes: large, small, and non-mammalian, and pooled statistics for each class are given in the shaded regions. Weathered data is also summarized on the table.

For exploratory purposes, we also compared the rib-shaft texture of two non-mammalian species (an ostrich and a fish). As Figure 25 shows, group mean comparisons (Tukey HSD) indicate that the ostrich rib-shaft roughness is statistically similar to the large ungulate rib roughness (5.0± 0.3 µm vs. 3.3± 0.5 um, respectively, p=0.9957) and that the fish rib-shaft texture (Ra= 5.6± 0.5µm) was statistically grouped with the smaller non-ungulate mammal types (Ra = 5.6± 0.5µm vs. 5.0± 0.3 µm, respectively, p=0.7806). Since the non-mammalian species had rib-shaft texture more similar to their size classes and not taxonomic clade, animal size as opposed to taxon, may be the predominant factor in determining rib-shaft texture. However, more samples of non-mammalian and mammalian species would need to be analyzed before this implication is confirmed.

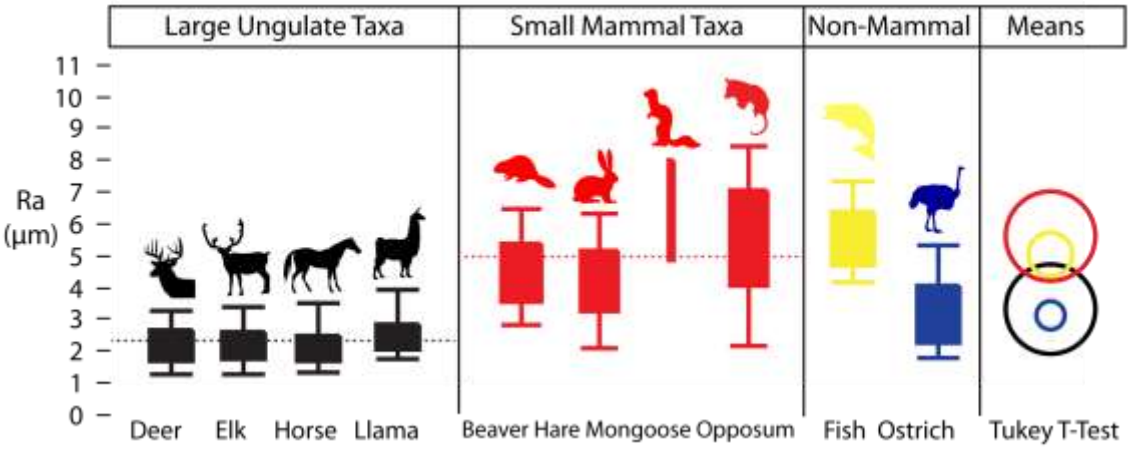

Figure 25: Boxplot of rib-shaft surface roughness (Ra) for several different species. Animals are assigned statistically distinct groups: large ungulate taxa, small mammal taza, and non-mammal taxa. The mean and standard deviation is indicated by colored circles to the right. Results indicate that the non-mammalian taxa plot closer to their respective size class.

Surface Texture of Weathered Bone

Subaerial bone weathering in arid environments is a progressive process starting with the development of small cracks that propagate into much larger cracks (Behrensmeyer, 1978; Tappen and Peske, 1970; Tuross et al., 1989). Since bone weathering is predictable and increasingly changes the size of cracks, measures of 3D surface roughness may provide alternative means for characterizing the degree of bone surface modification due to weathering. Based on our previous results, as long as 3D texture analyses are restricted to the rib shafts of large ungulates, variations in bone

surface texture are due to changes after death, likely as the result of weathering. Thus, we tested whether the bone surface roughness (Ra) correlates with the degree of weathering and provides means for quantifying weathering stages. To do so, we measured the Ra of weathered ungulate rib-shafts and compared this roughness metric with the ribs' assigned weathering stages. We analyzed 68 weathered bones; however, our sample sizes for each weathering stage were uneven because very few advanced weathering stages were available in the collections. We classified the weathered bones into five groups, representing four weathering stage: 0) unweathered bone; 1): very fine cracks on bone surface, no exfoliation or pitting; 1.5) fine-cracks on bone surface, some pitting, and small regions of exfoliation; 2) flaking of outer bone layers associated with cracks; and 3) considerable flaking and exfoliation with regions of fibrous texture. Weathering stages 4 and 5 were not considered in this study.

Based on average roughness values, we found that advancing weathering stages of rib shafts from large ungulate skeletons were characterized by rougher surfaces. After confirming dissimilarity between weathering stages with ANOVA (p-value <0.0001), we found that the distribution in roughness values is statistically distinct for each weathering stage (Figure 26). As predicted, the lower weathering stages are characterized by less rough surfaces, and the degree of roughness increases with each measured weathering stage. A linear regression (r^2= 0.6) shows that surfaces become more rough by 4.5 um vertical deviation from the mean-line with each increased weathering stage. These results indicate that a distinct surface roughness range will correlate with the weathering stages and suggests that surface roughness analyses may provide means to quantitatively analyze the weathering stages of fossil assemblages. In fact, roughness analyses were even able to statistically distinguished sub-weathering stages (weathering stage 1.5, Figure 26), which suggests that using quantifiable textural data may increase the temporal sensitivity of weathering stage analyses.

The scope of our study is limited because we primarily used adult mammalian rib bones. Our study does not take into account variation due to ontogenetic change (Brown et al., 2009; Tumarkin-Deratzian, 2006), other bones in the skeleton, and other vertebrate

types. Our results are also restricted to subaerial weathering in arid environments. Studies of bone weathering in different climates have found that bones are more affected by bioerosion activity (root damage or microbes) in wetter climates (Andrews and Cook, 1985; Fernández-Jalvo et al., 2010; Tappen, 1994). Lastly, 3D surface measuring instruments are found to vary (Leach and Haitjema, 2010; Rhee et al., 2005; Schwaller et al., 2009), and, without calibrating other instruments to ours, exact Ra values measured on other instruments should not be compared with our data; although we predict quantifying weathering stages on other instruments will be successful.

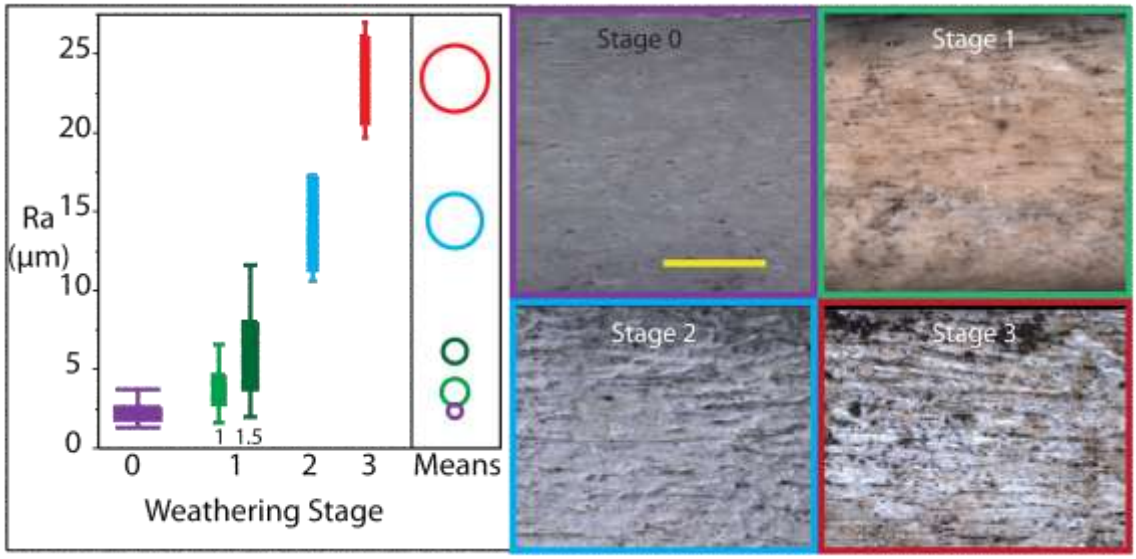

Figure 26: Box-plot indicating that surface roughness values from each weathering stage are statistically distinct. As expected, each weathering stage is progressively rougher. Images of representative bone surface for each weathering stage are provided on the right.

CONCLUSION

Bone weathering analyses are widely used to assess temporal information like accumulation rates, time since death, and time-averaging of modern and fossil bone assemblages. This principal works because bone surface texture degrades in a predictable fashion due to subaerial exposure in arid environments. In addition to traditional descriptive methods for describing bone weathering stages, we tested whether textural analyses already in practice by engineers may also provide means for characterizing weathering stages. To do this, we first identified a region of unweathered bone that was

texturally similar within a skeleton and across species to ensure variations measured in weathering analyses were the result of post-mortem changes and not due to initial bone surface differences.

For adult ungulate specimens, we found that the rib shaft is a good region to use in comparative weathering stage analyses because it is texturally similar within a skeleton and across species. Conversely, locations of tissue connectivity, like the rib-head and –shaft, should be avoided or analyzed separately because these regions are initially rougher. Comparisons of Ra measured from the rib shafts of large ungulates and smaller non-ungulate mammals indicate that surface texture is statistically similar in each group, but smaller mammals tend to have rougher bone texture compared to larger ungulate mammals. Of note, ribs from two non-mammalian vertebrates were more similar in texture to their respective weight class than to each other.

The average roughness parameter Ra was found to be a reliable predictor of weathering stage. Over 60 adult ungulate rib shafts collected from the ground surface in South Africa were assigned a weathering stage and measured using 3D textural analyses. The average surface roughness value of these weathered ribs was found to be statistically distinct for each weathering stage, suggesting that Ra, and potentially other 3D surface characterization parameters, may provide alternative means for analyzing the degree of bone weathering and estimating the temporal resolution of a fossil assemblage. However, due to the scope of our study, more analyses are needed to extend our interpretations to juvenile specimens, other vertebrate taxa, weathering in wetter climates, and data collected on other instruments.

Quantifying bone weathering stages using surface texture parameters has many advantages. Using the average roughness parameter Ra, and potentially other textural parameters, to characterize the degree of bone weathering may enable more reliable comparative taphonomic analyses by reducing inter-observer variation. Since surface texture analyses can incorporate data at the micron-level, we've shown that weathering stage analyses based on 3D roughness data may provide more time-specific weathering analyses. Lastly, the data provided by textural analyses in bone weathering studies may

be more compatible for use in multivariate statistics because it is continuous numerical data.

References

Allison, P. A., 1988a, The role of anoxia in the decay and mineralization of proteinaceous macro-fossils: Paleobiology, p. 139-154.

-, 1988b, Taphonomy of the Eocene London clay biota: Palaeontology, v. 31, no. 4, p. 1079-1100.

Allison, P. A., Smith, C. R., Kukert, H., Deming, J. W., and Bennett, B. A., 1991, Deep-water taphonomy of vertebrate carcasses: a whale skeleton in the bathyal Santa Catalina Basin: Paleobiology, p. 78-89.

Altschul, S. F., Gish, W., Miller, W., Myers, E. W., and Lipman, D. J., 1990, Basic local alignment search tool: Journal of molecular biology, v. 215, no. 3, p. 403-410.

Amano, K., and Little, C. T., 2005, Miocene whale-fall community from Hokkaido, northern Japan: Palaeogeography, Palaeoclimatology, Palaeoecology, v. 215, no. 3, p. 345-356.

Amon, D. J., Glover, A. G., Wiklund, H., Marsh, L., Linse, K., Rogers, A. D., and Copley, J. T., 2013, The discovery of a natural whale fall in the Antarctic deep sea: Deep Sea Research Part II: Topical Studies in Oceanography.

Ananyina, Y. V., 2010, Parasitic and free-living leptospirae (Leptospiraceae): Ecological and genetic features: Biology bulletin, v. 37, no. 7, p. 705-708.

Andrews, P., and Cook, J., 1985, Natural modifications to bones in a temperate setting: Man, p. 675-691.

Araujo, R., 2010, Endemism Versus Dispersion: Contribution of Microbial Genetics for Forensic Evidences: Open Forensic Science Journal, v. 3, p. 14-21.

Ascenzi, A., and Silvestrini, G., 1984, Bone-boring marine micro-organisms: an experimental investigation: Journal of Human Evolution, v. 13, no. 6, p. 531-536.

Astibia, H., Payros, A., Suberbiola, X. P., Elorza, J., Berreteaga, A., Etxebarria, N., Badiola, A., and Tosquella, J., 2005, Sedimentology and taphonomy of sirenian remains from the Middle Eocene of the Pamplona Basin (Navarre, western Pyrenees): Facies, v. 50, no. 3-4, p. 463-475.

Bailey, J. V., Raub, T. D., Meckler, A. N., Harrison, B. K., Raub, T., Green, A. M., and Orphan, V. J., 2010, Pseudofossils in relict methane seep carbonates resemble endemic microbial consortia: Palaeogeography, Palaeoclimatology, Palaeoecology, v. 285, no. 1, p. 131-142.

Balzer, A., Gleixner, G., Grupe, G., SCHMIDT, H. L., Schramm, S., and TURBAN-JUST, S., 1997, IN VITRO DECOMPOSITION OF BONE COLLAGEN BY SOIL BACTERIA: THE IMPLICATIONS FOR STABLE ISOTOPE ANALYSIS IN ARCHAEOMETRY*: Archaeometry, v. 39, no. 2, p. 415-429.

Bauer, M., Kube, M., Teeling, H., Richter, M., Lombardot, T., Allers, E., Würdemann, C. A., Quast, C., Kuhl, H., and Knaust, F., 2006, Whole genome analysis of the marine Bacteroidetes 'Gramella forsetii'reveals adaptations to degradation of

polymeric organic matter: Environmental Microbiology, v. 8, no. 12, p. 2201-2213.
Behrensmeyer, A. K., 1978, Taphonomic and ecologic information from bone weathering: Paleobiology, p. 150-162.
Behrensmeyer, A. K., and Kidwell, S. M., 1985, Taphonomy's contributions to paleobiology: Paleobiology, v. 11, no. 1, p. 105-119.
Belaústegui, Z., de Gibert, J. M., Domènech, R., Muñiz, F., and Martinell, J., 2012, Clavate borings in a Miocene cetacean skeleton from Tarragona (NE Spain) and the fossil record of marine bone bioerosion: Palaeogeography, Palaeoclimatology, Palaeoecology, v. 323, p. 68-74.
Bell, L., and Elkerton, A., 2008, Unique marine taphonomy in human skeletal material recovered from the medieval warship Mary Rose: International Journal of Osteoarchaeology, v. 18, no. 5, p. 523-535.
Benninger, L. A., Carter, D. O., and Forbes, S. L., 2008, The biochemical alteration of soil beneath a decomposing carcass: Forensic science international, v. 180, no. 2, p. 70-75.
Best, M. M., and Kidwell, S. M., 2009, Bivalve taphonomy in tropical mixed siliciclastic-carbonate settings. I. Environmental variation in shell condition.
Beutler, M., Milucka, J., Hinck, S., Schreiber, F., Brock, J., Mußmann, M., Schulz-Vogt, H. N., and de Beer, D., 2012, Vacuolar respiration of nitrate coupled to energy conservation in filamentous Beggiatoaceae: Environmental microbiology, v. 14, no. 11, p. 2911-2919.
Bond, D., Wignall, P. B., and Racki, G., 2004, Extent and duration of marine anoxia during the Frasnian–Famennian (Late Devonian) mass extinction in Poland, Germany, Austria and France: Geological Magazine, v. 141, no. 02, p. 173-193.
Bong, C. W., Obayashi, Y., and Suzuki, S., 2013, Succession of protease activity in seawater and bacterial isolates during starvation in a mesocosm experiment: Aquat Microb Ecol, v. 69, p. 33-46.
Boumba, V. A., Ziavrou, K. S., and Vougiouklakis, T., 2008, Biochemical pathways generating post-mortem volatile compounds co-detected during forensic ethanol analyses: Forensic science international, v. 174, no. 2, p. 133-151.
Bown, T. M., and J Kraus, M., 1981, Vertebrate fossil-bearing paleosol units (Willwood Formation, Lower Eocene, northwest Wyoming, USA): Implications for taphonomy, biostratigraphy, and assemblage analysis: Palaeogeography, Palaeoclimatology, Palaeoecology, v. 34, p. 31-56.
Brett, C. E., and Baird, G. C., 1986, Comparative taphonomy: a key to paleoenvironmental interpretation based on fossil preservation: Palaios, p. 207-227.
Bromley, R. G., Comparative analysis of fossil and recent echinoid bioerosion, *in* Proceedings Palaeontology1975.
Brook, I., 2008, Microbiology and management of joint and bone infections due to anaerobic bacteria: Journal of Orthopaedic Science, v. 13, no. 2, p. 160-169.

Brown, C. M., Russell, A. P., and Ryan, M. J., 2009, Pattern and transition of surficial bone texture of the centrosaurine frill and their ontogenetic and taxonomic implications: Journal of Vertebrate Paleontology, v. 29, no. 1, p. 132-141.

Brownie, J., Shawcross, S., Theaker, J., Whitcombe, D., Ferrie, R., Newton, C., and Little, S., 1997, The elimination of primer-dimer accumulation in PCR: Nucleic acids research, v. 25, no. 16, p. 3235-3241.

Buchan, A., González, J. M., and Moran, M. A., 2005, Overview of the marine Roseobacter lineage: Applied and environmental microbiology, v. 71, no. 10, p. 5665-5677.

Butler, I. B., and Rickard, D., 2000, Framboidal pyrite formation via the oxidation of iron (II) monosulfide by hydrogen sulphide: Geochimica et Cosmochimica Acta, v. 64, no. 15, p. 2665-2672.

Canfield, D. E., and Raiswell, R., 1991, Pyrite formation and fossil preservation: Taphonomy: Releasing the data locked in the fossil record, v. 9, p. 337-387.

Carter, D. O., Yellowlees, D., and Tibbett, M., 2007, Cadaver decomposition in terrestrial ecosystems: Naturwissenschaften, v. 94, no. 1, p. 12-24.

Child, A., 1995a, Microbial taphonomy of archaeological bone: Studies in Conservation, v. 40, no. 1, p. 19-30.

-, 1995b, Towards and understanding of the microbial decomposition of archaeological bone in the burial environment: Journal of Archaeological Science, v. 22, no. 2, p. 165-174.

Choi, W.-C., Kang, S.-J., Jung, Y.-T., Oh, T.-K., and Yoon, J.-H., 2011, Oceanisphaera ostreae sp. nov., isolated from seawater of an oyster farm, and emended description of the genus Oceanisphaera Romanenko et al. 2003: International journal of systematic and evolutionary microbiology, v. 61, no. 12, p. 2880-2884.

Clarke, J. B., 2004, A mineralogical method to determine cyclicity in the taphonomic and diagenetic history of fossilized bones: Lethaia, v. 37, no. 3, p. 281-284.

Cutler, A. H., Behrensmeyer, A. K., and Chapman, R. E., 1999, Environmental information in a recent bone assemblage: roles of taphonomic processes and ecological change: Palaeogeography, Palaeoclimatology, Palaeoecology, v. 149, no. 1, p. 359-372.

Dahlgren, T. G., Wiklund, H., Kallstrom, B., Lundalv, T., Smith, C. R., and Glover, A. G., 2006, A shallow-water whale-fall experiment in the north Atlantic: Cahiers de Biologie Marine, v. 47, no. 4, p. 385.

Daniel, J. C., and Chin, K., 2010, The role of bacterially mediated precipitation in the permineralization of bone: Palaios, v. 25, no. 8, p. 507-516.

Danise, S., Cavalazzi, B., Dominici, S., Westall, F., Monechi, S., and Guioli, S., 2012, Evidence of microbial activity from a shallow water whale fall (Voghera, northern Italy): Palaeogeography, Palaeoclimatology, Palaeoecology, v. 317, p. 13-26.

Darroch, S. A., Laflamme, M., D SCHIFFBAUER, J., and Briggs, D. E., 2012, Experimental formation of a microbial death mask: Palaios, v. 27, no. 5, p. 293-303.

Davis, P. G., 1997, The bioerosion of bird bones: International Journal of Osteoarchaeology, v. 7, no. 4, p. 388-401.

Del Fabbro, C., Scalabrin, S., Morgante, M., and Giorgi, F. M., 2013, An Extensive Evaluation of Read Trimming Effects on Illumina NGS Data Analysis: PloS one, v. 8, no. 12, p. e85024.

Deming, J. W., Reysenbach, A. L., Macko, S. A., and Smith, C. R., 1997, Evidence for the microbial basis of a chemoautotrophic invertebrate community at a whale fall on the deep seafloor: Bone-colonizing bacteria and invertebrate endosymbionts: Microscopy research and technique, v. 37, no. 2, p. 162-170.

Donald, R., and Southam, G., 1999, Low temperature anaerobic bacterial diagenesis of ferrous monosulfide to pyrite: Geochimica et Cosmochimica Acta, v. 63, no. 13, p. 2019-2023.

Eberth, D. A., Rogers, R. R., Fiorillo, A. R., Rogers, R., Eberth, D., and Fiorillo, A., 2007, A practical approach to the study of bonebeds: Bonebeds: Genesis, Analysis and Paleobiological Significance, p. 265-331.

Evangelista, K. V., and Coburn, J., 2010, Leptospira as an emerging pathogen: a review of its biology, pathogenesis and host immune responses: Future microbiology, v. 5, no. 9, p. 1413-1425.

Evans, A. A., and Donahue, R. E., 2008, Laser scanning confocal microscopy: a potential technique for the study of lithic microwear: Journal of Archaeological Science, v. 35, no. 8, p. 2223-2230.

Farrand, M., 1970, Framboidal sulphides precipitated synthetically: Mineralium Deposita, v. 5, no. 3, p. 237-247.

Fernández-Jalvo, Y., Andrews, P., Pesquero, D., Smith, C., Marín-Monfort, D., Sánchez, B., Geigl, E.-M., and Alonso, A., 2010, Early bone diagenesis in temperate environments: Part I: Surface features and histology: Palaeogeography, Palaeoclimatology, Palaeoecology, v. 288, no. 1, p. 62-81.

Fiorillo, A. R., 1991, Taphonomy and depositional setting of Careless Creek Quarry (Judith River Formation), Wheatland County, Montana, USA: Palaeogeography, Palaeoclimatology, Palaeoecology, v. 81, no. 3, p. 281-311.

Fiorillo, A. R., Padian, K., and Musikasinthorn, C., 2000, Taphonomy and Depositional Setting of the Placerias Quarry (Chinle Formation: Late Triassic, Arizona): Palaios, v. 15, no. 5, p. 373-386.

Freese, E., Rütters, H., Köster, J., Rullkötter, J., and Sass, H., 2009, Gammaproteobacteria as a possible source of eicosapentaenoic acid in anoxic intertidal sediments: Microbial ecology, v. 57, no. 3, p. 444-454.

Fujiwara, Y., Kato, C., Masui, N., Fujikura, K., and Kojima, S., 2001, Dual symbiosis in the cold-seep thyasirid clam Maorithyas hadalis from the hadal zone in the Japan Trench, western Pacific: Marine Ecology Progress Series, v. 214, p. 151-159.

Fürsich, F., and Oschmann, W., 1993, Shell beds as tools in basin analysis: the Jurassic of Kachchh, western India: Journal of the Geological Society, v. 150, no. 1, p. 169-185.

Giancamillo, A. D., Giudici, E., Andreola, S., Porta, D., Gibelli, D., Domeneghini, C., Grandi, M., and Cattaneo, C., 2010, Immersion of piglet carcasses in water–The applicability of microscopic analysis and limits of diatom testing on an animal model: Legal medicine, v. 12, no. 1, p. 13-18.

Giovannoni, S. J., Tripp, H. J., Givan, S., Podar, M., Vergin, K. L., Baptista, D., Bibbs, L., Eads, J., Richardson, T. H., and Noordewier, M., 2005, Genome streamlining in a cosmopolitan oceanic bacterium: science, v. 309, no. 5738, p. 1242-1245.

Goffredi, S. K., Johnson, S. B., and Vrijenhoek, R. C., 2007, Genetic diversity and potential function of microbial symbionts associated with newly discovered species of Osedax polychaete worms: Applied and environmental microbiology, v. 73, no. 7, p. 2314-2323.

Goffredi, S. K., and Orphan, V. J., 2010, Bacterial community shifts in taxa and diversity in response to localized organic loading in the deep sea: Environmental Microbiology, v. 12, no. 2, p. 344-363.

Goffredi, S. K., Wilpiszeski, R., Lee, R., and Orphan, V. J., 2008, Temporal evolution of methane cycling and phylogenetic diversity of archaea in sediments from a deep-sea whale-fall in Monterey Canyon, California: The ISME journal, v. 2, no. 2, p. 204-220.

González, J. M., Kiene, R. P., and Moran, M. A., 1999, Transformation of Sulfur Compounds by an Abundant Lineage of Marine Bacteria in the α-Subclass of the ClassProteobacteria: Applied and environmental microbiology, v. 65, no. 9, p. 3810-3819.

González Riga, B. J., and Astini, R. A., 2007, Preservation of large titanosaur sauropods in overbank fluvial facies: a case study in the Cretaceous of Argentina: Journal of South American Earth Sciences, v. 23, no. 4, p. 290-303.

Grimes, S. T., Brock, F., Rickard, D., Davies, K. L., Edwards, D., Briggs, D. E., and Parkes, R. J., 2001, Understanding fossilization: experimental pyritization of plants: Geology, v. 29, no. 2, p. 123-126.

Grimes, S. T., Davies, K. L., Butler, I. B., Brock, F., Edwards, D., Rickard, D., Briggs, D. E., and Parkes, R. J., 2002, Fossil plants from the Eocene London Clay: the use of pyrite textures to determine the mechanism of pyritization: Journal of the Geological Society, v. 159, no. 5, p. 493-501.

Grine, F., Ungar, P., and Teaford, M., 2002, Error rates in dental microwear quantification using scanning electron microscopy: Scanning, v. 24, no. 3, p. 144-153.

Grote, J., Schott, T., Bruckner, C. G., Glöckner, F. O., Jost, G., Teeling, H., Labrenz, M., and Jürgens, K., 2012, Genome and physiology of a model Epsilonproteobacterium responsible for sulfide detoxification in marine oxygen depletion zones: Proceedings of the National Academy of Sciences, v. 109, no. 2, p. 506-510.

Grünke, S., Lichtschlag, A., de Beer, D., Kuypers, M., Lösekann-Behrens, T., Ramette, A., and Boetius, A., 2010, Novel observations of Thiobacterium, a sulfur-storing

Gammaproteobacterium producing gelatinous mats: The ISME journal, v. 4, no. 8, p. 1031-1043.
Haiyan, R., Shulan, J., Dao, W., and Chengwu, C., 2007, Degradation characteristics and metabolic pathway of 17α-ethynylestradiol by< i> Sphingobacterium</i> sp. JCR5: Chemosphere, v. 66, no. 2, p. 340-346.
Hefti, E., Trechsel, U., Rüfenacht, H., and Fleisch, H., 1980, Use of dermestid beetles for cleaning bones: Calcified Tissue International, v. 31, no. 1, p. 45-47.
Higgs, N. D., Glover, A. G., Dahlgren, T. G., and Little, C. T., 2011, Bone-boring worms: Characterizing the morphology, rate, and method of bioerosion by Osedax mucofloris (Annelida, Siboglinidae): The Biological Bulletin, v. 221, no. 3, p. 307-316.
Hogler, J. A., 1994, Speculations on the role of marine reptile deadfalls in Mesozoic deep-sea paleoecology: Palaios, p. 42-47.
Hollund, H., Jans, M., Collins, M., Kars, H., Joosten, I., and Kars, S., 2012, What happened here? Bone histology as a tool in decoding the postmortem histories of archaeological bone from Castricum, The Netherlands: International Journal of Osteoarchaeology, v. 22, no. 5, p. 537-548.
Holz, M., and Barberena, M. C., 1994, Taphonomy of the south Brazilian Triassic paleoherpetofauna: pattern of death, transport and burial: Palaeogeography, Palaeoclimatology, Palaeoecology, v. 107, no. 1, p. 179-197.
Inagaki, F., Takai, K., Kobayashi, H., Nealson, K. H., and Horikoshi, K., 2003, Sulfurimonas autotrophica gen. nov., sp. nov., a novel sulfur-oxidizing ε-proteobacterium isolated from hydrothermal sediments in the Mid-Okinawa Trough: International journal of systematic and evolutionary microbiology, v. 53, no. 6, p. 1801-1805.
Jans, M., Nielsen-Marsh, C., Smith, C., Collins, M., and Kars, H., 2004, Characterisation of microbial attack on archaeological bone: Journal of Archaeological Science, v. 31, no. 1, p. 87-95.
Jans, M. M., 2008, Microbial bioerosion of bone–a review, Current developments in bioerosion, Springer, p. 397-413.
Jensen, M., and Thomsen, E., 1987, Ultrastructure, dissolution and" pyritization" of Late Quaternary and Recent echinoderms: Bulletin of the Geological Society of Denmark, v. 36, no. 3-4, p. 275-287.
Jiang, W.-T., Horng, C.-S., Roberts, A. P., and Peacor, D. R., 2001, Contradictory magnetic polarities in sediments and variable timing of neoformation of authigenic greigite: Earth and Planetary Science Letters, v. 193, no. 1, p. 1-12.
Jones, E. G., Collins, M. A., Bagley, P. M., Addison, S., and Priede, I. G., 1998, The fate of cetacean carcasses in the deep sea: observations on consumption rates and succession of scavenging species in the abyssal north-east Atlantic Ocean: Proceedings of the Royal Society of London. Series B: Biological Sciences, v. 265, no. 1401, p. 1119-1127.
Jordan, E. M., Thompson, F. L., Zhang, X.-H., Li, Y., Vancanneyt, M., Kroppenstedt, R. M., Priest, F. G., and Austin, B., 2007, Sneathiella chinensis gen. nov., sp. nov., a

novel marine alphaproteobacterium isolated from coastal sediment in Qingdao, China: International journal of systematic and evolutionary microbiology, v. 57, no. 1, p. 114-121.

Jorgensen, B., and Revsbech, N., 1985, Diffusive boundary layers and the oxygen uptake of sediments and detritus: Limnology and oceanography, v. 30, no. 1, p. 111-122.

Kaim, A., Kobayashi, Y., Echizenya, H., Jenkins, R. G., and Tanabe, K., 2008, Chemosynthesis-based associations on Cretaceous plesiosaurid carcasses: Acta Palaeontologica Polonica, v. 53, no. 1, p. 97-104.

Kaiser, T. M., and Brinkmann, G., 2006, Measuring dental wear equilibriums—the use of industrial surface texture parameters to infer the diets of fossil mammals: Palaeogeography, Palaeoclimatology, Palaeoecology, v. 239, no. 3, p. 221-240.

Kaiser, T. M., and Katterwe, H., 2001, The application of 3D-microprofilometry as a tool in the surface diagnosis of fossil and sub-fossil vertebrate hard tissue. An example from the Pliocene Upper Laetolil Beds, Tanzania: International Journal of Osteoarchaeology, v. 11, no. 5, p. 350-356.

Kemp, K. M., Jamieson, A. J., Bagley, P. M., McGrath, H., Bailey, D. M., Collins, M. A., and Priede, I. G., 2006, Consumption of large bathyal food fall, a six month study in the NE Atlantic: Marine Ecology Progress Series, v. 310, p. 65-76.

Kenrick, P., and Edwards, D., 1988, The anatomy of Lower Devonian Gosslingia breconensis Heard based on pyritized axes, with some comments on the permineralization process: Botanical journal of the Linnean Society, v. 97, no. 2, p. 95-123.

Kiel, S., 2008, Fossil evidence for micro-and macrofaunal utilization of large nekton-falls: examples from early Cenozoic deep-water sediments in Washington State, USA: Palaeogeography, Palaeoclimatology, Palaeoecology, v. 267, no. 3, p. 161-174.

Kiel, S., Goedert, J. L., Kahl, W.-A., and Rouse, G. W., 2010, Fossil traces of the bone-eating worm Osedax in early Oligocene whale bones: Proceedings of the National Academy of Sciences, v. 107, no. 19, p. 8656-8659.

Kirchman, D. L., 2002, The ecology of Cytophaga–Flavobacteria in aquatic environments: FEMS Microbiology Ecology, v. 39, no. 2, p. 91-100.

Knoblauch, C., Sahm, K., and Jørgensen, B. B., 1999, Psychrophilic sulfate-reducing bacteria isolated from permanently cold Arctic marine sediments: description of Desulfofrigus oceanense gen. nov., sp. nov., Desulfofrigus fragile sp. nov., Desulfofaba gelida gen. nov., sp. nov., Desulfotalea psychrophila gen. nov., sp. nov. and Desulfotalea arctica sp. nov: International Journal of Systematic and Evolutionary Microbiology, v. 49, no. 4, p. 1631-1643.

Ko, A. I., Goarant, C., and Picardeau, M., 2009, Leptospira: the dawn of the molecular genetics era for an emerging zoonotic pathogen: Nature Reviews Microbiology, v. 7, no. 10, p. 736-747.

Kodama, Y., and Watanabe, K., 2004, Sulfuricurvum kujiense gen. nov., sp. nov., a facultatively anaerobic, chemolithoautotrophic, sulfur-oxidizing bacterium

isolated from an underground crude-oil storage cavity: International journal of systematic and evolutionary microbiology, v. 54, no. 6, p. 2297-2300.
Koenig, A. E., Rogers, R. R., and Trueman, C. N., 2009, Visualizing fossilization using laser ablation–inductively coupled plasma–mass spectrometry maps of trace elements in Late Cretaceous bones: Geology, v. 37, no. 6, p. 511-514.
Kozich, J. J., Westcott, S. L., Baxter, N. T., Highlander, S. K., and Schloss, P. D., 2013, Development of a dual-index sequencing strategy and curation pipeline for analyzing amplicon sequence data on the MiSeq Illumina sequencing platform: Applied and environmental microbiology, v. 79, no. 17, p. 5112-5120.
Kraft, B., Engelen, B., Goldhammer, T., Lin, Y. S., Cypionka, H., and Könneke, M., 2013, Desulfofrigus sp. prevails in sulfate-reducing dilution cultures from sediments of the Benguela upwelling area: FEMS microbiology ecology, v. 84, no. 1, p. 86-97.
Krumbein, W., and Garrels, R., 1952, Origin and classification of chemical sediments in terms of pH and oxidation-reduction potentials: The Journal of Geology, p. 1-33.
Kuever, J., Rainey, F., and Widdel, F., 2005a, Order V. Desulfuromonales ord. nov: Bergey's Manual of Systematic. Proteobacteria. Part C The Alpha-, Beta-, Delta-, and Epsilonproteobacteria. New York: Springer Science+ Business Media, Inc, p. 1005-1020.
Kuever, J., Rainey, F., and Widdel III, F., 2005b, Order III. Desulfobacterales ord. nov: Bergey's Manual of Systematic Bacteriology, v. 2, no. Part C, p. 959.
Larkin, J. M., and Strohl, W. R., 1983, Beggiatoa, Thiothrix, and Thioploca: Annual Reviews in Microbiology, v. 37, no. 1, p. 341-367.
Leach, R., and Haitjema, H., 2010, Bandwidth characteristics and comparisons of surface texture measuring instruments: Measurement Science and Technology, v. 21, no. 3, p. 032001.
Ludwig, W., Schleifer, K.-H., and Whitman, W. B., 2009, Revised road map to the phylumFirmicutes, Bergey's Manual® of Systematic Bacteriology, Springer, p. 1-13.
Lundsten, L., Schlining, K. L., Frasier, K., Johnson, S. B., Kuhnz, L. A., Harvey, J. B., Clague, G., and Vrijenhoek, R. C., 2010, Time-series analysis of six whale-fall communities in Monterey Canyon, California, USA: Deep Sea Research Part I: Oceanographic Research Papers, v. 57, no. 12, p. 1573-1584.
Machado de Oliveira, J., Siqueira, J., Rôças, I., Baumgartner, J., Xia, T., Peixoto, R., and Rosado, A., 2007, Bacterial community profiles of endodontic abscesses from Brazilian and USA subjects as compared by denaturing gradient gel electrophoresis analysis: Oral microbiology and immunology, v. 22, no. 1, p. 14-18.
MacLean, L., Tyliszczak, T., Gilbert, P., Zhou, D., Pray, T., Onstott, T., and Southam, G., 2008, A high-resolution chemical and structural study of framboidal pyrite formed within a low-temperature bacterial biofilm: Geobiology, v. 6, no. 5, p. 471-480.

Marchiafava, V., Bonucci, E., and Ascenzi, A., 1974, Fungal osteoclasia: a model of dead bone resorption: Calcified tissue research, v. 14, no. 1, p. 195-210.

Marinellama, S., 1995, Cellulitis and sepsis due to Sphingobacterium: Jama2002, v. 228, p. 16.

Markowitz, V. M., Chen, I.-M. A., Palaniappan, K., Chu, K., Szeto, E., Grechkin, Y., Ratner, A., Jacob, B., Huang, J., and Williams, P., 2012, IMG: the integrated microbial genomes database and comparative analysis system: Nucleic acids research, v. 40, no. D1, p. D115-D122.

Markowitz, V. M., Korzeniewski, F., Palaniappan, K., Szeto, E., Werner, G., Padki, A., Zhao, X., Dubchak, I., Hugenholtz, P., and Anderson, I., 2006, The integrated microbial genomes (IMG) system: Nucleic acids research, v. 34, no. suppl 1, p. D344-D348.

Martill, D. M., and Unwin, D. M., 1997, Small spheres in fossil bones: blood corpuscles or diagenetic products?: Palaeontology, v. 40, no. 3, p. 619-624.

Marynowski, L., RAKOCInski, M., and Zaton, M., 2007, Middle Famennian (Late Devonian) interval with pyritized fauna from the Holy Cross Mountains (Poland): organic geochemistry and pyrite framboid diameter study: Geochemical Journal, v. 41, no. 3, p. 187-200.

Meldahl, K. H., and Flessa, K. W., 1990, Taphonomic pathways and comparative biofacies and taphofacies in a Recent intertidal/shallow shelf environment: Lethaia, v. 23, no. 1, p. 43-60.

Miller, J. H., 2011, Ghosts of Yellowstone: multi-decadal histories of wildlife populations captured by bones on a modern landscape: PloS one, v. 6, no. 3, p. e18057.

Moore, J. R., 2012, Do terrestrial vertebrate fossil assemblages show consistent taphonomic patterns?: Palaios, v. 27, no. 4, p. 220-234.

Moran, M. A., González, J. M., and Kiene, R. P., 2003, Linking a bacterial taxon to sulfur cycling in the sea: studies of the marine Roseobacter group: Geomicrobiology Journal, v. 20, no. 4, p. 375-388.

Mußmann, M., Hu, F. Z., Richter, M., de Beer, D., Preisler, A., Jørgensen, B. B., Huntemann, M., Glöckner, F. O., Amann, R., and Koopman, W. J., 2007, Insights into the genome of large sulfur bacteria revealed by analysis of single filaments: PLoS biology, v. 5, no. 9, p. e230.

Nelson, D. C., Wirsen, C. O., and Jannasch, H. W., 1989, Characterization of large, autotrophic Beggiatoa spp. abundant at hydrothermal vents of the Guaymas Basin: Applied and Environmental Microbiology, v. 55, no. 11, p. 2909-2917.

Norris, R. D., 1986, Taphonomic gradients in shelf fossil assemblages; Pliocene Purisima Formation, California: PALAIOS, v. 1, no. 3, p. 256-270.

Nuhfer, E. B., and Pavlovic, A. S., 1979, Association of Kaolinite with Pyritic Framboids: DISCUSSION: Journal of Sedimentary Research, v. 49, no. 1.

Ohfuji, H., and Rickard, D., 2005, Experimental syntheses of framboids—a review: Earth-Science Reviews, v. 71, no. 3, p. 147-170.

Pfretzschner, H.-U., 2004, Fossilization of Haversian bone in aquatic environments: Comptes Rendus Palevol, v. 3, no. 6, p. 605-616.

Popa, R., Kinkle, B. K., and Badescu, A., 2004, Pyrite framboids as biomarkers for iron-sulfur systems: Geomicrobiology Journal, v. 21, no. 3, p. 193-206.

Pruesse, E., Quast, C., Knittel, K., Fuchs, B. M., Ludwig, W., Peplies, J., and Glöckner, F. O., 2007, SILVA: a comprehensive online resource for quality checked and aligned ribosomal RNA sequence data compatible with ARB: Nucleic acids research, v. 35, no. 21, p. 7188-7196.

Quast, C., Pruesse, E., Yilmaz, P., Gerken, J., Schweer, T., Yarza, P., Peplies, J., and Glöckner, F. O., 2012, The SILVA ribosomal RNA gene database project: improved data processing and web-based tools: Nucleic acids research, p. gks1219.

Raiswell, R., Whaler, K., Dean, S., Coleman, M., and Briggs, D., 1993, A simple three-dimensional model of diffusion-with-precipitation applied to localised pyrite formation in framboids, fossils and detrital iron minerals: Marine Geology, v. 113, no. 1, p. 89-100.

Ranieri, M., and Boor, K., 2009, < i> Short communication:</i> Bacterial ecology of high-temperature, short-time pasteurized milk processed in the United States: Journal of dairy science, v. 92, no. 10, p. 4833-4840.

Reeb, V., Kolel, A., McDermott, T. R., and Bhattacharya, D., 2011, Good to the bone: microbial community thrives within bone cavities of a bison carcass at Yellowstone National Park: Environmental Microbiology, v. 13, no. 9, p. 2403-2415.

Revsbech, N. P., 1989, An oxygen microsensor with a guard cathode: Limnology and Oceanography, v. 34, no. 2, p. 474-478.

Revsbech, N. P., and Jørgensen, B., 1986, Microelectrodes: their use in microbial ecology: Adv. Microb. Ecol, v. 9, p. 293-352.

Rhee, H.-G., Vorburger, T. V., Lee, J. W., and Fu, J., 2005, Discrepancies between roughness measurements obtained with phase-shifting and white-light interferometry: Applied optics, v. 44, no. 28, p. 5919-5927.

Sagemann, J., Bale, S. J., Briggs, D. E., and Parkes, R. J., 1999, Controls on the formation of authigenic minerals in association with decaying organic matter: An experimental approach: Geochimica et Cosmochimica Acta, v. 63, no. 7, p. 1083-1095.

Sassen, R., Roberts, H. H., Carney, R., Milkov, A. V., DeFreitas, D. A., Lanoil, B., and Zhang, C., 2004, Free hydrocarbon gas, gas hydrate, and authigenic minerals in chemosynthetic communities of the northern Gulf of Mexico continental slope: relation to microbial processes: Chemical Geology, v. 205, no. 3, p. 195-217.

Schloss, P. D., Westcott, S. L., Ryabin, T., Hall, J. R., Hartmann, M., Hollister, E. B., Lesniewski, R. A., Oakley, B. B., Parks, D. H., and Robinson, C. J., 2009, Introducing mothur: open-source, platform-independent, community-supported software for describing and comparing microbial communities: Applied and environmental microbiology, v. 75, no. 23, p. 7537-7541.

Schuller, D., Kadko, D., and Smith, C. R., 2004, Use of< sup> 210</sup> Pb/< sup> 226</sup> Ra disequilibria in the dating of deep-sea whale falls: Earth and Planetary Science Letters, v. 218, no. 3, p. 277-289.

Schulz, E., Calandra, I., and Kaiser, T. M., 2010, Applying tribology to teeth of hoofed mammals: Scanning, v. 32, no. 4, p. 162-182.

Schwaller, P., Züst, R., and Michler, J., 2009, Quantitative Topographical Characterization of Thermally Sprayed Coatings by Optical Microscopy: Journal of thermal spray technology, v. 18, no. 1, p. 96-102.

Shade, A., McManus, P. S., and Handelsman, J., 2013, Unexpected diversity during community succession in the apple flower microbiome: MBio, v. 4, no. 2, p. e00602-00612.

Shapiro, R. S., and Spangler, E., 2009, Bacterial fossil record in whale-falls: petrographic evidence of microbial sulfate reduction: Palaeogeography, Palaeoclimatology, Palaeoecology, v. 274, no. 3, p. 196-203.

Shipman, P., 1981, Life history of a fossil: an introduction to taphonomy and paleoecology, Harvard University Press Cambridge.

Skei, J., 1988, Formation of framboidal iron sulfide in the water of a permanently anoxic fjord-Framvaren, South Norway: Marine Chemistry, v. 23, no. 3, p. 345-352.

Smith, C. R., and Baco, A. R., 2003, Ecology of whale falls at the deep-sea floor: Oceanography and Marine Biology: An Annual Review Volume, v. 41, p. 311-354.

Stackebrandt, E., and Goebel, B., 1994, Taxonomic note: a place for DNA-DNA reassociation and 16S rRNA sequence analysis in the present species definition in bacteriology: International Journal of Systematic Bacteriology, v. 44, no. 4, p. 846-849.

Stemp, W. J., 2013, A Review of Quantification of Lithic Use-Wear using Laser Profilometry: A Method Based on Metrology and Fractal Analysis: Journal of Archaeological Science.

Stemp, W. J., and Stemp, M., 2003, Documenting stages of polish development on experimental stone tools: surface characterization by fractal geometry using UBM laser profilometry: Journal of archaeological science, v. 30, no. 3, p. 287-296.

Sweeney, R., and Kaplan, I., 1973, Pyrite framboid formation; laboratory synthesis and marine sediments: Economic Geology, v. 68, no. 5, p. 618-634.

Tappen, M., 1994, Bone weathering in the tropical rain forest: Journal of Archaeological Science, v. 21, no. 5, p. 667-673.

Tappen, N., and Peske, G. R., 1970, Weathering cracks and split-line patterns in archaeological bone: American Antiquity, p. 383-386.

Thamdrup, B., Fossing, H., and Jørgensen, B. B., 1994, Manganese, iron and sulfur cycling in a coastal marine sediment, Aarhus Bay, Denmark: Geochimica et Cosmochimica Acta, v. 58, no. 23, p. 5115-5129.

Thole, S., Kalhoefer, D., Voget, S., Berger, M., Engelhardt, T., Liesegang, H., Wollherr, A., Kjelleberg, S., Daniel, R., and Simon, M., 2012, Phaeobacter gallaeciensis

genomes from globally opposite locations reveal high similarity of adaptation to surface life: The ISME journal, v. 6, no. 12, p. 2229-2244.
Tringe, S. G., Von Mering, C., Kobayashi, A., Salamov, A. A., Chen, K., Chang, H. W., Podar, M., Short, J. M., Mathur, E. J., and Detter, J. C., 2005, Comparative metagenomics of microbial communities: Science, v. 308, no. 5721, p. 554-557.
Trueman, C., and Martill, D., 2002, The long–term survival of bone: the role of bioerosion: Archaeometry, v. 44, no. 3, p. 371-382.
Trueman, C. N., Behrensmeyer, A. K., Tuross, N., and Weiner, S., 2004, Mineralogical and compositional changes in bones exposed on soil surfaces in Amboseli National Park, Kenya: diagenetic mechanisms and the role of sediment pore fluids: Journal of Archaeological Science, v. 31, no. 6, p. 721-739.
Tumarkin-Deratzian, A. R. V., David, R.; Dodson, Peter, 2006, Bone surface texture as an ontogenetic indicator in long bones of the Canada goose Branta canadensis (Anseriformes: Anatidae): Zoological Journal of the Linnean society, v. 148, no. 2, p. 133-168.
Turner-Walker, G., and Jans, M., 2008, Reconstructing taphonomic histories using histological analysis: Palaeogeography, Palaeoclimatology, Palaeoecology, v. 266, no. 3, p. 227-235.
Tuross, N., Behrensmeyer, A., Eanes, E., Fisher, L., and Hare, P., 1989, Molecular preservation and crystallographic alterations in a weathering sequence of wildebeest bones: Applied Geochemistry, v. 4, no. 3, p. 261-270.
Verna, C., Ramette, A., Wiklund, H., Dahlgren, T. G., Glover, A. G., Gaill, F., and Dubilier, N., 2010, High symbiont diversity in the bone-eating worm Osedax mucofloris from shallow whale-falls in the North Atlantic: Environmental microbiology, v. 12, no. 8, p. 2355-2370.
Vietti, L. A., Bailey, J. V., Fox, D. L., and Rogers, R. R., (submitted), Rapid formation of framboidal sulfides on bone sulfides from a simulated marine carcass-fall: Palaios.
Wang, F., Jiang, H., Shi, K., Ren, Y., Zhang, P., and Cheng, S., 2012, Gut bacterial translocation is associated with microinflammation in end-stage renal disease patients: Nephrology, v. 17, no. 8, p. 733-738.
Wignall, P., and Newton, R., 1998, Pyrite framboid diameter as a measure of oxygen deficiency in ancient mudrocks: American Journal of Science, v. 298, no. 7, p. 537-552.
Wignall, P. B., Newton, R., and Brookfield, M. E., 2005, Pyrite framboid evidence for oxygen-poor deposition during the Permian–Triassic crisis in Kashmir: Palaeogeography, Palaeoclimatology, Palaeoecology, v. 216, no. 3, p. 183-188.
Wilkin, R., and Barnes, H., 1996, Pyrite formation by reactions of iron monosulfides with dissolved inorganic and organic sulfur species: Geochimica et Cosmochimica Acta, v. 60, no. 21, p. 4167-4179.
-, 1997, Formation processes of framboidal pyrite: Geochimica et Cosmochimica Acta, v. 61, no. 2, p. 323-339.

Wilkin, R. T., Barnes, H. L., and Brantley, S. L., 1996, The size distribution of framboidal pyrite in modern sediments: An indicator of redox conditions: Geochimica et Cosmochimica Acta, v. 60, no. 20, p. 3897-3912.

Williams, K. P., Sobral, B. W., and Dickerman, A. W., 2007, A robust species tree for the alphaproteobacteria: Journal of bacteriology, v. 189, no. 13, p. 4578-4586.

Wings, O., 2004, Authigenic minerals in fossil bones from the Mesozoic of England: poor correlation with depositional environments: Palaeogeography, Palaeoclimatology, Palaeoecology, v. 204, no. 1, p. 15-32.

Yamamoto, M., and Takai, K., 2011, Sulfur metabolisms in epsilon-and gamma-Proteobacteria in deep-sea hydrothermal fields: Frontiers in microbiology, v. 2.

Youssef, N., Elshahed, M. S., and McInerney, M. J., 2009, Microbial processes in oil fields: culprits, problems, and opportunities: Advances in applied microbiology, v. 66, p. 141-251.

Zhou, C., and Jiang, S.-Y., 2009, Palaeoceanographic redox environments for the lower Cambrian Hetang Formation in South China: Evidence from pyrite framboids, redox sensitive trace elements, and sponge biota occurrence: Palaeogeography, Palaeoclimatology, Palaeoecology, v. 271, no. 3, p. 279-286.